Benzimidazole and Benzothiazole Based Chemosensors For Biologically Important Analytes

A Dissertation

Submitted in partial fulfillment for the degree of

Doctor of Philosophy

Abhijit Gogoi

(Roll No. 10612241)

Thesis Supervisor: Prof. Gopal Das

Department of Chemistry

Indian Institute of Technology Guwahati

Assam -781039, India

Benzimidazole and Benzothiazole Based Chemosensors For Biologically Important Analytes

A Dissertation

Submitted in partial fulfillment for the degree of

Doctor of Philosophy

Abhijit Gogoi

(Roll No. 10612241)

Thesis Supervisor: Prof. Gopal Das

Department of Chemistry

Indian Institute of Technology Guwahati

Assam-781039, India

Dedicated to

my parents

INDIAN INSTITUTE OF TECHNOLOGY GUWAHATI

Department of Chemistry

STATEMENT

I do hereby declare that the matter embodied in this thesis is the result of investigations carried out by me in the Department of Chemistry, Indian Institute of Technology Guwahati, India, under the guidance of Prof. Gopal Das, Department of Chemistry, Indian Institute of Technology Guwahati, India.

In keeping with the general practice of reporting scientific observations, due acknowledgements have been made wherever this work is based on the findings of other investigators.

26th October, 2015 **Abhijit Gogoi**

IIT Guwahati

INDIAN INSTITUTE OF TECHNOLOGY GUWAHATI

Department of Chemistry

CERTIFICATE

This is to certify that Mr. Abhijit Gogoi has been working under my supervision since January, 20011 as a regular registered Ph. D. student. His thesis entitled **"Benzimidazole and Benzothiazole Based Chemosensors for Biologically Important Analytes"** is authentic record of the results obtained from the research work carried out under my supervision in the Department of Chemistry, Indian Institute of Technology Guwahati, Assam, India. I am forwarding his thesis to submit for the award of degree of Doctor of Philosophy, from this institute. I hereby certify that he has fulfilled all the requirements, according to the rules of this institute regarding the investigations embodied in his thesis and this work has not been submitted elsewhere for a degree.

Prof. Gopal Das
(Thesis Supervisor)
Professor
Department of Chemistry
IIT Guwahati
Assam - 781039, India

Acknowledgement

At this final stage of truly memorable journey towards my intellectual destination, it is really hard to list all the people who sincerely helped me and I would like to thank all of them who have made this thesis possible. I would like to express my deepest gratitude to my father Lombudor Gogoi and mother Rina Gogoi, two people with irrational and unbreakable belief on me. Their unconditional love and support made me reach this stage of my life. I am highly indebted to my thesis supervisor Prof. Gopal Das for his kind support, insightful advice and encouragement. I earnestly thank him for his nice guidance, freedom to work, encouragement and inspiration which helped me to enrich myself.

Besides my supervisor, I would also like to give sincere gratitude to my doctoral committee members, Dr. Lal Mohan Kundu, Dr. Debasis Manna and Dr. Subhradip Ghosh for their advices and valuable suggestions. I shall always be obliged to Prof. Aiyagari Ramesh for his admirable support throughout my research work. I also wish to thank staff members of chemistry department especially Nilotpal da. I would also thank Dr. BLD for the help he has rendered through these years. My sincere thanks to the staffs of central instrument facility, for their help and in hand guidance to several analytical instruments, required during my research work.

I take this opportunity to thank my Lab members and friends, Bedo da, Bimlesh da, Sandeep da, Arghya da, Jiban, Chirantan da, Nazbul, Romen, Barun, Soham, Nilotpal, Rupinder, Utsab, Biswajit and Madhurima for their co-operation and inspiration in my research work, without which it would not been easy to complete the PhD thesis. It was great to work and spend times with these interesting human beings and I will always cherish the memories of their jokes, laughter and humor throughout my life. I wish them great success in every aspects of their life.

I also owe my obligations to my other seniors, batch mates and juniors of PhD fraternity of the chemistry department for their help and support.

In context to the thesis work, I had opportunity to mingle with friends of Biosciences & Bioengineering, IIT Guwahati. I owe my gratitude to Sudip, Thiyagaranjan, Sandipan, Poulomi for their unconditional support and all the help they extended from time to time whenever required.

I take this opportunity to thank my friend Saurav, Sarat, Baglari, Rintu, Preetismita, Ruprekha and Ankana, for being a source of my encouragement and love through this time. Also big thanks to Anupal, Trididp, Ashim, Arindam, Amlan, Hiranya, Jugal, Sourav and Sayan for supporting me in countless occasions. I would like to pay my sincere thanks to my school, college and university teachers, their motivation and help has guided me to reach this far.

Finally, I would like to thank the Microsoft Corporation for presenting the MS word, from grammar check to synonyms, from equation to symbols.

***A**bhijit*

The contents of this thesis entitled "**Benzimidazole and Benzothiazole Based Chemosensors For Biologically Important Analytes**" have been divided into six chapters based on the results of experimental work performed during the research period.

Chapter 1: Introduction

In the core of various biological, environmental and chemical process there are either cationic or anionic species which control those process. In the human proteome, one third of all proteins and half of all enzymes require metals for their structures or functions. Similarly, deepened understanding of the multifarious roles that anions play in biology, industrial processes and in the environment is essential for their application in various experimental fields such as bio-medicine, pollution control etc. Smartly designed molecular chemosensors can infer valuable information regarding their presence in biology, environmental and chemical process through differential output signals. The chemosensors are consisting mainly of two moieties, a binding unit responsible for the molecular recognition and a signalling unit to signal the recognition event. Interaction with the guest analyte can change the electron distribution of the chemosensor and thereby causes variation in signal outputs. Tsien *et. al*. in early 1980 marked the beginning of the golden era of chemosensors with a fluorescent calcium sensor and since then it expands promptly in different dimensions such as biology, medicine, military security, new materials, nano-devices and environmental science etc. However, the definition of 'chemosensor' was first given by Czarnik in 1993 as: ''A compound of abiotic origin that complexes to an analyte reversibly with a concomitant fluorescent signal transduction'' and it constitutes only the active transduction unit of a sensor.

There are different strategies and types of chemosensors which signals the presence of targeted species through different output signals both *in vivo* as well as *in vitro*. However, simplicity and high sensitivity of organic small molecular fluorescent chemosensors have made them the most attractive hosts in the sensing world. In this regard, our aim is to focus on benzimidazole and benzothiazole functionalities for designing new chemosensors. Such functionalities are ubiquitous and play vital roles in human body. In addition to this, histidine residues from imidazole ring is present in the active sites of most metalloproteins. Imidazole is also known to form hydrogen bonds with drugs and proteins. Furthermore, benzimidazole and similar class of compounds are rich in various properties. They are generally fluorescent, have both hydrogen bond acceptors as well as donors groups. Thus, on suitable substitution they would become fluorescence chemosensors to various non fluorescent species such as pH, picric acid, temperature, metals, anions etc.

Chapter 2: Experimental methods and characterization

In this chapter, a detailed information's about the various reagents used in the synthesis of the receptors/probes, their synthetic procedures, crystallization details, binding study, specifications of analytical instruments employed in the characterization of synthesized compounds are discussed.

Chapter 3: Benzothiazole Functionalized Sensor for Zn(II) and $H_2PO_4^-$: Response in NIR region

This chapter describes the synthesis and different photophysical behaviour of a novel benzothiazole functionalized ninhydrin based chemosensor **L_1**. The new chemosensor **L_1**, impels excellent colorimetric response to Zn^{2+}, which make the probe usable for naked eye detection of Zn^{2+} ion. The same solution is also exhibit 'turn-on' fluorometric response in near infra-red region (NIR). These spectral changes are significant enough to enable naked eye detection of Zn^{2+} ion in physiological medium also. Most importantly, the sensitivity of **L_1** for Zn^{2+} ion is also preserve in presence of its congener Cd^{2+} and most of the other tested metal ions even when present in excess. The Job's plot from the titration data suggests a 1:1 (**L_1** : Zn^{2+}) binding stoichiometry and the calculated detection limit is 6 nM. Nature of the Zn^{2+} binding mode with **L_1** is also analyse with ^{1}H NMR titration. Furthermore, the '**L_1**-Zn^{2+}' ensemble can selectivity sense and differentiate $H_2PO_4^-$ from pyrophosphate, ATP, ADP etc. nucleotides and other common anions through swithching off fluorescence emission at the same wavelength.

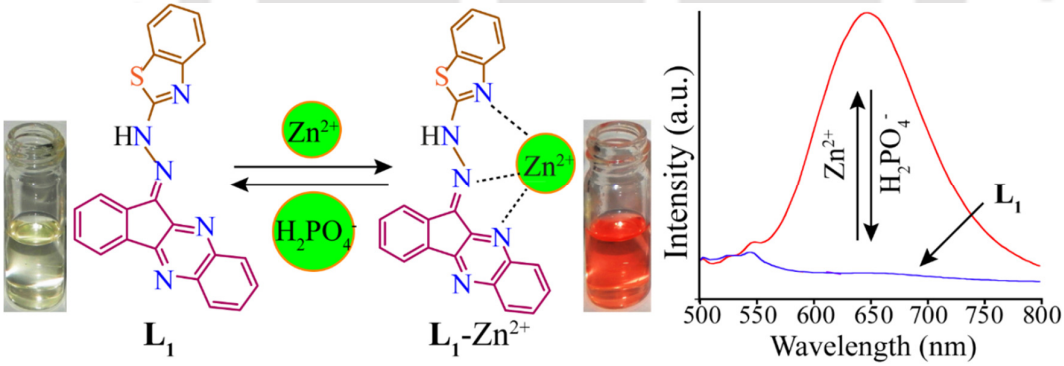

Scheme 1. A comprehensive representation of the research work included in chapter 3.

Chapter 4: Benzothiazole Functionalized Sensor for Zn(II), Cd(II), PPi and $H_2PO_4^-$: Multi ion sensing platform at Physiological condition

The different photophysical behaviours of a benzothiazole containing chemosensor (**L_2**) with various ananlytes are discussed in this chapter. **L_2** responds to Zn^{2+} ion based on CHEF process, which thereby impels a switch on response in optical and fluorescence emission spectra, promoting it to a dual probe for the naked eye detection of Zn^{2+} through change in colour and fluorescence in physiological condition. The selectivity and sensitivity for Zn^{2+} ion is

maintained over most of the biologically important cations except copper. Again similar to Zn^{2+} ion, Cd^{2+} also impels a 'turn-on' response in fluorescence spectra whereas the copper induced coloured solution is fluorescent inactive. Furthermore, both the Zn^{2+} and Cd^{2+} ensembles of **L_2** also respond to $H_2PO_4^-$ and $P_2O_7^{4-}$ anions in the same buffered medium as 'turn-off' sensors. The present study also demonstrates the utility of solution-coated dip paper strip of **L_2** for rapid detection of Zn^{2+} ion. Chemosensor **L_2** is also found to be reversible and recyclable towards Zn^{2+} and pyrophosphate ions over more than six cycles and responds to a INHIBIT logic gate. ^{1}H NMR titration and theoretical calculations are also conducted for the detailed understanding of the zinc binding with **L_2**.

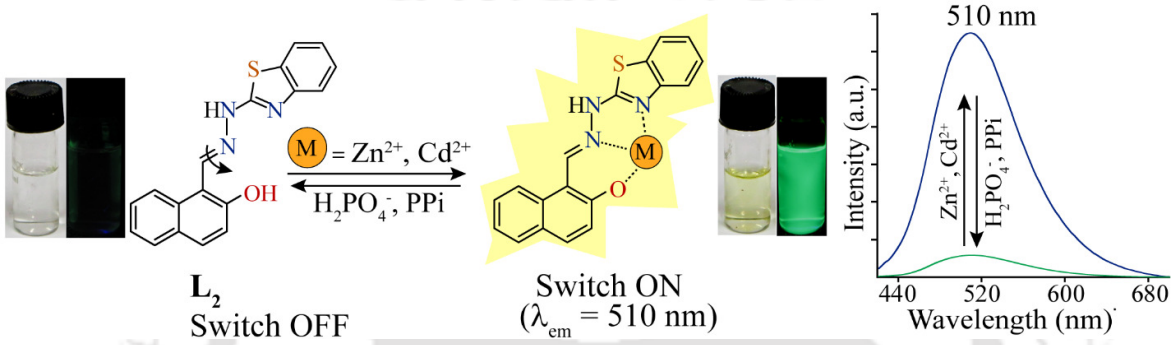

Scheme 2. A comprehensive representation of the research work included in chapter 4.

Chapter 5: Benzothiazole Functionalized Sensor for Zn(II) and PPi: Nano-molar sensing in Physiological condition and in Live Cells

This chapter give detailed information about a novel benzothiazole containing Schiff base (**L_3**), which renders relay recognition of Zn^{2+} and PPi in physiological medium. The Zn^{2+} sensing is evidence in mixed buffered medium and also in the physiological milieu in presence of HSA, BSA and SBF. In presence of Zn^{2+}, the colorless chemosensor solution displays a strong greenish fluorescence and thus enabled naked eye detection of the metal. The chemosensor exhibits a strong affinity ($K = 1.25\times10^5\ M^{-1}$) for Zn^{2+} even in the presence of the other interfering metal ions and is ultrasensitive as it can respond even to 1 nM Zn^{2+} (LOD for Zn^{2+} = 71 ppb). A facile application of the chemosensor can be demonstrate through successful detection of Zn^{2+} using the sensor-coated paper strips. The Zn^{2+}-chemosensor ensemble also responds to PPi in the same experimental medium through fluorescence quenching. Such sequential 'off-on-off' type fluorescence response of the chemosensor upon alternate addition of Zn^{2+} and PPi is further helpful to construct a INHIBIT logic gate. On the basis of the selectivity of chemosensor for Zn^{2+} in physiological medium and its biocompatible attribute, the probe could facilitate fluorescence-based sensing of intracellular Zn^{2+} in live HeLa cells. It is

envisaged that the developed probe holds considerable potential as a Zn^{2+} sensor for future environmental and biomedical applications.

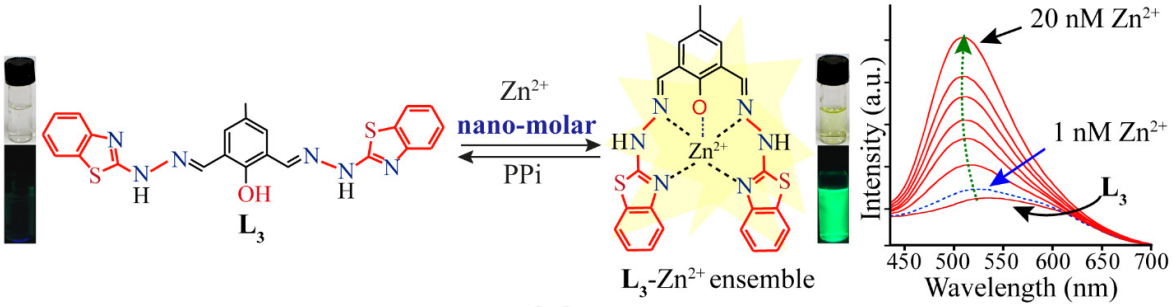

Scheme 3. A comprehensive representation of the research work included in chapter 5.

Chapter 6: Benzimidazole Functionalized Sensor for PPi: Aggregation-Induced Metal-Free Chemosensing Platform

The photophysical properties of a promising AIE active chemosensor (**L_4**) for the selective "switch-on" colorimetric and fluorimetric detection of pyrophosphate anion (PPi) in physiological medium are discussed in this chapter. Interaction with the PPi anion boosted the fluorescence through aggregation, which is well supported by FESEM, AFM, and DLS experiments. At the same time, the color of the solution has also changed which is detectable with naked eye.

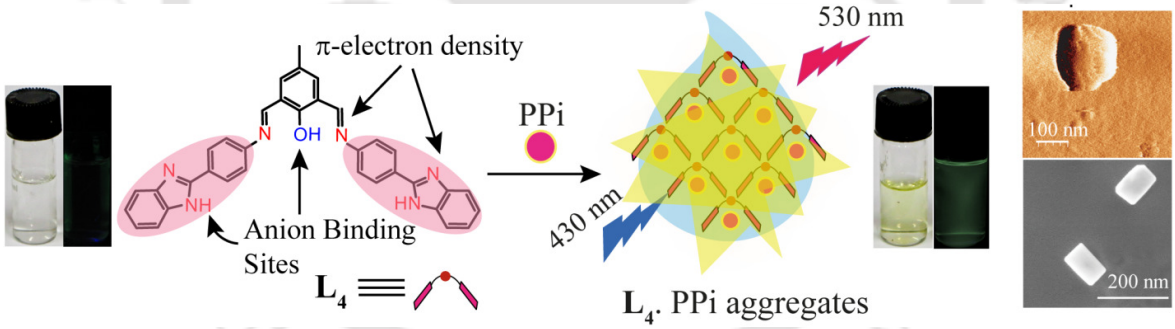

Scheme 4. A comprehensive representation of the research work included in chapter 6.

The high sensitivity for the PPi anion is observed in both aggregated and nonaggregate (solution) form of the chemosensor. Importantly, the PPi selectivity does not alter even in the presence of a higher concentration of other competing anions, including biologically relevant anions. Again, other phosphorus containing anions such as AMP, ADP, ATP etc. produce no change in the fluorescence emissive behavior of **L_4**. A handmade paper based test also describes the potential applicability of the **L_4** in the PPi sensing. Finally, on the basis of the nontoxic nature of the probe, the PPi-induced enhanced fluorescence emission could be garnered to ascertain inherent levels of PPi produced in live HeLa cells.

Contents

Chapter 3

Benzothiazole Functionalized Sensor for Zn(II) and $H_2PO_4^-$: Response in NIR region

Chapter 4

Benzothiazole Functionalized Sensor for Zn(II), Cd(II), PPi and $H_2PO_4^-$: Multi ion sensing platform at Physiological condition

Chapter 1

Introduction

Chapter 1

Design and synthesis of fluorescent chemosensors for sensing cations and anions

1.1 Why cations and anions are targeted?

Cations and anions are indispensable for every forms of life, as they play crucial roles in many biological and environmental process. In human body, metal ions regulate the osmotic pressure, catalysis, metabolism, biomineralization and signalling processes. The metal cofactors are essential for functioning of all nucleic acids and an estimated one-third to one-half of all proteins, including DNA and RNA polymerases contains metals.[1-2] Most biological organisms requires higher concentrations of alkali and alkaline earth metals such as sodium, potassium and calcium. They are involved in crucial biological processes such as transmission of nerve pulses, muscle contraction and regulation of cell activity etc. Apart from this, human body also contains a few transition metal ions such as iron, copper, zinc, manganese, cobalt, nickel, molybdenum, tungsten, chromium and vanadium in very lower concentrations. Iron provides the oxygen-carrying capacity of heme and acts as a cofactor in many enzymatic reactions. Zinc is an essential factor for many biological process and for some pathological process. Other transition metal ions such as mercury, lead and cadmium are toxic for living organisms, and thus their early detection in the environment is desirable.[3-5] However, the full distribution of metals used by an organism, is largely uncharacterized.

On the other hand, due to the variable sizes and shapes of anions, the anion chemistry is more challenging and infrequent to that of metal ion chemistry.[6] The phosphates ions are the central building blocks of two of the most fundamental molecules in living systems DNA and RNA; they are constituents of membrane lipids (in the form of phospholipids) and are involved in essential biological processes *viz.* energy storage, gene regulation, and signal transduction.[7-8] Moreover, phosphates are essential for medicinal drugs and fertilizers. Again, pollution from phosphates and phosphorylated compounds can cause eutrophication in the aquatic ecosystem also.[9-10] Halides play major roles both in environment and in biological process. Fluoride ion is essential for good dental health, but its overexposure (fluorosis) can have detrimental effects such as kidney failure and debilitating skeletal defects.[11] Chloride (usually from sodium chloride) is essential for good human health, it regulates blood pressure, maintains the metabolism process and the acid‑base balance within the body. The cyanide anion is toxic for mammals, it inhibits cellular respiration

by binding strongly with a heme unit of cytochrome c oxidase, inhibiting the protein from functioning and resulting fatal consequences.[12]

1.2 Advantages of fluorescence based assays

Thus the list of interesting analytes to be detected is lengthy, and consequently there is a need to develop rapid and low-cost testing methods for those analytes in areas like biology, chemical and environment. In this regard, fluorescence based sensing of analytes is the most popular technique, as it is fast, sensitive, easy to handle and do not consume the analytes. This technique is based on an interesting property known as the 'Stokes shift' which states that the position of output emission is always at higher wavelength than the excitation spectra.[13] One of the first scientific report which narrate the uses of luminescence as an analytical tool was Harvey in 1923.[14] However, chemical sensing using fluorescence to signal a molecular recognition event was first demonstrated during the early 1980s when Tsien *et al.* reported the synthesis of the first fluorescent calcium chemosensor.[15-16] Since then an enormous effort has been made for the rational design of new fluorescent sensors, and the field started to expand in various dimensions of science such as biology, analytical science, environmental science etc. However, the terminology 'chemosensor' was given in 1994 only by Czarnik as: ''A compound of abiotic origin that complexes to an analyte reversibly with a concomitant fluorescent signal transduction''.[17-18]

1.3 Receptor design and its essential properties

For designing a fluorescent chemosensor either for metal ion or for anion, it essentially requires two units- a well functionalized chelating or binding unit and one signalling unit usually a fluorophore to absorb and emit light. For chelating with metal ions, the binding unit essentially requires the presence of electronegative atoms such as N, O and S, while it is usually the NH and CH fragments from various functionalities which bind to the guest anions. The signalling unit can be attached directly to the binding unit to continue π conjugation in the system or can be separated through a suitable spacer.[19-22] The later model grows up with the strong contribution of De Silva and co-workers.

The probe detects the guest analytes through any of the four mechanisms which are discussed in section 1.4. However, to behave like a chemosensor, binding to the guest analyte must causes some change in the electron distribution of the probe. This thereby lead to two type changes in fluorescence emission spectra- i) change in intensity, commonly known as 'turn on/off' and ii) change in position of wavelength response known as 'ratiometric' approach. Again, there are various mechanisms which transformed these changes in electron distributions of the probes after binding to the guest analytes into optical output signals. Among them, PET (Photoinduced

electron transfer),[23-24] ICT (Internal charge transfer)[25-26] FRET (Forster resonant energy transfer)[27-28] and ESIPT (Excited state intramolecular proton transfer)[29] are the most common. PET process modulates the intensity of fluorescence emission, whereas ICT, ESIPT and FRET process mainly modulates the position of wavelength emission (ratiometric approach). Apart from this, in recent days, certain site selective functional groups are purposefully added to the chemosensor, to push it to a desired location inside the cells where the activity of certain ions can be visualized. Thus, along with the proper binding groups proper choices of fluorophores and sensing technique are essential for the desired photophysical behaviours of the chemosensor.

Brightness and the position of peaks in the absorption/emission spectra are the two main features of fluorescent chemosensors which need to be renovated every time. Theoretical brightness is the product of multiplication of quantum efficiency with excition coefficient and thus a measure of light efficiency.[30] A brighter chemosensor is expected to be more successful in the complex biological world when other interfering ions and molecules are also present. Many of such biomolecules can absorb and emits light in UV and visible region. Thus background signal from cellular milieu is higher when the tested chemosensor also absorb at higher energy range. Besides, after absorbing the radiation the excited molecules can interact with the oxygen molecules to form reactive oxygen species, which damages the cells. Generally, higher energy, lower wavelength light causes more damages than the longer wavelength light.[31-34] Thus, fluorescent sensors which can absorb and emits at higher wavelength are more demanding.

Water solubility and fast response time are other two important features of an ideal chemosensor. Most organic chemosensors are insoluble in water and this restricted their applicability in practical world. Thus, different functionalities and technologies are innovated to apply them in aqueous medium, uses of hydrophilic side chains and making them charged are among such techniques. However, the use of aggregation of smartly designed chemosensor molecules for sensing ions is relatively new and very interesting technique.

1.3.1 Why benzimidazole or benzothiazole?

Imidazole and its derivatives are belong to an interesting class of compounds and deserve special attention. Imidazole is amphoteric in nature and possess both anion binding as well as cation binding sites. The imidazole functionality is indispensable in human body and mostly encountered as histamine and histidine. More interestingly, active sites of most metalloproteins contain an imidazole ring from histidine residue.[35] The acidity of the NH proton of the imidazole can be tuned with suitable substitutions on imidazole ring for anion binding. Besides, such functionalities can also be charged positively to get additional assistance in anion binding and water solubility. Again

the benzimidazole functionality has portrayed its importance in vitamin B_{12} where the benzimidazole N is bonded to cobalt ion (Figure 1.1). Apart from the aforementioned properties, benzimidazole is even fluorescent active, and thus can also behave like a chromophore.

Many of the benzothiazole containing organic compounds are also used as fungicides. Benzothiazole derivatives are important in medicinal chemistry due to their potential application as anticancer, antimicrobial, anticonvulsant, antiviral, antitubercular, antimalarial, anthelmintic, analgesic, anti-inflammatory, antidiabetic, antifungal, antibacterial, antioxidant etc.[36] Based on this observation, we choose to develop fluorescent benzimidazole and benzothiazole based chemosensors for sensing cations and anions.

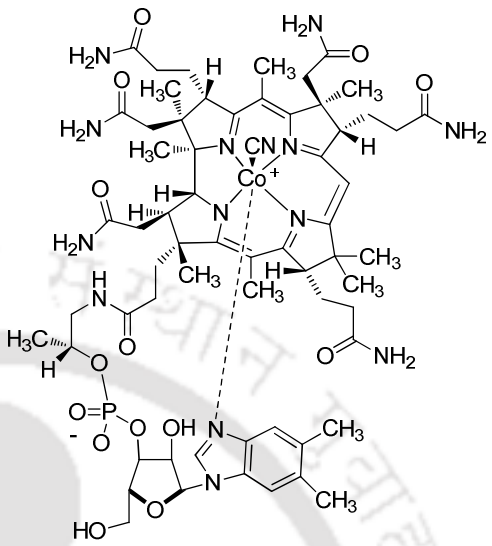

Figure 1.1 Structure of Vitamin B_{12}.

1.4 Types of reaction mechanisms in the sensing event

The host can sense the presence of the guest analyte through any of four following reactions mechanisms- 1) protonation-deprotonation, 2) complexation (including direct and displacement complexation), 3) cleavage and formation of covalent bonds and 4) redox reactions.[37] In the first type of the sensing mechanism, the sensed guest either causes protonation or deprotonation of the host, and thereby modulates the optical signals. Cations and anions can also form or rupture weak covalent bonds in a chemosensor like the case in a protection-deprotection event. Chemodosimeter is the common name to this type of probes and this interaction is completely irreversible in nature. In the last category, the probe responds to the guest via redox reactions without rupturing any bond. However, for the sake of this thesis, only the complexation based chemosensors are discussed here.

The non-covalent interactions between the host and guest is the main backbone in designing a complexation based chemosensor. This type is further divided into two sub classes known as direct complexation and competitive displacement complexation.

1.4.1 Direct complexation: In this strategy, the binding unit and the signaling unit (reporter) are covalently linked, and the resulting probes could directly form supramolecular complexes with the analyte via the following ways: coordination, electrostatic interaction, or hydrogen bonding (Scheme 1.1). Such probes are usually known for their rapid spectroscopic response and good

reversibility, which are rather suited for monitoring the dynamic changes in the analyte concentrations. Although, there are huge numbers of such chemosensors available in the literature with various functionalities, the examples which are discussed here are limited to imidazole, benzimidazole, benzoxzole and benzothiazole functionalities only.

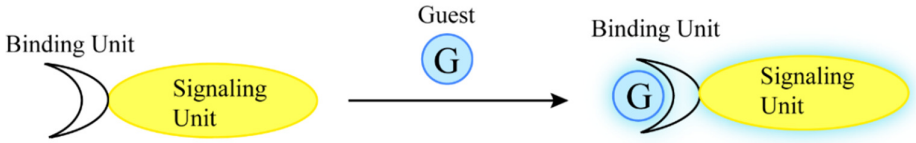

Scheme 1.1 Schematic presentation of direct complexation in sensing.

1.4.1.1 Fluorescent chemosensors for metal ions

The usual affinity of the metal ions for the electronegative atoms such as N, O and S is the key to develop such chemosensors.[38] However, for the selectivity issue, one of the following criteria is essential: (1) matchable ring/cavity size of the chemosensor for a given ion, such as crown ethers with different ring sizes for alkali and alkaline earth metal ions; (2) presence of suitable number and positions of donor atoms in the chemosensor for convenient formation of five- and six-membered ring complexes with metal ions, like the probes with EGTA (ethylene glycol tetraacetic acid) moiety for Ca^{2+}; and (3) soft–hard acid–base principle, such as the soft sulfur-containing receptors has high affinity for soft metal ions (e.g., Ag^{+} and Hg^{2+}). After the binding, the various electronic and energy transfer process just like PET, ICT and FRET signals this binding event. Here are a few examples of such chemosensors for various metal ions along with their corresponding sensing mechanisms.

A benzimidazole substituted BODIPY chemosensor **1**, shows good selectivity for Hg^{2+} ion over other heavy metal ions (HMT) both *in vivo* as well as *in vitro* (Figure 1.2).[39] In the chemosensor design, BODIPY(boron-dipyrromethene) is the main fluorophore and the benzimidazole functionality is introduced as binding site. The detection of Hg^{2+} is associated with a blue-shift in optical spectra and a simultaneous increase in the fluorescence emission intensity. This change in optical spectra is attributed to a decrease in charge delocalization upon binding to Hg^{2+}. The authors claimed that in the sensing process, two sensor molecules are bonded to a single mercury ion, where lone pairs of the benzimidazole nitrogen coordinate to the mercury ion. This thereby block the PET mechanism and resulting solution became fluorescent.

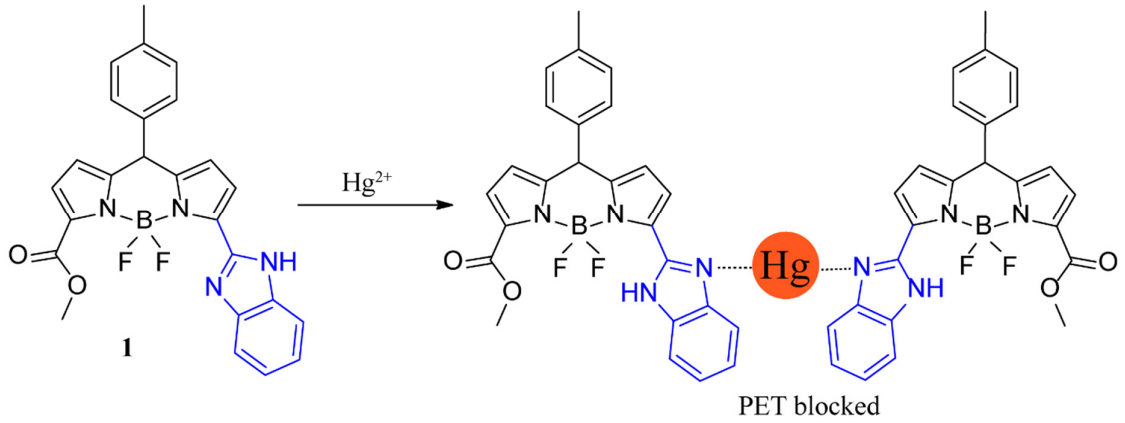

Figure 1.2 Structure of chemosensor **1** and its plausible binding mechanism.

Apart from the role of chelator for metal ion, the benzimidazole can also be used as a fluorophore. In a similar attempt, *Chuburu et.al* has modified cyclam with a benzimidazole functionality to get fluorescence assistance.[40] Now, the chemosensor (**2**) exhibits nearly 12 fold enhancement in fluorescence emission intensity after the addition of Zn^{2+} ion (Figure 1.3). The Zn^{2+} is expected to be penta coordinated and the participation of all the amine functions in the metal coordination prevents the photoinduced electron transfer (PET) effect and promotes a good chelation-enhanced fluorescence (CHEF) effect.

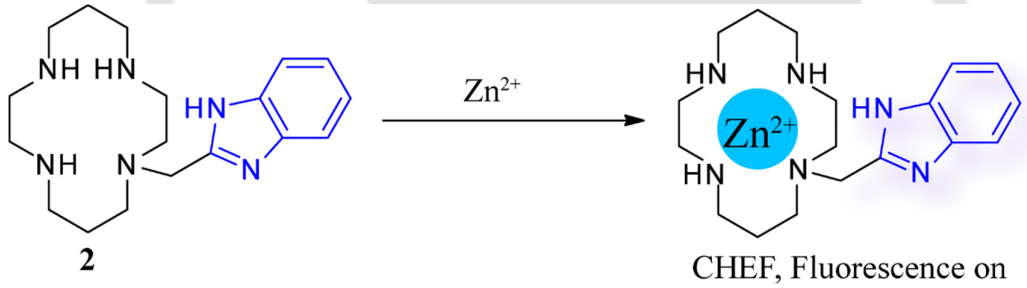

Figure 1.3 Structure of chemosensor **2** and its plausible binding mechanism.

Both the aforementioned chemosensors are 'off-on' type, and as the chemosensor **2** contains only benzimidazole functionality, its fluorescence emission response is in the UV range. However, use of rhodamine functionality in chemosensor **3** has improved its optical properties in the sensing event.[41] In the new chemosensor, benzothiazole is the binding core and the rhodamine functionality is the signalling unit. The chemosensor is selective to Hg^{2+} ion at physiological pH (Figure 1.4) and exhibits more than 1000 fold increase in fluorescence emission. Again, has been proved that the benzothiazole moiety is essential for the selective recognition of Hg^{2+} ion and it also facilitates the formation of the six-membered spirocycle, the reason for enhanced optical properties. Analysis of the single crystal of the possible intermediate suggests the coordination of the Hg^{2+} is through N atoms of the hydrazine unit and benzothiazole moiety.

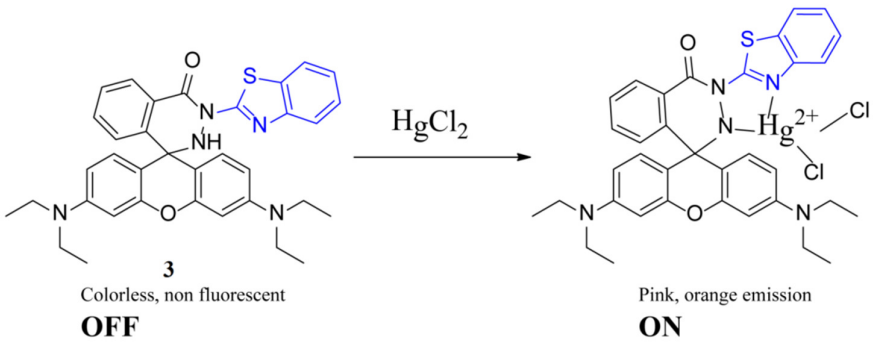

Figure 1.4 Structure of chemosensor **3** and its plausible binding mechanism.

In a more complicated signal transduction mechanism, benzimidazole functionalities are used design a rhodamine–benzimidazole conjugate (**4**), based on the resonance energy transfer from benzimidazole to a rhodamine moiety (Figure 1.5).[42] Apart from this, the benzimidazole functionalities are also the sites for metal binding. The new chemosenor is a ratiometric probe only to Cu^{2+}, and the obtained colorimetric and fluorescence emission changes are easily debatable with naked eye. In the absence of Cu^{2+}, there is minimum spectral overlap between benzimidazole emission and rhodamine absorption due to the closed spirolactam form. However, the binding of Cu^{2+} induces opening of the spirolactam ring which thereby enhances that spectral overlap resulting in enhanced fluorescence through FRET process.

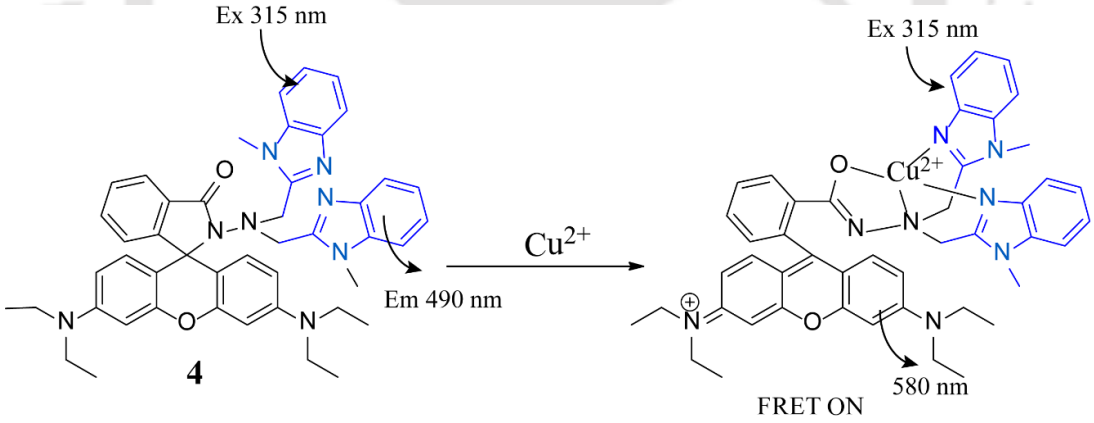

Figure 1.5 A FRET based chemosensor **4** and its plausible binding mechanism.

1.4.1.2 Chemosensors for anions

The design of chromogenic and fluorogenic probes with high sensitivity and selectivity for anions is challenging because of the strong hydration effects of anions in an aqueous system. Benzimidazole type of probes have the advantage here as they can also be charged to get the additional electrostatic assistance. Both NH and N functionalities of the imidazole/benzimidazole act as hydrogen bond donor (H donor) and acceptor (H acceptor) respectively to stabilize the host-guest complex. Apart from this, the CH of the charged imidazole/benzimidazole is also a good H

donor. A few of such chemosensors and their corresponding sensing mechanisms are discussed below.

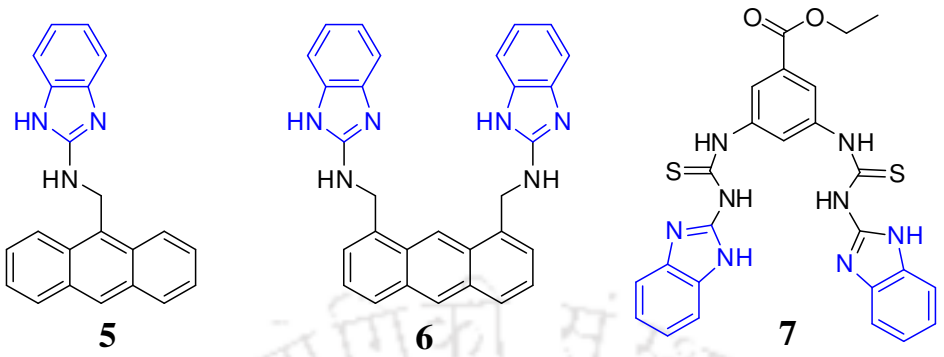

Figure 1.6 Molecular structures of PET based chemosensors **5**-**7**.

The neutral acyclic benzimidazole modified anthracene containing chemosensors **5** and **6**, are reported to recognize multiple ions through PET caused fluorescence quenching (Figure 1.6).[43] The monopodal receptor **5** display strong fluorescence emission in acetonitrile which is quenched upon addition of halides, acetate and $H_2PO_4^-$. However, chemosensor **6** with two benzimidazole functionalities, shows stronger affinity for those anions due to the participation of all four NH groups in anchoring the anion. Again, it prefers acetate over fluoride in the same experimental medium. However, a thiourea and ester modified probe **7** by the same research group has shown better selectivity even in mixed water medium.[44] The new fluorescent probe is only selective to PO_4^{3-} and again a PET process is reported to be the cause of fluorescence emission quenching. The benzimidazole core is the signaling unit in this occasion which also determines the selectivity of the chemosensor.

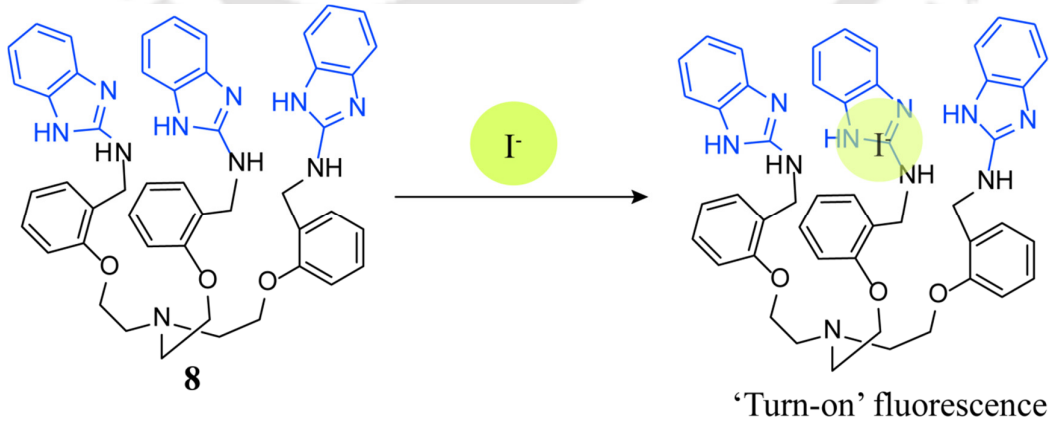

Figure 1.7 Plausible binding of I^- with the chemosensor **8**.

In an another example, a neutral benzimidazole based chemosensor **8** on a tripodal framework, shows good selectivity for iodide over other anions such as F^-, Cl^-, Br^-, HSO_4^-, NO_3^-, CH_3COO^-,

and $H_2PO_4^-$ (Figure 1.7).[45] It is a good example of benzimidazole showing dual functionalities i.e. as anion binding core and as signalling unit to report the binding event. The authors claimed that the best fitting of the iodide anion in the preorganized cavity of the molecule is the reason for iodide selectivity.

The anthracene-coupled benzimidazolium based ortho-phenylenediamine derivative **9** exhibits good selectivity towards carboxylates (Figure 1.8).[46] This cleft liked receptor design preferentially bind to $CH_3CO_2^-$, F^- and $H_2PO_4^-$ over other anions, in which both N–H---O and $(C–H)^+$---O hydrogen bonds are cooperatively recognizing the anions. However, chemosensor **10** selectively recognizes tetrabutylammonium dihydrogen phosphate in CH_3CN through quenching of anthracene emission (Figure 1.8).[47] Instead of tetrabutylammonium dihydrogen phosphate, the aqueous metahnolic solution of the probe **10** exhibit moderate fluorescence quenching with sodium salts of phosphate, hydrogen phosphate, and dihydrogen phosphate. Apart from this, chemosensor **10** also sensitive to tetrabutylammonium hydrogen sulfate in aqueous CH_3OH.

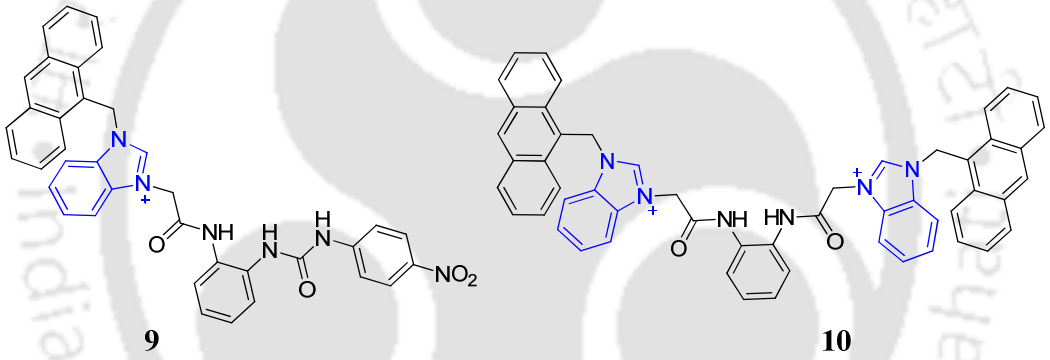

Figure 1.8 Structures of benzimidazolium based chemosensor **9** and **10**.

1.4.2 Competitive displacement complexation

In this approach, a pre-synthesized supramolecular assembly of a receptor or host (H) with a reporter (I) is made to interact with the incoming guest ion. Due to the stronger affinity of the guest ion than the reporter for the receptor, the reporter is replaced which leads to change in spectroscopic properties (Scheme 1.2)[48-52] A reporter can be metal ions or a dye molecule in most occasions. In fact, this strategy resembles to the classical complexiметric titration in analytical chemistry where different indicators or dyes are used to check the end point. The colorimetric detection of Mg^{2+} using EDTA and Eriochrome Black T is an example of competitive displacement complexation. The initially formed red coloured complex between Mg^{2+} and Eriochrome Black T (EBT), is titrated with EDTA. At the end point, the EDTA expelled the EBT due to higher stability of the resulting Mg^{2+}-EDTA complex and the free EBT turned the solution blue.

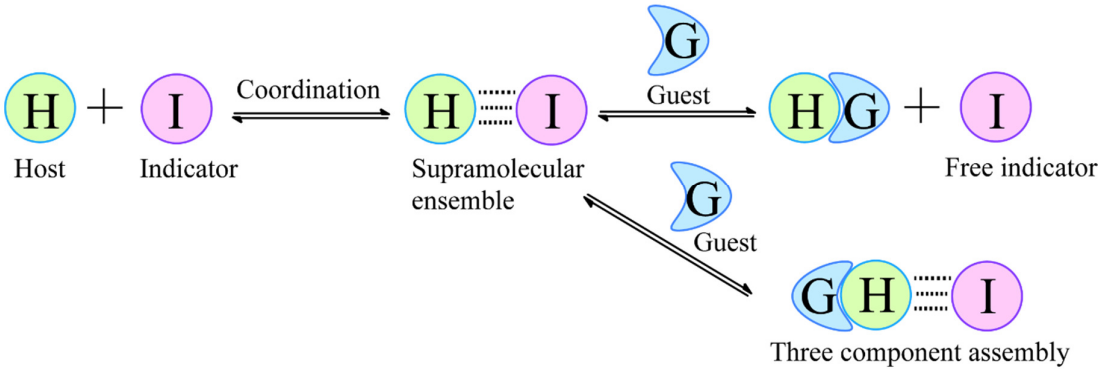

Scheme 1.2. Schematic presentation of competitive displacement complexation in sensing.

Inouye and Shinkai and their co-workers were the first to report this sensing technique around 1994.[48-49] In 1998, inspired by the antibody based biosensors in immune assays, Anslyn and co-workers had reported the sensing of citrate anion through the indicator displacement assay technique.[50] For that, the group had prepared a supramolecular ensemble of a three-guanylation-appended receptor and a fluorescein indicator and made it to interact with citrate ion. The citrate anion displaces the fluorescein from the host cavity causing it to flourish independently in solution.

Today, this approach has earned a special position in the field anion sensing with the metal–chemosensor ensemble.[51-52] As mentioned earlier, the anions are relatively bigger and have lower charge to size ratio than the metal ions, which is accountable for their higher solvation energy. Thus, the anion sensing is an intriguing task in aqueous medium. Due to the obvious affinity of the anion for a cation, a metal-chemosensor ensemble could counter this problem. The success of this technique is based on the strong bonding between the metal and guest anion causing a decomplexation procedure to signal the anion binding. This technique is also widely employed by nature to inhibit the role of metalloenzymes, like the case in alkaline phosphatases. For this reason, synthetic zinc(II) complexes are commonly got attracted towards phosphate anions. A few such examples of such metal-chemosensor ensembles functioning as secondary analytes for anions are discussed below.

In an direct instance of anion induced decomplexation, phosphate anion displaces the copper ion from an assembly of '**11**-Cu^{2+}' in mixed aqueous medium and thereby restored the fluorescence of the naked probe (Figure 1.9).[53] Other anions like F^-, Cl^-, Br^-, HSO_4^-, NO_3^-, $CH_3CO_2^-$, CN^- and ClO_4^- failed to cause decomplexation and resulted in no change in emission of the ensemble.

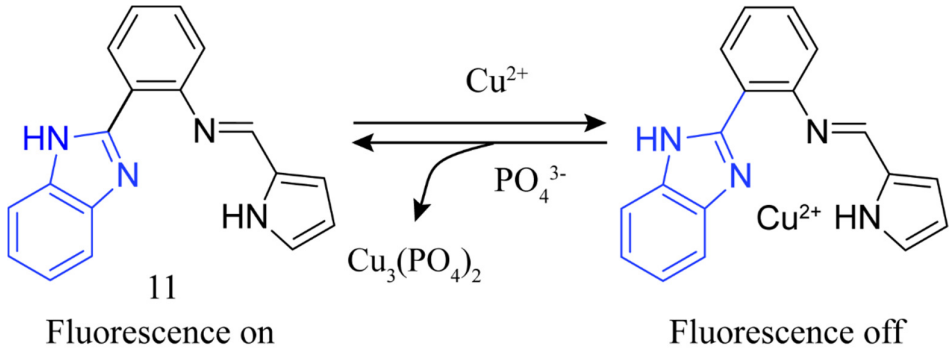

Figure 1.9 Sensing of PO_4^{3-} based on competitive displacement complexation technique.

Thus, the aforementioned chemosensor-metal ensemble responds in 'off-on' fashion to phosphate anion at the same wavelength. However, realizing the superiority of the ratiometric probes over intensity based probes, Pang *et. al.* has introduced Keto-enol tatumerism functionality in designing the chemosensor **12**. Such tatumers absorbs at different wavelengths and thereby emit at different wavelength positions in fluorescence emission spectra. In the design of the chemosensor **12** (Figure 1.10), the benzothiazole unit is deliberately substituted at 'ortho' to the phenolic OH, so that it can undergoes an excited state electron transfer phenomenon from OH to N known as ESIPT (excited state intramolecular proton transfer).[54] Thus, a Keto-enol tautomerism is possible in the excited state. In the **12**-Zn^{2+} ensemble the ESIPT is off due to bonding of oxide with Zn^{2+} ion. However, on addition of PPi, the coordination environment has changed and OH is freed to undergo ESIPT process.

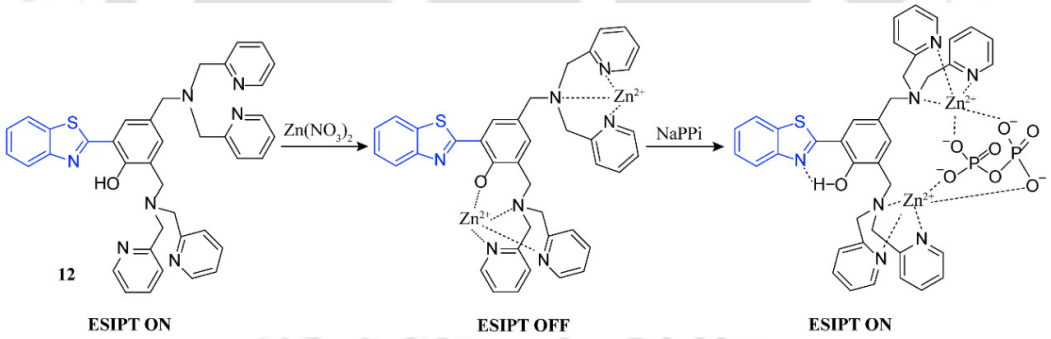

Figure 1.10 Structure of chemosensor **12** and the plausible binding mechanism in PPi sensing with the **12**-Zn^{2+} ensemble.

Relatively low cost in the synthesis yet high selectivity, sensitivity and easy handling have made small molecular chemosensors as the most attractive and widely studied species to target various hosts both *in vivo* and *in vitro*. Thus we decided to synthesize benzimidazole and benzothiazole functionalized small molecular probes for sensing cations and anions.

1.5 Aim of the thesis and future perspective

In spite of the abundant exciting properties of imidazole or similar class of compounds, they are not that common in designing chemosensors for cations and anions. Besides the amphoteric behaviour of the imidazole ring, such functionalities can also behave like a flurophore also. Thus, we aimed in designing new chemosensors with benzimidazole and benzothiazole functionalities for sensing biologically important ions. We also targeted to improve their sensitivity and selectivity, folds of fluorescence emissions in excitation and fluorescence emission spectra of the chemosensors after interacting with the guest analyte.

The impact of a NIR emissive fluorescent probe is noteworthy in the real application world. Light in the longer wavelength region like far red or NIR region (650-900 nm) possesses the advantages such as good tissue penetration, low auto-fluorescence, and biological damage, and is thus favorable for *in vivo* imaging. Therefore, design of chromogenic and fluorogenic probes for biologically important cations and anions with longer emission wavelength is our first target.

But, there are vast numbers of ions available in nature with different chemical and physiological impacts on biology, environment, defence etc. In this context, fluorescent probes which can respond to different ions through variable signal outputs are also creditable. But, selectivity is interrogated when ions of akin chemical properties are also present, like Zn^{2+} in presence of Cd^{2+}; Cd^{2+} in presence of Hg^{2+}; F^- in presence of CN^-; F^- in presence of OAc^- etc. Thus, smart designs of chemosensors to discriminate such ions in physiological medium are always demanded. For this, the probe must equipped with different binding functionalities. Our target functionality i.e. the benzothiazole possess a soft sulphur and a hard nitrogen atom, and thus a fluorescence based discrimination of some of those aforesaid ions are expected with a chemosensor functionalized with same. We are also interested in testing those chemosensors in the real biological environment.

However, the biological medium water is the main obstacle in an anion sensing event and most chemosensors are failed to exhibit the same selectivity and sensitivity as shown in organic aprotic solvents. Therefore various modifications of existing chemosensors and new techniques are developed to counter this problem, but each of them have their own limitations. A relatively new phenomena known as aggregation induced emission (AIE) might be helpful at this point as it essentially requires water or concentrated doses of the chemosensor to operate efficiently. Thus, development of benzimidazole functionalized AIE active anion chemosensor is also a target of our study.

References

1. S. J. Lippard, J. M. Berg, Principles of Bioinorganic Chemistry; University Science Books: Mill Valley, CA, 1994.
2. Biological Inorganic Chemistry, 1st ed.; Bertini, I., Gray, H. B., Stiefel, E. I., Valentine, J. S., Eds.; University Science Books: Sausalito, CA, 2007.
3. Biological Inorganic Chemistry, 1st ed.; I. Bertini, H. B. Gray, E. I. Stiefel and J. S. Valentine, Eds.; University Science Books: Sausalito, CA, 2007.
4. C. L. Dupont, S. Yang, B. Palenik and P. E. Bourne, *Proc. Natl. Acad. Sci. U.S.A*., 2006, **103**, 17822-17827.
5. V. N. Gladyshev and Y. Zhang, *Met. Ions Life Sci.*, 2013, **12**, 529-580.
6. J. W. Steed and J. L. Atwood, Cation-Binding Hosts in Supramolecular Chemistry, John Wiley & Sons, Ltd, Chichester, 2nd edn, 2009.
7. A. T. Aron, K. M. Ramos-Torres, J. A. Cotruvo, Jr. and Christopher J. Chang, *Acc. Chem. Res.*, 2015, **48**, 2434–2442.
8. A. E. Hargrove, S. Nieto, T. Zhang, J. L. Sessler and E. V. Anslyn; *Chem. Rev*., 2011, **111**, 6603–6782.
9. Phosphorus in the Global Environment: Transfers, Cycles, and Management; Wiley: New York, 1995.
10. C. F. Mason, Biology of Freshwater Pollution; Longman: New York, 1991.
11. L. S. Kaminsky, M. C. Mahoney, J. Leach, J. Melius and M. J. Miller, *Oral Biol. Med*., 1990, **1**, 261–281.
12. M. A. Holland and L. M. Kozlowski, *Clin. Pharm*., 1986, **5**, 737-741.
13. G. G. Stokes, *Philos. Trans. R. Soc. London*, 1852, **142**, 463–562
14. E. N. Harvey, *Science*, 1923, **57**, 501–503
15. R. Y. Tsien, *Biochemistry*, 1980, **19**, 2396-2404.
16. G. Grynkiewicz, M. Poenie and R. Y. Tsien, *J. Biol. Chem*., 1985, **260**, 3440-3450.
17. J. P. Desvergne and A. W. Czarnik., Chemosensors of Ion and Molecule Recognition (NATO Science Series, Serie C: Mathematical and Physical Sciences), Kluwer Academic, London, 1997.
18. Fluorescent Chemosensors for Ion and Molecule Recognition, American Chemical Society, Washington DC, 1993, 538.
19. R. P. Haugland, The Handbook: A Guide to Fluorescent Probes and Labelling Technologies, 10th ed.; Molecular Probes: Eugene, OR, 2005.
20. X. Chen, M. Sun and H. M. Ma, *Curr. Org. Chem*., 2006, **10**, 477-489.
21. Fluorescent Chemosensors for Ion and Molecule Recognition, American Chemical Society, Washington DC, 1993, 538.
22. W. Shi and H. M. Ma, *Chem. Commun*., 2012, **48**, 8732-8744.
23. A. P. de Silva, H. Q. N. Gunaratne, T. Gunnlaugsson, A. J. M. Huxley, C. P. McCoy, J. T. Rademacher and T. E. Rice, *Chem. Rev.*, 1997, **97**, 1515-1566.
24. R. A. Bissell, A. P. de Silva, H. Q. N. Gunaratne, P. L. M. Lynch, G. E. M. Maguire and K. R. A. S. Sandanayake, *Chem. Soc. Rev*., 1992, **21**, 187-195.
25. B. Valeur and I. Leray, *Coord. Chem. Rev.*, 2000, **205**, 3-40.
26. M. Yuan, Y. Li, J. Li, X. Liu, J. Lv, J. Xu, H. Liu, S. Wang and D. Zhu, *Org. Lett.*, 2007, **9**, 2313-2316.
27. J. Wu, W. Liu, J. Ge, H. Zhang and P. Wang, *Chem. Soc. Rev*., 2011, **40**, 3483-3495.
28. A. P. Demchenko, K.-C. Tang and P.-T. Chou, *Chem. Soc. Rev*., 2013, **42**, 1379-1408.
29. A. Douhal, F. Lahmani, A. H. Zewail, *Chem. Phys.*, 1996, **207**, 477–498.
30. N. C. Shaner, P. A. Steinbach and R. Y. Tsien, *Nat. Methods* 2005, **2**, 905-909.
31. A. Grzelak, B. Rychlik and G. Bartosz, *Free Radical Biol. Med.*, 2001, **30**, 1418-1425.
32. R. A. Hoebe, C. H. Van Oven, T. W. J. Gadella Jr, P. B. Dhonukshe, C. J. F. Van Noorden, E. M. Manders, *Nat. Biotechnol*., 2007, **25**, 249-253.
33. B. F. Godley, F. A. Shamsi, F. Q. Liang, S. G. Jarrett, S. Davies and M. Boulton, *J. Biol. Chem*., 2005, **280**, 21061-21066.
34. J. E. Aubin, *J. Histochem. Cytochem*., 1979, **27**, 36-43.
35. I. Bertini, A. Sigel and H. Sigel, Handbook on Metalloproteins, Marcel and Dekker, New York, 2001.
36. R. S. Keri, M. R. Patil, S. A. Patil and S. Budagumpi, Eur. J. Med. Chem. 2015, 89, 207-251.
37. X. Li, X. Gao, W. Shi and H. Ma, *Chem. Rev*., 2014, **114**, 590-659.
38. J. F. Callan, A. P. de Silva, D. C. Magri, *Tetrahedron,* 2005, **61**, 8551-8588.
39. S, Madhu, D, K, Sharma, S, K, Basu, S. Jadhav, A. Chowdhury and M. Ravikanth, *Inorg. Chem*., 2013, **52**, 11136-11145.
40. A. E. Majzoub, C. Cadiou, I. D.-Olivier, B. Tinant and F. Chuburu, *Inorg. Chem*., 2011, **50**, 4029-4038.

41. Z. Yang, L. Hao, B. Yin, M. She, M. Obst, A. Kappler and J. Li, *Org. letters*., 2013, **15**, 4334-4337.
42. S. Goswami, S. Maity, A. C. Maity, A. K. Maity, A. K. Das and P. Saha, *RSC Adv*., 2014, **4**, 6300-6305.
43. J. Kang, H. S. Kim and D. O. Jang, *Tet. Let.*, 2005, **46**, 6079-6082.
44. G. W. Lee, N. Singh and D. O. Jang, *Tet. Let.*, 2008, **49**, 1952-1956.
45. N. Singh and D. O. Jang, *Org. Lett*., 2007, **9**, 1991-1994.
46. K. Ghosh and I. Saha, *Tet. Let*., 2008, **49**, 4591-4595.
47. K. Ghosh, I. Saha and A. Patra, *Tet. Let.*, 2009, **50**, 2392-2397.
48. M. Inouye, K. I. Hashimoto and K. Isagawa, *J. Am. Chem. Soc*., 1994, **116**, 5517-5518.
49. K. N. Koh, K. Araki, A. Ikeda, H. Otsuka and S. Shinkai, *J. Am. Chem. Soc*., 1996, **118**, 755-758.
50. A. Metzger and E. V. Anslyn, *Angew. Chem., Int. Ed.,* 1998, **37**, 649-652.
51. X. Lou, D. Ou, Q. Li and Z. Li, *Chem. Commun*., 2012, **48**, 8462-8477.
52. J. Wu, B. Kwon, W. Liu, E. V. Anslyn, P. Wang and J. S. Kim, *Chem. Rev*., 2015, **115**, 7893-7943.
53. P. Saluja, N. Kaur, N. Singh and D. O. Jang, *Tet. Let.*, 2012, **53**, 3292–3295.
54. J. Wang, X. Liua and Y. Pang, *J. Mater. Chem. B*, 2014, **2**, 6634-6638.

Chapter 2

Materials and Methods

Chapter 2

This chapter deals with the generalized materials and methodology followed to synthesize and characterize the probes. It also describes the general equipments and different experimental set ups/calculations used to study the interaction with different cations and anions.

2.1 General Information and Materials.

All the materials used for synthesis are purchased from commercial suppliers. The absorption spectra are recorded on a Perkin-Elmer Lamda-750 UV-Vis spectrophotometer using 10 mm path length quartz cuvettes in the range 250-700 nm wavelength, while fluorescence measurements are conducted on a Horiba Fluoromax-4 spectrofluorometer using 10 mm path length quartz cuvettes at 298 K. Mass spectra of the probes are obtained using Waters Q-ToF Premier mass spectrometer. NMR spectra are recorded on a Varian FT-400 MHz instrument as well as on a BRUKER-600 MHz and the chemical shifts are presented in parts per million (ppm) on the scale. The following abbreviations are used to describe spin multiplicities in ^{1}H NMR spectra: s = singlet; d = doublet; t = triplet; m = multiplet. IR spectra are recorded on a Perkin Elmer-Spectrum One FT-IR spectrometer with KBr disks in the range 4000-450 cm^{-1}.

2.2 Synthesis and characterization of the compounds

2.2.1 Synthesis of L_1 [(E)-2-(2-(11H-indeno[1,2-b]quinoxalin-11-ylidene)hydrazinyl)benzo[d] thiazole]:

Room temperature stirring of ninhydrin (1.02 mmol) and o-phenylene diamine (1.5 mmol) in methanol with few drops of concentrated sulphuric acid for 3 hours give a flappy orange like precipitate (**L**, **Scheme 3.1**). To the solution of **L** (1.02 mmol) in ethanol, 2-hydrazinobenzothiazole (1.5 mmol) and few drops of concentrated sulphuric acid are added. The resulting solution is stirred for 4 hours at room temperature. It give an orange red type precipitate which then filtered and wash with ethanol and finally with water to give pure $\mathbf{L_1}$. Yield = 70%; ^{1}H NMR (400 MHz, $CDCl_3$, TMS): 13.471(s, 1H), 8.250(d, 1H), 8.151(t, 2H), 7.992(d, 1H), 7.781(m, 4H), 7.568(m, 2H), 7.419(t, 1H), 7.254(d, 1H). ^{13}C: 166.872, 153.509, 151.984, 147.317, 141.952, 140.411, 138.082, 137.558, 135.077, 131.950, 131.609, 130.865, 130.395, 129.803, 129.727, 129.660, 126.297, 123.231, 122.457, 121.357, 120.742, 94.653. ESI-MS: m/z Calculated for $C_{22}H_{13}N_5S$ [$\mathbf{L_1}$] = 379.04, found [$\mathbf{L_1} + H^+$] = 380.1019.

2.2.2 Synthesis of L_{1C} [(E)-11-(2-phenylhydrazono)-11H-indeno[1,2-b]quinoxaline] :

Similarly condensation of **L** (1.02 mmol) with phenyl hydrazine (1.5 mmol) with a few drops of concentrated sulphuric acid in ethanol give $\mathbf{L_{1C}}$. Yield = 75 %.

^{1}H NMR (400 MHz, $CDCl_3$, TMS): 12.874(s, 1H), 8.180(d, 1H), 8.139(m, 2H), 7.795(d, 1H), 7.7541(m, 4H), 7.561(t, 2H), 7.480(t, 1H), 7.060(t, 1H), ^{13}C: 1153.212, 147.645, 143.511, 141.437, 140.583, 140.011, 132.476, 131.851, 129.921, 129.822, 129.647, 129.365, 129.304, 128.495, 122.455, 120.350, 114.173, 66.058. ESI-MS: m/z Calculated for $C_{21}H_{14}N_4$ [**L1C**] = 322.12, found [**L1C** + H^+] = 323.1382.

2.2.3 Synthesis of L2 [(E)-1-((2-(benzo[d]thiazol-2-yl)hydrazono)methyl)naphthalen-2-ol]:

The synthesis of the **L2** and **L2C** are described in **Scheme 4.1**. 2-hydrazinobenzothiazole (165 mg, 1 mmol) and 2-hydroxyl-1-naphthaldehyde (172 mg, 1 mmol) are dissolved in 20 mL of ethanol and refluxed for 6 hr. The pale yellow type precipitate is then filtered and wash with cold ethanol to give pure form of **L2** with 84% yield.

^{1}H NMR [400 MHz, $CDCl_3$, $SiMe_4$, δ(ppm)]: 12.391 (1H, s), 9.288 (1H, s), 8.122-8.101 (1H, d), 7.798-7.776 (2H, t), 7.537–7.492 (2H, m), 7.383-7.346 (2H, m), 7.281-7.239 (3H, m), 7.101-7.061 (1H, t), 6.22 (1H, d), 3.28 (8H, q), 1.11 (12H, t). ^{13}C NMR [100 MHz, $CDCl_3$, $SiMe_4$, δ (ppm)]: 166.275, 158.352, 148.514, 132.094, 131.972, 128.967, 128.174, 127.236, 126.344, 125.551, 123.331, 121.760, 121.692, 120.220, 118.977, 113.737, 108.994. ESI-MS (positive mode, m/z): Calculated for $C_{18}H_{13}N_3OS$: 319.0799. Found: 320.08586. (**L2** + H^+) IR analysis: 3445 cm^{-1} (broad, -OH), 1627cm^{-1} (sharp, -C=N).

2.2.4 Synthesis of L2C [(E)-2-(2-(naphthalen-1-ylmethylene)hydrazinyl)benzo[d]thiazole]:

Synthesis of **L2C** is similar to that of **L2**. 2-hydrazinobenzothiazole is refluxed with 1-naphthaldehyde for 6 hours. It give a yellowish type precipitate which is then washed with cold ethanol to give pure **L2C** with 70% yield.

^{1}H NMR [600 MHz, $CDCl_3$, $SiMe_4$, δ (ppm)]: 8.836-8.822 (1H, d), 8.703 (1H, s), 7.904-7.871 (3H, t), 7.681-7.668 (1H, d), 7.623–7.610 (1H, t), 7.560-7.508 (3H, m), 7.341-7.321 (1H, t), 7.144-7.140 (1H, t). ^{13}C NMR [100 MHz, $CDCl_3$, SiMe4, δ (ppm)]: 133.178, 129.731, 129.327, 128.991, 128.053, 126.856, 126.444, 125.445, 125.148, 124.721, 123.904, 120.991, 120.480, 117.209. ESI-MS (positive mode, m/z): Calculated for $C_{18}H_{13}N_3S$: 303.08. Found: 304.098. (**L2c** + H^+). IR analysis: 1614 cm^{-1} (sharp, -C=N)

2.2.5 Synthesis of L3 [2,6-bis((E)-(2-(benzo[d]thiazol-2-yl)hydrazono)methyl)-4-methylphenol]:

Condensation of freshly prepared 2,6-Diformyl-4-methylphenol[1] with 2-hydrazinobenzothiazole for 4 hours yielded a yellowish precipitate, which is then filtered and washed with cold methanol to obtain pure **L3** (**Scheme 5.1**). % Yield = 85.

^{1}H NMR of **L3** (400 MHz, DMSO-d_6): 12.267 (bs, 1H), 8.484 (s, 2H), 7.727-7.753 (d, 2H), 7.561 (s, 2H), 7.354-7.229 (m, 4H), 7.128-7.091 (t, 2H), 2.319 (s, 3H). ^{13}C NMR (600 MHz):

166.58, 153.78, 133.41, 128.43, 126.28, 121.92, 121.66, 120.16, 20.12. ESI-MS (positive mode, m/z) Calculated [$\mathbf{L_3}$ + H^+] = 459.1062, found mass: 459.1042.

2.2.6 Synthesis of $\mathbf{L_{3C}}$ [2,2'-((2E,2'E)-2,2'-((5-methyl-1,3-phenylene)bis(methanylylidene))bis (hydrazin-1-yl-2-ylidene))bis(benzo[d]thiazole]:

Similarly, condensation of 2,6-Diformyl-benzene with 2-hydrazinobenzothiazole for 4 hours gives gave a yellowish type precipitate of $\mathbf{L_{3C}}$. % Yield = 80.

^{1}H NMR of $\mathbf{L_{3C}}$ (400 MHz, DMSO-d_6): 12.353(bs, 1H), 8.181(s, 2H), 7.981(s, 1H), 7.801-7.603 (m, 4H), 7.528-7.454 (m, 3H), 7.310 (t, 2H), 7.125 (t, 2H). ^{13}C NMR: 167.180, 134.94, 129.12, 127.386, 126.059, 124.125, 121.765, 120.94. ESI-MS (positive mode, m/z) Calculated [$\mathbf{L_{3C}}$ + H^+] = 429.1004, found mass: 429.0948.

2.2.7 Synthesis of $\mathbf{L_4}$ [2,6-bis-((4-(1H-benzo[d]imidazol-2-yl)phenyl)imino) methyl)-4 methyl phenol] :

Condensation of 2,6-Diformyl-4-methylphenol with 4-(1H-benzo[d]imidazol-2-yl)aniline for 4 hours forms a reddish type precipitate, which is then purified with column chromatography to obtain pure $\mathbf{L_4}$ (**Scheme 6.1**). The chemical structure is fully characterized with ^{1}H NMR, ^{13}C NMR and mass analysis.

^{1}H NMR of $\mathbf{L_4}$ (400 MHz, DMSO-d_6): 10.216 (s, 2H), 8.008(d, 4H), 7.851-7.818 (s, 2H), 7.764-7.710(m, 2H), 7.472(d, 2H), 6.769(s, 4H), 2.332 (s, 3H). ^{13}C NMR: 192.25, 154.09, 149.81, 137.30, 131.47, 129.85, 128.81, 125.15, 1253.34, 122.55, 113.63, 113.11, 107.93, 19.55. ESI-MS (positive mode, m/z) Calculated [$\mathbf{L_4}$ + H^+] = 459.1062, found mass: 459.1042.

2.3 X-Ray crystallography

The intensity data are collected using a Bruker SMART APEXII CCD diffractometer, equipped with a fine focus 1.75 kW sealed tube Mo-Kα radiation (λ = 0.71073 Å) at 298(2) K, with increasing ω (width of 0.3° per frame) at a scan speed of 3 s per frame. The SMART software is used for data acquisition. Data integration and reduction are undertaken with SAINT and XPREP[2] software. Multi-scan empirical absorption corrections are applied to the data using the program SADABS.[3] Structures are solved by direct methods using SHELXS-97 and are refined by full-matrix least squares on F2 using SHELXL-97 program package.[4] In the crystal structure, non-hydrogen atoms are refined anisotropically. Hydrogen atoms attached to all carbon atoms are geometrically fixed. Structural illustrations have been generated using MERCURY 3.0 for Windows.[5] Crystal data, as well as details of data collection and refinement for $\mathbf{L_1}$ are summarized below.

2.4 UV–Vis and Fluorescence Spectral Studies

Stock solutions of various ions (1×10^{-3} M) are prepared in deionized water. Perchlorate or nitrate salts are used for metal ions while tetrabutyl/tetraethyl or sodium salts of the corresponding anions and nucleotides are used for the preparation of anion stock solutions. The stock solution of $\mathbf{L_{1\text{-}4}}$ and $\mathbf{L_{1C\text{-}3C}}$ (5×10^{-3} M) are prepared in DMSO. For the titration experiments, a 1×10^{-3} M solution of the chemosensor taken in a quartz optical cell of 1 cm optical path length is titrated with incremental concentration of cation/anion stock solutions in the experimental medium. For the competitive selectivity experiment, fluorescence emission of the 'chemosensor-sensed guest' ensemble is collected in the absence and presence of the competitive ions in excess (10 equivalent).

2.5 Evaluation of the Apparent Binding Constant

Chemosensor $\mathbf{L_{1\text{-}4}}$ with an effective concentration of 10.0×10^{-6} M is used for the emission titration studies with the sensed guest ions.

Chemosensor $\mathbf{L_1}$ with an effective concentration of 10 μM in an acetonitrile is used for the emission titration studies with a Zn^{2+} solution. A stock solution of $Zn(ClO_4)_2$, having a concentration of 0.2 mM in an acetonitrilesolution is used. The effective Zn^{2+} concentration is varied between 0 and 60 μM for this titration.

The basic equation (1) for determination of the ligand-metal complexation is:

$$D + nM = C \qquad (1)$$

Where D is the ligand molecule; M is the metal ion, and C is the complex.

The binding constant K of the metal complex is determined by equation (2), assuming the concentration of free metal is about equal to its total concentration ($[M] \approx [M]_t$),[6-8]

$$(F\text{-}F_0)/(F\text{-}F_m) = [C]/[D] = K[M]^n \qquad (2)$$

Where F_0, F, and F_m are the corrected fluorescence emission intensity (λ = 654 nm) of the complex at initial, interval t, and the final state at which the complex is fully formed upon addition of metal ion, respectively. The binding constant K is determined from the plot of the linear regression of $\log[(F\text{-}F_0)/(F_m\text{-}F)]$ vs. log[M] in equation (3), derived from equation (2), to obtain the intercept as log K and the slope as n.

$$\text{Log } [(F\text{-}F_0)/(F\text{-}F_m)] = \log K + n \log[M] \qquad (3)$$

In case of $\mathbf{L_2}$, $\mathbf{L_3}$ and $\mathbf{L_4}$, the apparent binding constants for the formation of respective Host-guest complexes are calculated using equation 4 (Benesi Hildebrand equation).[6]

$$1/(I-I_0) = 1/\{K(I_{max}-I_0)C\} + 1/(I_{max}-I_0) \quad (4)$$

I_0 is the fluorescence emission intensity of the host at emission maximum (λ_{max}), I is the observed emission at that particular wavelength in the presence of a certain concentration of the analyte (C), I_{max} is the maximum emission value that is obtained at λ_{max} during titration with varying analyte concentration, K is the apparent binding constant (M^{-1}) and is determined from the slope of the linear plot. Similarly, the binding constants for the anions are also calculated using equation 4.

2.6 Finding the Detection Limit

The detection limits are calculated on the basis of the fluorescence titrations data. The fluorescence emission spectrum of the blank chemosensor (**L_{1-4}**) is measured 10 times, and the standard deviation of blank measurement iss achieved. To gain the slope, the ratio of the fluorescence emission at λ_{max} is plotted as a concentration of corresponding guest ion.

So the detection limit is calculated with the following equation

$$\text{Detection limit} = 3\sigma/k \quad (5)$$

where σ is the standard deviation of blank measurement, and k is the slope between the ratio of fluorescence emission versus respective analyte concentration.

Similarly, the detection limits for the sensed anions are also calculated using the 5, where σ is the standard devaiation of chemosensor (**L_{2-3}**)-metal ensembles and k is the slope between the ratio of fluorescence emission versus respective anions concentrations.

2.7 Sensing of Zn(II) in Physiological Milieu

To investigate the potential of **L_3** as a probe for intracellular detection of Zn^{2+}, the subsequent endeavour is to study its interaction in milieu replicating the conditions relevant in an *in vitro* system. To that end, two proteins are chosen, bovine serum albumin (BSA) and human serum albumin (HSA), and the interaction study between **L_3** and Zn^{2+} is studied. Stock solutions of the proteins are prepared at a final concentration of 4 mg/mL. Proteins are then titrated from the stock solution in a cuvette with preformed **L_3**-Zn^{2+} complex. To further validate the biological importance of **L_3**, the interaction of **L_3** with Zn^{2+} is also studied in simulated body fluid (SBF), whose ionic composition is similar to that of human extracellular fluid. SBF is prepared as reported previously.[9]

2.8 Cytotoxic Effect of L_3, L_3-Zn^{2+} and L_3-Zn^{2+}-PPi Ensemble

The cytotoxic effect of **L_3** and **L_3**.Zn^{2+} complex and **L_3**-Zn^{2+}-PPi ensemble on HeLa cells (human cervical carcinoma cells) are determined by an MTT assay as per the manufacturer instruction (Sigma-Aldrich, MO, USA). HeLa cells are initially cultured in a 25 cm^2 tissue culture flask in DMEM medium supplemented with 10% (v/v) FBS, penicillin (100 μg mL^{-1}) and streptomycin (100 μg mL^{-1}) under a humidified atmosphere of 5% CO_2 until the cells are approximately 90% confluent. Prior to MTT assay, cells are passaged and seeded into 96 well tissue culture plates at a cell density of 10^4 cells per well and incubated with varying concentrations of **L_3**, **L_3**-Zn^{2+} complex, **L_3**-Zn^{2+}-PPi ensemble, Zn^{2+} and PPi solution (15, 30, 60, 90 and 120 μM) and incubated for a period of 24 h under 5% CO_2. Following incubation, the growth media is carefully aspirated, and fresh DMEM containing MTT solution is added to the wells. The plate is incubated for 4 h at 37°C. Subsequently, the supernatant is collected and the insoluble colored formazan product is solubilized in DMSO and its absorbance is measured in a microtiter plate reader (Infinite M200, TECAN, Switzerland) at 550 nm. The assay is performed in six sets for each concentration of the test samples. Data analysis and determination of standard deviation is performed with Microsoft Excel 2013 (Microsoft Corporation). In the MTT assay, the absorbance for the control cells (solvent control) is considered as 100% cell viability and the absorbance for the treated cells are compared to determine % cell viability with respect to the solvent control.

2.9 Detection of Intracellular Zn^{2+} and PPi by Imaging

HeLa cells are initially cultured in a 25 cm^2 tissue culture flask containing DMEM medium supplemented with 10% FBS, penicillin (100 μg mL^{-1}) and streptomycin (100 μg mL^{-1}) in a CO_2 incubator. Prior to imaging studies, HeLa cells are seeded into a 6 well plate and grown in DMEM medium at 37°C till 80% confluency. Subsequently, the cells are washed thrice with sterile phosphate buffered saline (PBS), incubated with 15 μM **L_3** in DMEM at 37°C for 1 hour in a CO_2 incubator and their images are acquired using a fluorescence microscope (Eclipse Ti-U, Nikon, USA) with a filter that allowed green light emission. The cells are further wash with sterile PBS in order to remove excess **L_3** and then incubated for 1 hour with 30 μM $Zn(ClO_4)_2$ prepared in sterile PBS. The images of the cells are acquired with a fluorescence microscope. The cells are subsequently wash with sterile PBS and then incubated further with 30 μM PPi for 1 hour. Following incubation, the images of the cells are again acquired with a fluorescence microscope as mentioned earlier.

2.10 Dynamic light scattering studies. The particle size of the **L_4**-PPi aggregates is measured by dynamic light scattering (DLS) experiments on a Malvern Zetasizer Nano ZS instrument

equipped with a 4.0 mW He–Ne laser operating at a wavelength of 633 nm. The samples and the background are measured at room temperature (25° C) at a scattering angle of 173°. DLS experiments are carried out with an optically clear solution of **L4** (10 μM) in water in the presence of 10 equivalents of PPi ion. The solution is equilibrated for 30 minutes prior to taking the measurements.

2.11 Atomic Force Microscope (AFM) Studies. Glass cover slips (18 mm x 18 mm) are sterilized by immersion in sodium hypochlorite solution (0.5%) for 2 hours and rinsed thoroughly with sterile MilliQ grade water. To study the aggregation effect of **L4**, to a solution of **L4** (10 μM) in aqueous medium, 10 equivalents of PPi is added and mixed well. The mixture is then drop-casted on a glass cover slip followed by dessication prior to acquiring AFM images. Atomic force microscope images are captured with an Agilent 5500 AFM (Agilent Technologies, Chandler, AZ, USA). Cantilevers made of silicon nitride are used having a resonant frequency of ca. 150 to 250 kHz. Images are acquired in non-contact mode, with 10 μm x 10 μm size at a scan rate of 0.5- 1.0 line/s. Analysis of the topographic images of the surface is accomplished by using the WSxM v5.0 Develop 6.5 image viewer software.

2.12 Field Emission Scanning Electron Microscope (FESEM) Studies. FESEM imaging studies are conducted separately with (i) an aqueous solution of **L4** (10 μM) and (ii) an aqueous solution of **L4** (10 μM) mixed with 10 equivalents of PPi. The solutions are then drop-casted on a cover slip, followed by dessication prior to acquiring images in a field emission scanning electron microscope (Zeiss Sigma, USA).

2.13 Cytotoxic Effect on HeLa Cells. The cytotoxic effect of the probe and **L4**-PPi complex on cultured HeLa cells is determined by an MTT assay as per the manufacturer instruction (Sigma-Aldrich, MO, USA). HeLa cells are initially grown in a 25 cm^2 tissue culture flask in DMEM medium supplemented with 10% (v/v) FBS, penicillin (100 μg/mL) and streptomycin (100 μg/mL) under a humidified atmosphere of 5% CO_2 in an incubator until the cells are approximately 90% confluent. Prior to MTT assay, cells are trypsinized and seeded into 96 well tissue culture plates at a cell-density of 10^4 cells per well and incubated with varying concentrations (10, 20, 30, 40, 50 and 60 μM) of the probe, probe-PPi complex and the metal salt solution made in methanol solvent (0.1% v/v) and incubated for a period of 24 hours under 5% CO_2. Solvent control samples (cells incubated in 0.1% methanol) are also included in parallel sets. Following incubation, the growth media is carefully aspirated, and fresh DMEM containing MTT solution is added to the wells. The plate is incubated for 4 hours at 37° C. Following incubation, the supernatant is collected and the insoluble colored formazan product is

solubilized in DMSO and its absorbance is measured in a microtiter plate reader (Infinite M200, TECAN, Switzerland) at 550 nm. The assay is performed in six sets for each concentration of the test samples. Data analysis and determination of standard deviation is performed with Microsoft Excel 2010 (Microsoft Corporation). In the MTT assay, the absorbance for the solvent control cells is considered as 100% cell viability and the absorbance for the treated cells is compared to determine % cell viability with respect to the solvent control.

References

1. L. F. Lindoy, G. V. Meehan and N. Svenstrup, *Synthesis*, 1998, 7, 1029.
2. Saint, Smart and XPREP, Siemens Analytical X-ray Instruments Inc., Madison, Wisconsin, USA, 1995.
3. G. M. Sheldrick, SADABS: Software for Empirical Absorption Correction, University of Gottingen, Institute fur Anorganische Chemieder Universitat, Tammanstrasse 4, D-3400 Gottingen, Germany, 1999–2003.
4. G. M. Sheldrick, SHELXS-97, University of Gottingen, Germany, 1997; G. M. Sheldrick, SHELXL-97, Program for Crystal Structure Refinement; University of Gottingen, Germany, 1997.
5. Mercury 2.3, Supplied with Cambridge Structural Database; CCDC, Cambridge, U.K., 2007.
6. H. A. Benesi and J. H. Hildebrand, *J. Am. Chem. Soc*., 1949, **71**, 2703-2707.
7. K. A. Connors, Binding Constants; John Wiley & Sons: New York; 1987, 339.
8. B. Valeur, Molecular Fluorescence; Wiley-VCH: Weinheim; 2000, 339.
9. A. Oyane, H. M. Kim, T. Furuya, T. Kokubo, T. Miyazaki and T. Nakamura, *J. Biomed. Mater. Res*., 2003, **65**, 188-195.

Appendix 1

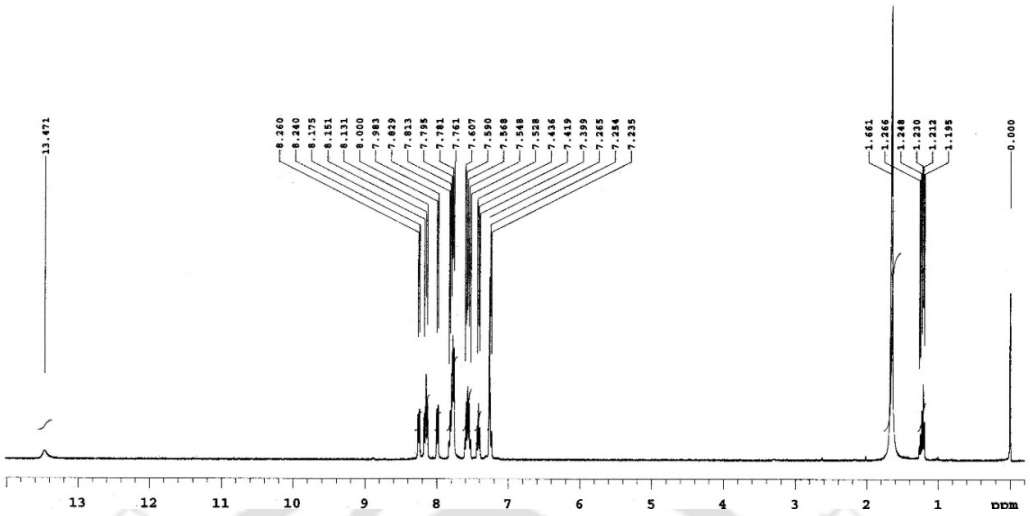

Figure A2.1 ^{1}H NMR of $\mathbf{L_1}$ in $CDCl_3$ solution at room temperature.

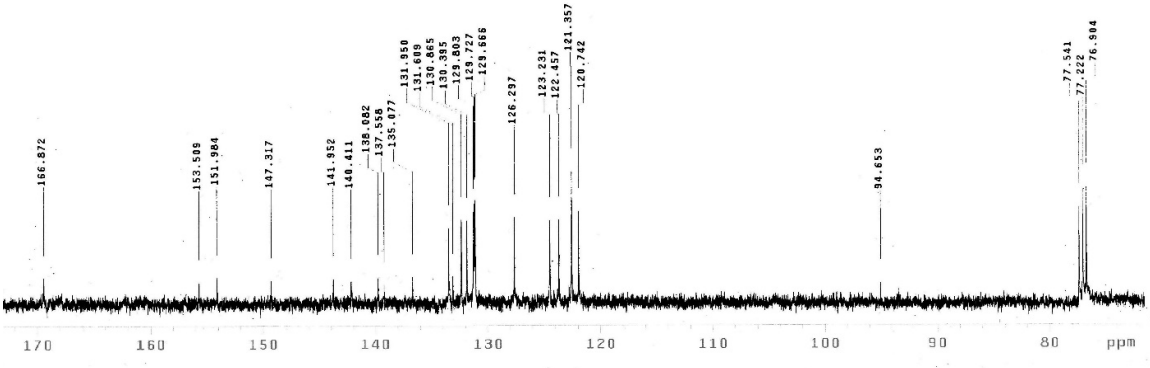

Figure A2.2 ^{13}C NMR of $\mathbf{L_1}$ in $CDCl_3$ solution at room temperature.

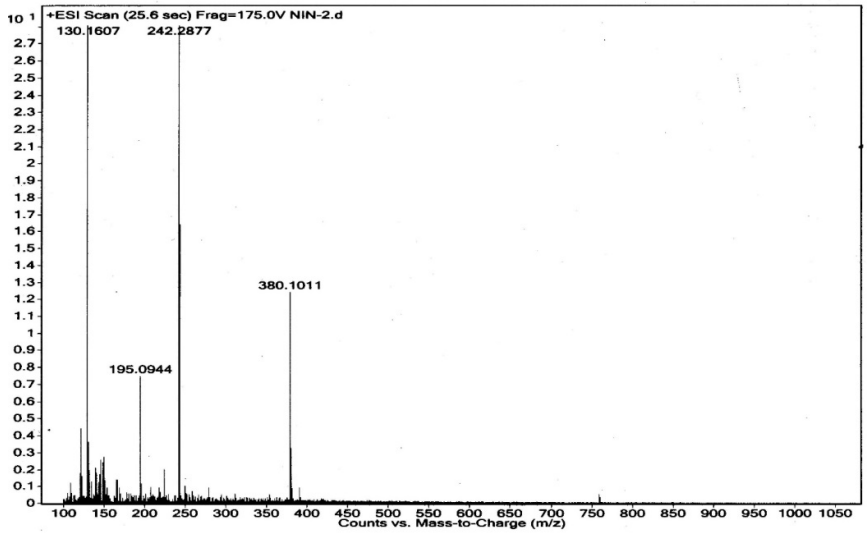

Figure A2.3 Mass Spectrum of $\mathbf{L_1}$ in positive mode.

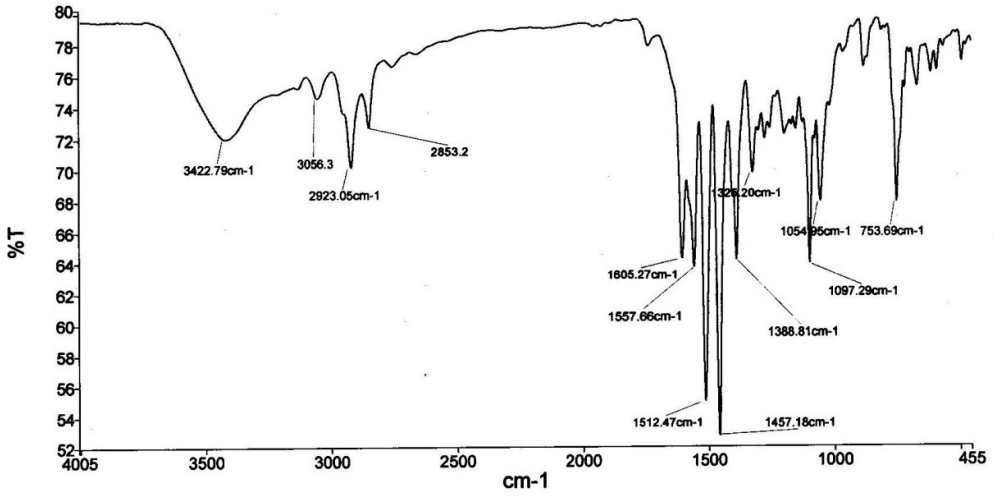

Figure A2.4 IR spectrum of $\mathbf{L_1}$ recorded on KBr disc.

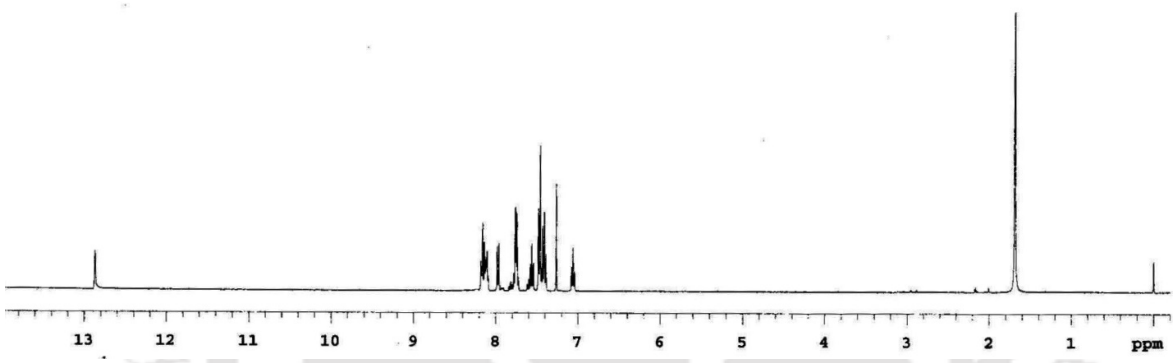

Figure A2.5 ^{1}H NMR of $\mathbf{L_{1C}}$ in $CDCl_3$ solution at room temperature.

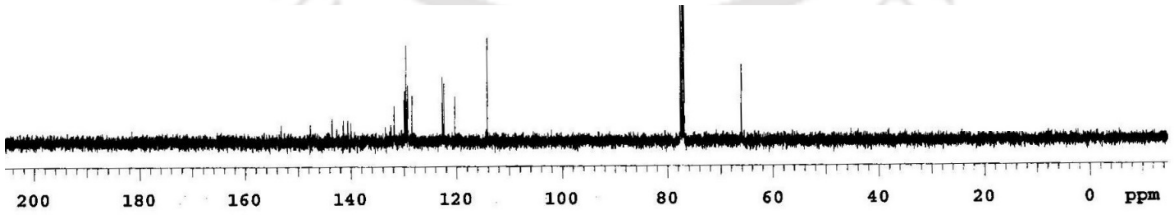

Figure A2.6 ^{13}C NMR of $\mathbf{L_{1C}}$ in $CDCl_3$ solution at room temperature.

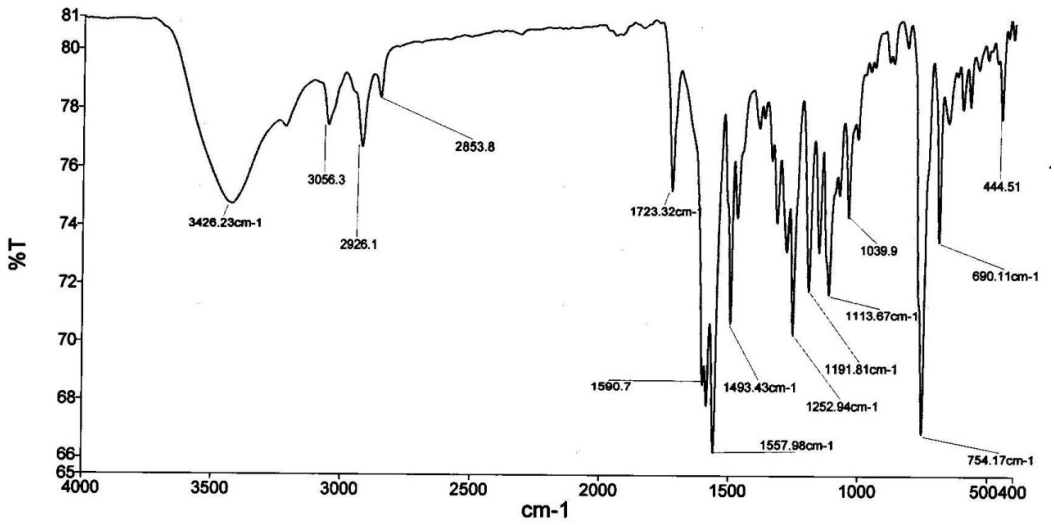

Figure A2.7 IR spectrum of $\mathbf{L_{1C}}$ recorded on KBr disc.

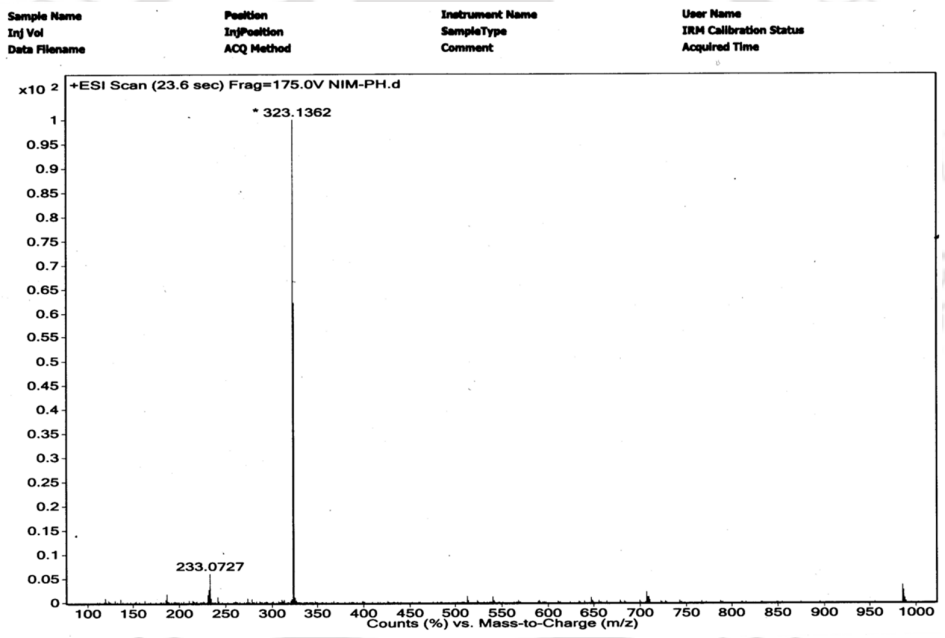

Figure A2.8 Mass Spectrum of $\mathbf{L_{1C}}$ in positive mode.

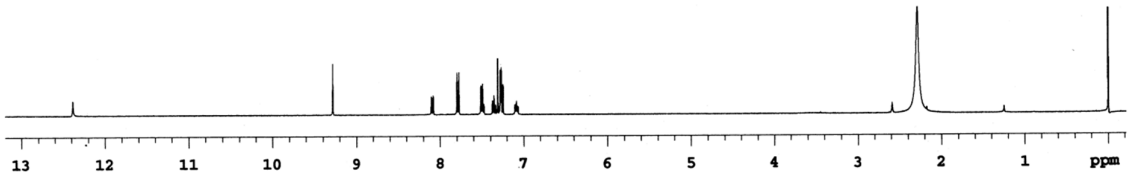

Figure A2.9 ^{1}H NMR of $\mathbf{L_2}$ in $CDCl_3$ with few drops of DMSO-d_6 at room temperature.

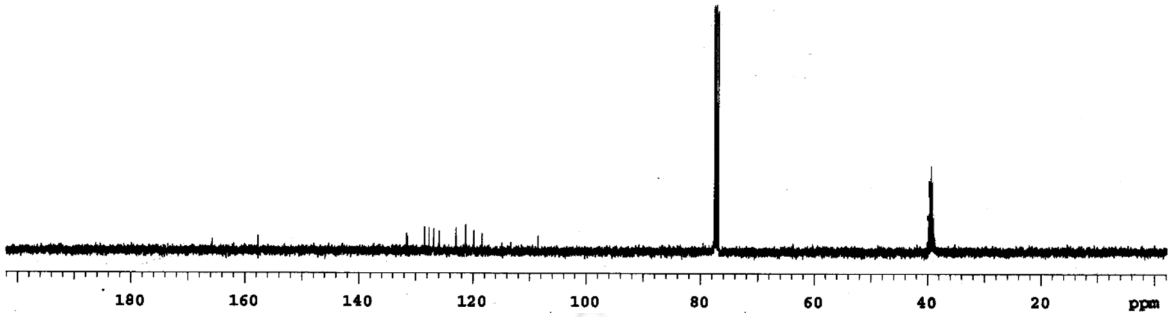

Figure A2.10 ^{13}C NMR of $\mathbf{L_2}$ in $CDCl_3$ with few drops of DMSO-d_6 at room temperature.

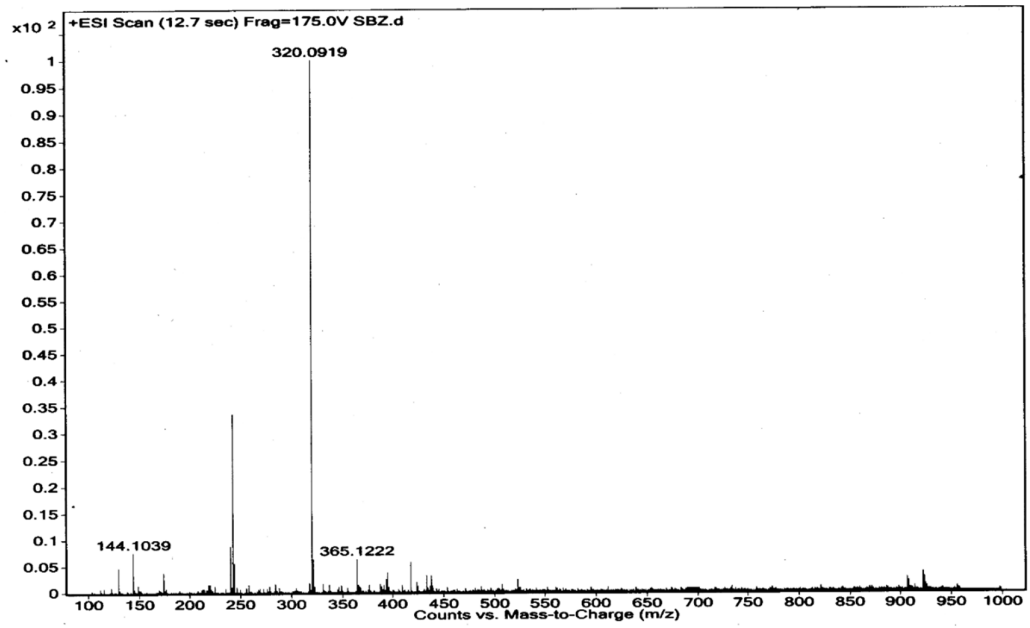

Figure A2.11 Mass Spectrum of $\mathbf{L_2}$ in positive mode.

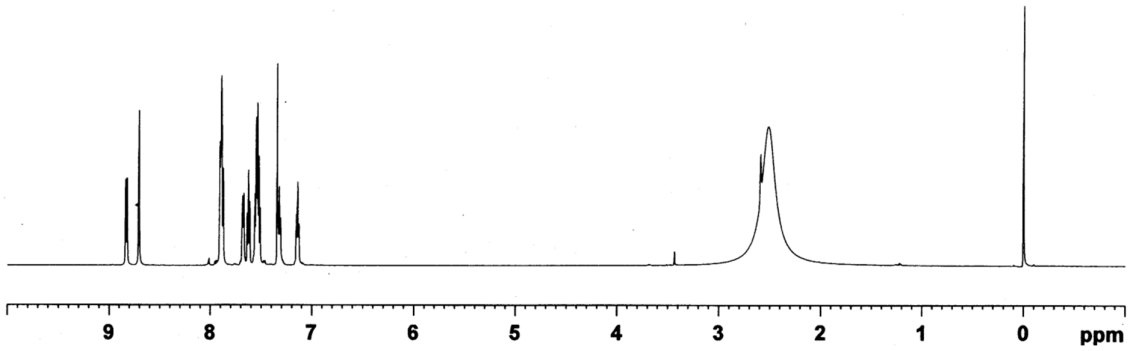

Figure A2.12 ^{1}H NMR of $\mathbf{L_{2C}}$ in $CDCl_3$ with few drops of DMSO-d_6 at room temperature.

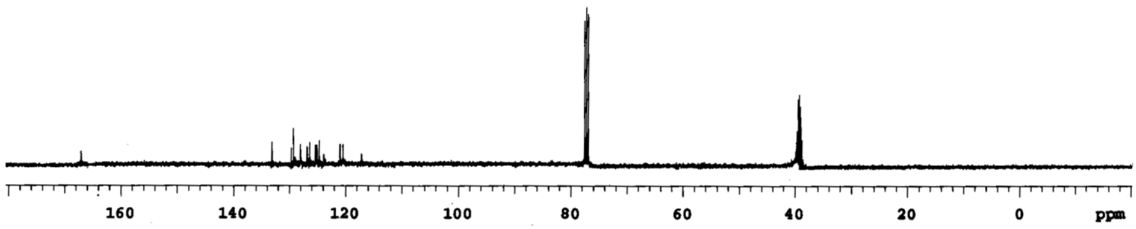

Figure A2.13 ^{13}C NMR of $\mathbf{L_{2C}}$ in $CDCl_3$ with few drops of DMSO-d_6 at room temperature.

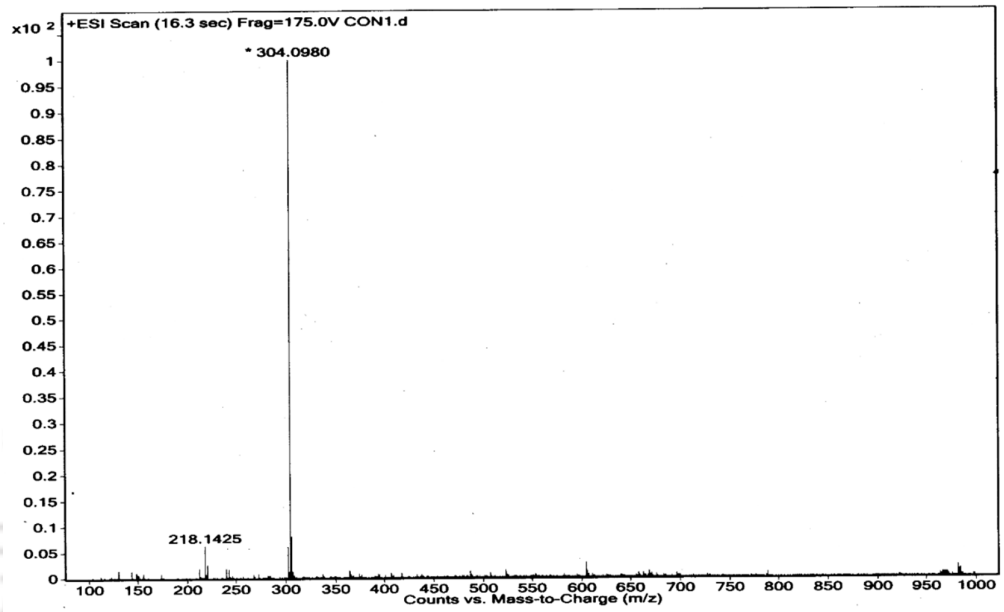

Figure A2.14 Mass spectrum of $\mathbf{L_{2C}}$ in positive mode.

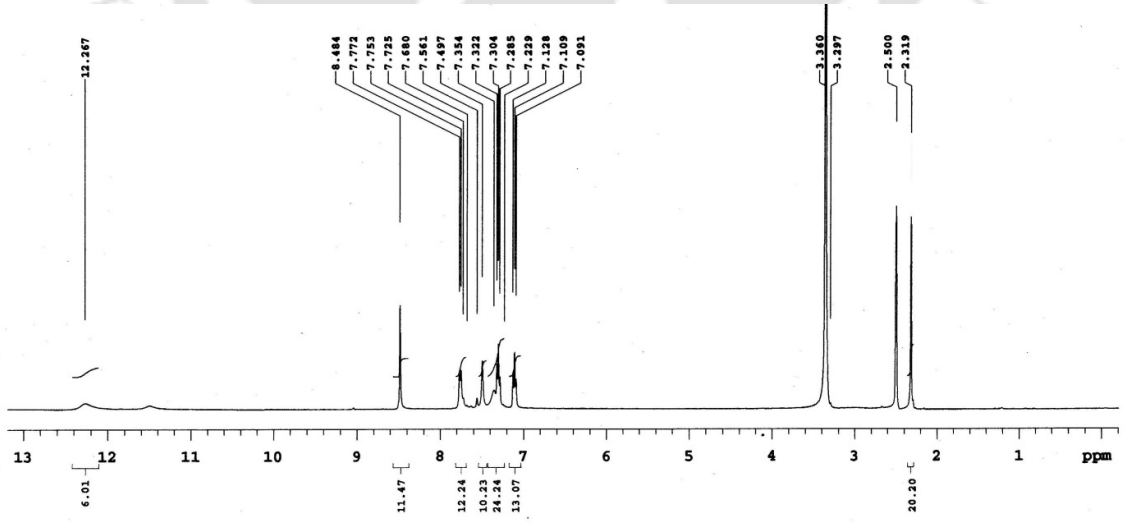

Figure A2.15 ^{1}H NMR of $\mathbf{L_3}$ in DMSO-d_6 solution at room temperature.

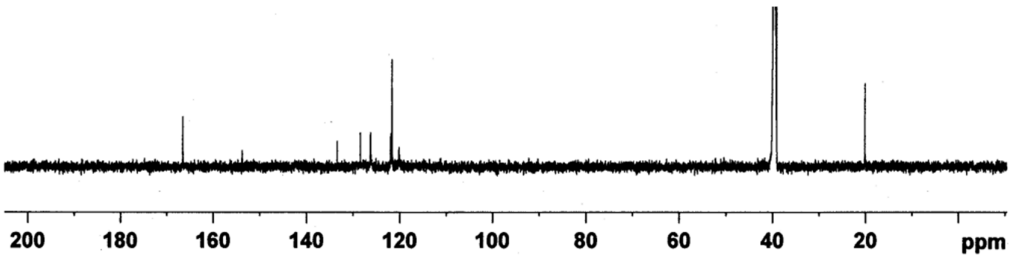

Figure A2.16 ^{13}C NMR of **L$_3$** in DMSO-d_6 solution at room temperature.

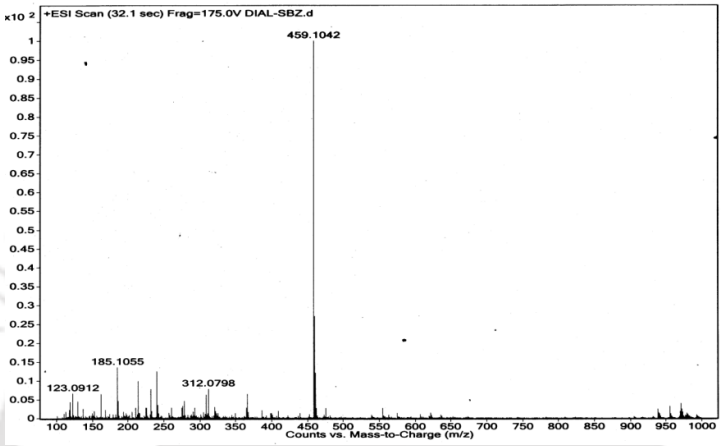

Figure A2.17 ESI-MS Mass Spectrum of **L$_3$** in positive mode.

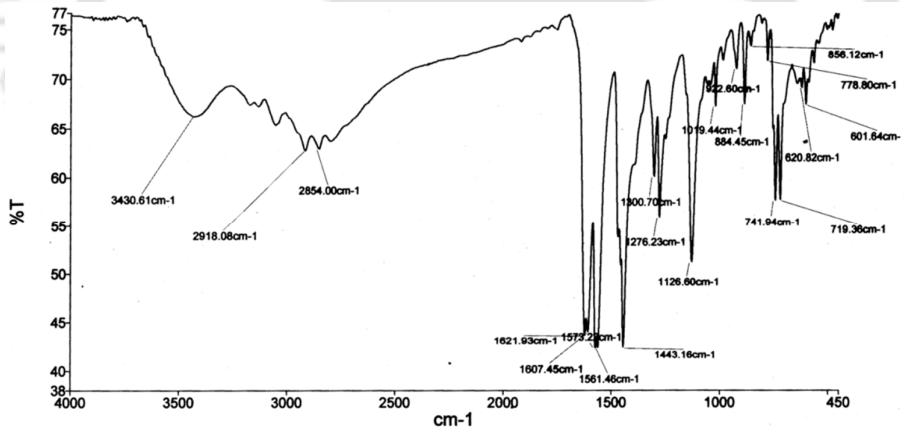

Figure A2.18 IR spectrum of **L$_3$** recorded on KBr disc.

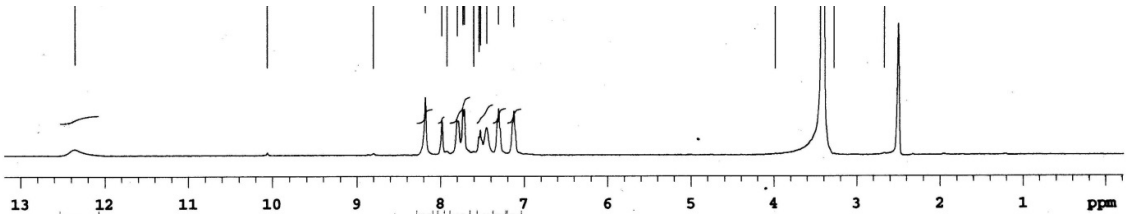

Figure A2.19 ^{1}H NMR of **L$_{3C}$** in DMSO-d_6 solution at room temperature.

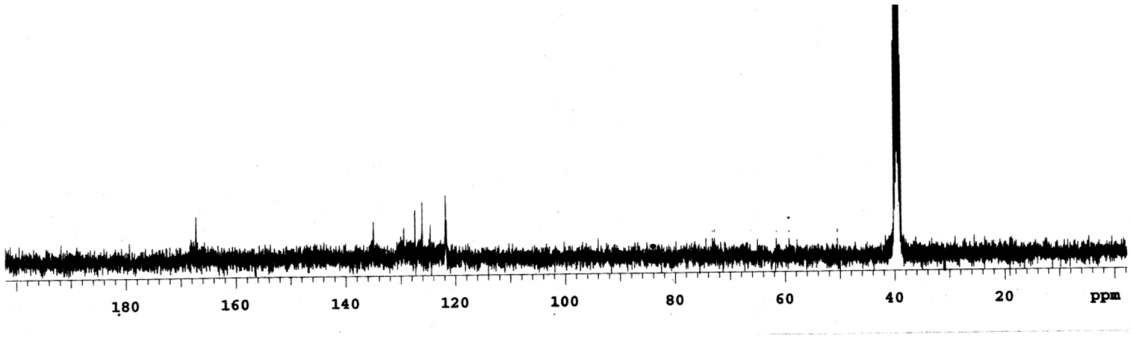

Figure A2.20 ^{13}C NMR of $\mathbf{L_{3C}}$ in DMSO-d_6 solution at room temperature.

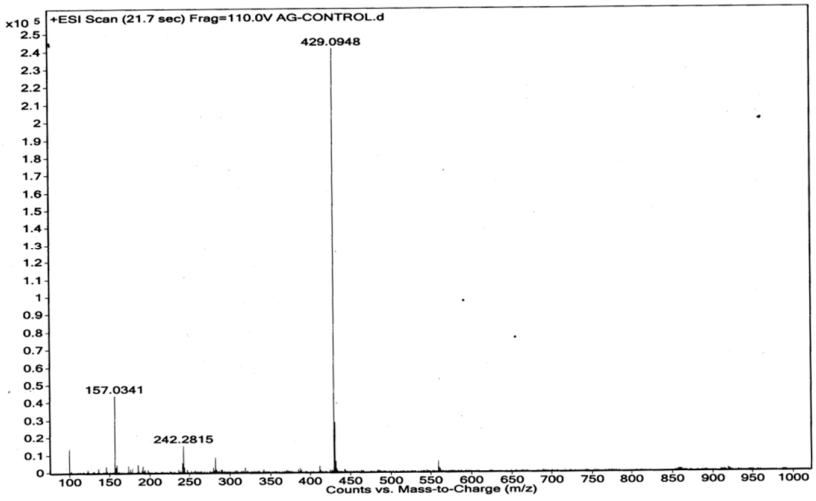

Figure A2.21 ESI-MS Mass Spectrum of $\mathbf{L_{3C}}$ in positive mode.

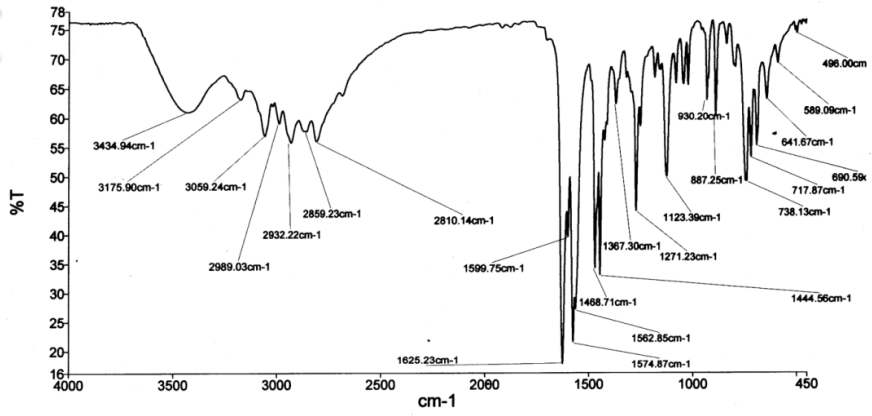

Figure A2.22 IR spectrum of $\mathbf{L_{3C}}$ recorded on KBr disc.

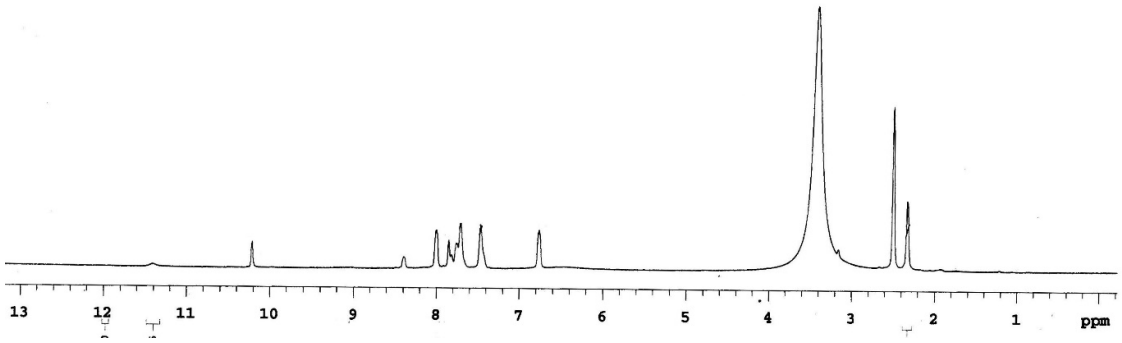

Figure A2.23 ^{1}H NMR of **L4** in DMSO-d_6 at room temperature.

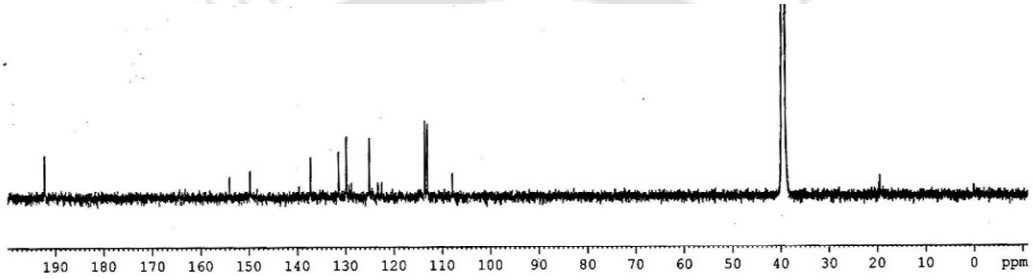

Figure A2.24 ^{13}C NMR of **L4** in DMSO-d_6 at room temperature.

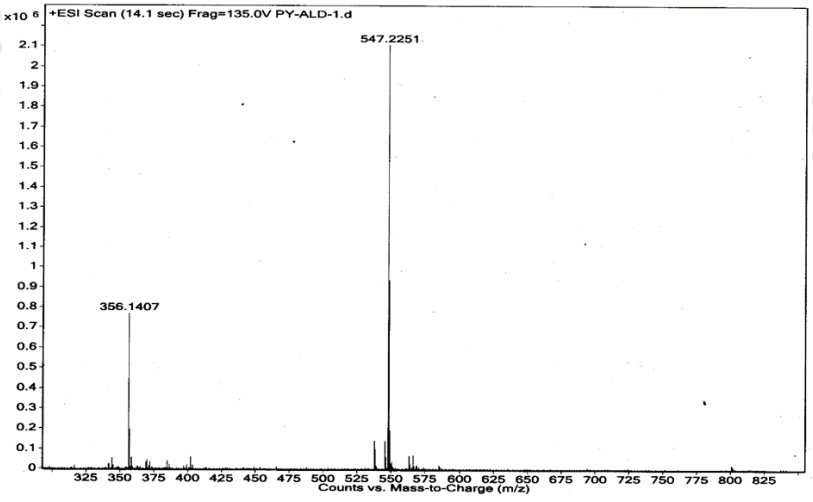

Figure A2.25 ESI-mass spectra of **L4** in positive mode.

Chapter 3

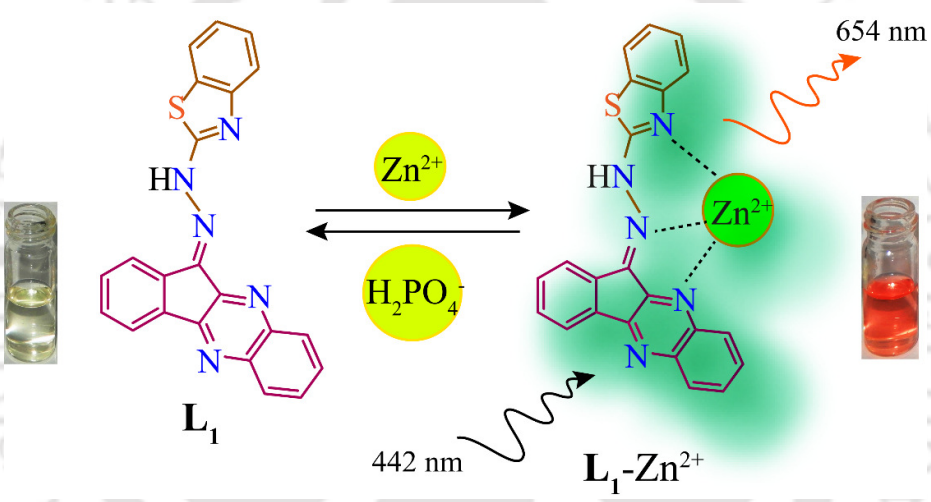

Benzothiazole Functionalized Sensor for Zn(II) and $H_2PO_4^-$: Response in NIR region

Chapter 3

3.1 Background and focus of the chapter

Metals are ubiquitous in nature and play critical roles in various fundamental processes, such as osmotic regulation, catalysis, metabolism, biomineralization, and signaling.[1] Among the metal ions, selective and sensitive detection of Zn^{2+} ion is an intriguing task due to its spectroscopically silent $3d^{10}$ configuration and the similar spectroscopic properties also exhibited by the toxic Cd^{2+} ion.[2] In terms of concentration in human body, Zn^{2+} ion is second most abundant transition metal ion after iron and involved in various key roles in biological systems including enzymatic catalysis, stabilization of protein structures and modulation of interactions between macromolecules. The total concentration of Zn^{2+} in mammalian cells is estimated to be in the range of 100 to 500 μM; the largest fraction is tightly bound to metalloproteins, whereas smaller portions are loosely bound to various readily exchangeable molecules and exist in some tissues such as the brain, intestine, pancreas, and retina.[3-4] Again, the disruption of Zn^{2+} homeostasis has been found to be associated with many neurological disorders such as Alzheimer's disease, Parkinson's disease, epilepsy and amyotrophic lateral sclerosis.[5-7]

Among the various available techniques for sensing metal ions, fluorescence based sensing is most attractive due to their high sensitivity, fast response time and the ease of handling. They enable high-contrast imaging of organs, soft tissues etc. and can unveil various metal related issues in bio-medical applications, environment etc. The first few generations of Zn^{2+} sensors were excited by UV light, which lead to severe photobleaching and photodamages. Thus, fluorescent chemosensors with higher wavelength emission are required, which can overcome the auto fluorescence from various biological entities and also can minimize the photo-damages. Thus, in the current decade, enormous efforts have been made in the synthesis of long range emissive fluorescent probes for metal ions. The NIR emissive (near infra-red) fluorescent chemosensors can penetrate very deep into the cells without much hampering them. Unfortunately, most of the existing NIR probes are derived from cyanine dyes, which suffer the poor stability issue.[8]

Again, use of metal-chemosensor ensembles for targeting anionic species is an increasing popular technique in the sensing world. The structural and geometrical flexibility of the metal-chemosensor ensemble can provide an excellent way of organizing the anion binding groups for optimal host-guest interactions.[9] Among the anions, sensing of biologically important

phosphorylated anions such as AMP, ADP, ATP, PPi, $H_2PO_4^-$ is of special interest. The dihydrogen phosphate plays a pivotal role in signal transduction, energy storage, and construction of the backbone of DNA and RNA.[10-11] However till today, fluorescent based chemosensors for $H_2PO_4^-$ ion are very limited and they responds to the aforementioned anion either through enhancement or quenching of fluorescence emission.[12-13]

Dipicolyl amine, quinolone, bipyridine, triazole and various cyclic and acyclic polyamine are the commonly used as binding units for designing a fluorescent probe for Zn^{2+}.[3,4] Owing to the varying chemosensor designs, different signal transduction mechanisms are operative, out of which PET (photoinduced electron transfer), ICT (internal charge transfer) and CHEF (chelation enhanced fluorescence) are most common. In this chapter, a benzothiazole unit is attached to a ninhydrin functionalized signalling unit to derive a new chemosensor (E)-2-(2-(11H-indeno[1,2-b]quinoxalin-11-ylidene) hydrazinyl) benzo [d] thiazole (**L_1**)(Scheme 31). The detailed synthetic procedure is described in the chapter 2.

The new chemosensor **L_1**, exhibits highly selective and sensitive 'turn-on' fluorescence response only to Zn^{2+} ion in NIR region. Although, a large number of synthetic receptors reports sensing of Zn^{2+} ion, synthetically simple chemosensors with 'turn-on' fluorescence emission in the NIR region are very limited.[17,18] Again, ninhydrin is known for its widespread applications in the fields of biochemical, analytical and forensic works.

3.2 Designing aspects of the chemosensor (L_1)

The chemosensor consists of a signalling unit (chromophore/ fluorophore) and a metal binding unit (binding core) integrated into one species through an imine bond. The benzothiazole unit thus increases the conjugation of the system and along with the quinoxaline core also act as good chelator for metal ions. A phenyl substituent control compound **L_{1C}** was also synthesized to understand the role of the benzothiazole functionality (Scheme 3.1).

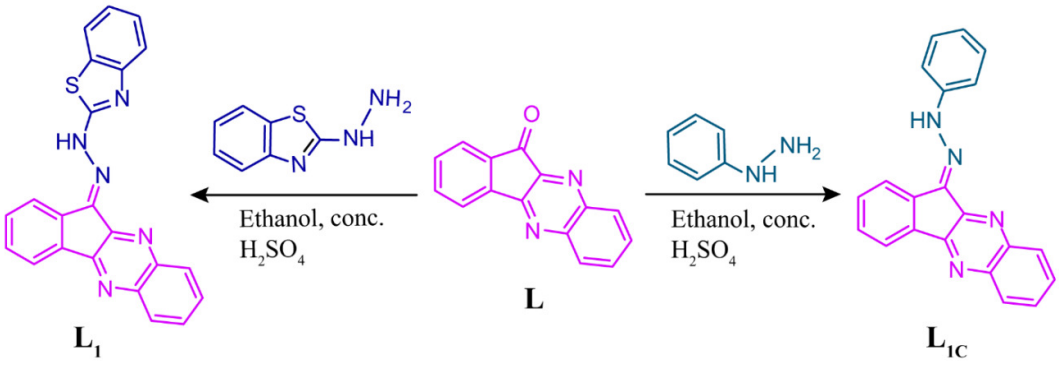

Scheme 3.1 Synthetic procedures of the probes.

3.3 Self-assembly of L_1 in solid state

Block shaped single crystals of **L_1** are grown from slow evaporation of its propanol solution. It crystallizes in monoclinic system with P21/c space group (Z = 4). The intramolecular N2—H---N4 (2.084 Å) hydrogen bonding made **L_1** to adopt a trans-amine orientation with respect to imine bond (C15---N1 = 1.305Å, C16---N2 = 1.364Å, C16---N3 = 1.309Å). The molecule is thus found to be almost planner and this facilitates the likelihood of further weaker interactions between the molecules.

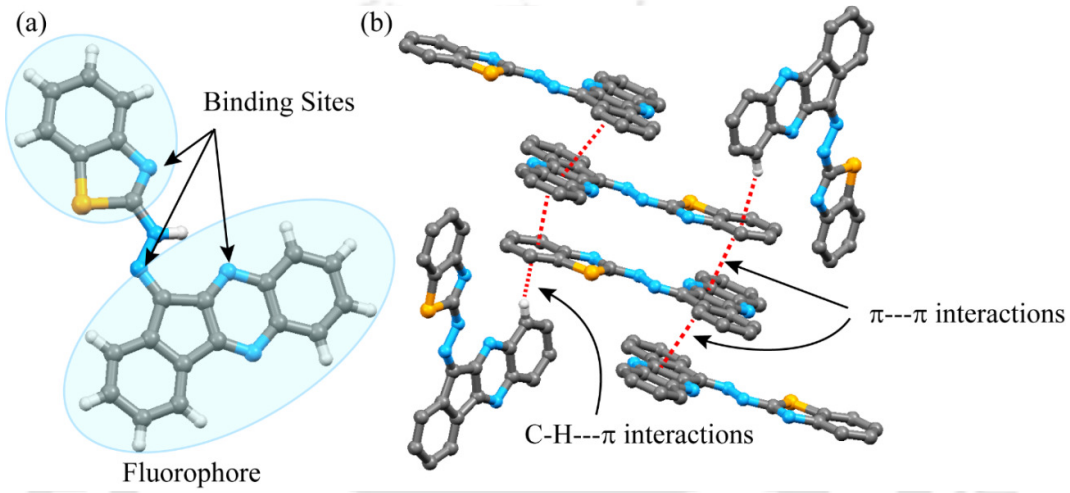

Figure 3.1 a) **L_1** with possible coordination sites for metal ions**.** (b) Various non-covalent interactions in the crystal structure.

The strong π---π interactions between the benzothiazole and the quinoxaline framework forces **L_1** molecules to arrange in a more or less parallel arrangement where both head to tail (benzothiazole to quinoxaline core) and tail to tail arrangements are visible (Figure 3.1b). A short C—H--- π (2.665 Å) interaction from the quinoxaline to the benzothiazole group further extends such interactions in other direction.

3.4 Absorption based selectivity and sensitivity study of L_1 with various metal ions

The sensing aptitude of the probe **L_1** for metal ions is investigated in acetonitrile solution with various metal ions such as Zn^{2+}, Cd^{2+}, Co^{2+}, Pb^{2+}, Ni^{2+}, Cu^{2+}, Fe^{3+}, Al^{3+}, Cr^{3+}, Hg^{2+}, Ag^{+}, Mg^{2+}, Ba^{2+}, Mn^{2+}, Na^{+}, K^{+}, Ca^{2+} etc. Before the addition of any metal ions, the naked probe **L_1** exhibits two characteristic absorption peaks nearly at 380 nm and at 442 nm in acetonitrile solution originating from π---π* transitions and long conjugation present in the polyaromatic system. A conspicuous change in UV-Vis spectral pattern is manifested only in presence of Zn^{2+} and Cu^{2+} ions (Figure 3.2a). Addition of Zn^{2+} ion to the acetonitrile solution of **L_1** produces new absorption peaks at 536 nm and at 418 nm with isobestic point at 468 nm. Concomitantly, the

colour of the solution has changed from light yellow to orange coloured solution. The response time is very fast which thus enable instantaneous visual detection of Zn^{2+} ion (Inset, Figure 3.2b). All these spectral changes indicates the formation a new UV-active Zn^{2+} complex with **L1**. Subsequently, to comprehend the Zn^{2+} induced changes, an acetonitrile solution of **L1** (10 μM) is also titrated with increasing concentrations of Zn^{2+} in the same experimental medium. Now, the figure 3.2b shows that with the progress of the titration, absorbance of the peak at 380 nm decreases but the new peak at 536 nm got intensified. Again, a plot of absorbance values of these peaks against the Zn^{2+} ion concentrations (μM) shows a linear correlation with each other over a wide Zn^{2+} concentration range (Figure A3.1 a). The Job's plot from this titration data suggests the formation of a 1:1 host-guest complex (Figure A3.1b). Again, addition of higher equivalents of Cu^{2+} ion (10 equivalents) to the acetonitrile solution of **L1** produces a new peak at 454 nm and a red shifted absorption maxima at 550 nm. The new isobestic points at 460 nm and 366 nm are the indicative of the formation of a new **L1**-Cu^{2+} complex. This also leads to a visual change in colour of the solution from light yellow to light pink. Since, the optical behaviour of **L1** is different for both Zn^{2+} and Cu^{2+} ion, it enables simultaneous detection of both the ions. More importantly, Cd^{2+} ion, the electronic congener of Zn^{2+} ion and other heavy metals, do not produce any significant change in the UV-Vis pattern of **L1**. Hereafter, fluorescence changes of the chemosensor with the same set of metal ions are also tested.

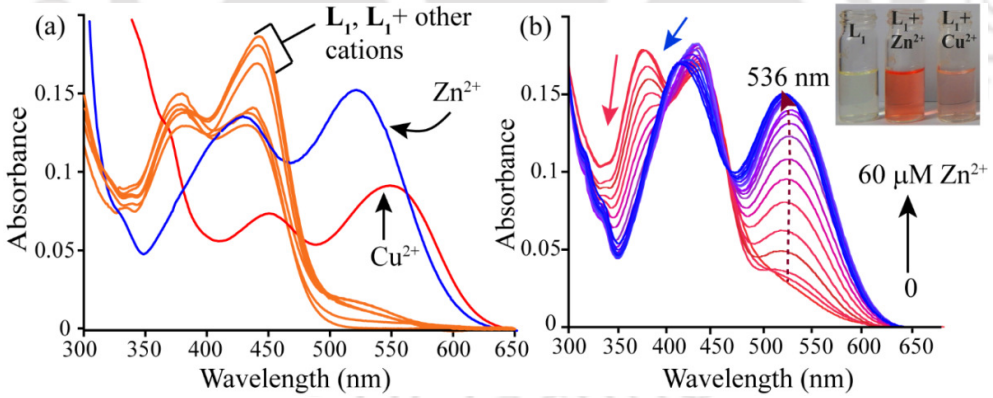

Figure 3.2 a) UV-Vis based selectivity study of **L1** with various metal ions. b) The change of **L1**'s absorption with increasing concentrations of Zn^{2+} (μM). **Inset:** The visual colour changes after addition of Cu^{2+} and Zn^{2+} to the acetonitrile solution of **L1**.

3.5 Fluorescence spectroscopic selectivity study of L1 with various metal ions

The probe **L1** is weakly fluorescent at 545 nm when excited either at 442 or at 468 nm, showed a weak emission maximum at (quantum yield <0.002) with a Stokes shift of 103 nm in acetonitrile. In good agreement with the finding of absorption spectral studies, Zn^{2+} ion promotes a significant fluorescent enhancement to chemosensor **L1** (Figure 3.3a). A new

emission maximum at 654 nm (Stokes shift of 130 nm) with 15.5 fold of fluorescent enhancement is recorded after addition of 10 equivalents of Zn^{2+} (Fluorescence quantum yield (Φ) = 0.11). However, the coloured Cu^{2+} solution is fluorescence inactive. And, likewise all other metal ions which includes Cd^{2+}, Co^{2+}, Pb^{2+}, Ni^{2+}, Fe^{3+}, Al^{3+}, Cr^{3+}, Hg^{2+}, Ag^{+}, Mg^{2+}, Ba^{2+}, Mn^{2+}, Na^{+}, K^{+} and Ca^{2+} cause no change to the sole fluorescence of **L1** (Figure 3.3b). Further, to track the Zn^{2+} induced fluorescence changes, titration experiment is also repeated with a 10 µM concentrated acetonitrile solution of **L1**. Figure 3.3c, clearly manifest a linear increase in fluorescence emission intensity nearly at 654 nm with increasing Zn^{2+} concentrations. The plot of fluorescent intensities at 654 nm versus Zn^{2+} ion concentrations exhibits a linear increase fluorescent intensity upto 20µM of Zn^{2+} and afterwards, the rate of enhancement is slowed down (Figure A3.1c). More importantly, the plot of log(FI) (fluorescence intensity) versus log[Zn^{2+}] is found to be linear (R^2 = 0.9902) in this concentration range (Figure A3.2a). The calculated lowest detection limit for Zn^{2+} is 6 nM based on 3σ/k method (Figure A3.2b). Again, the calculated binding constant is logK = 7.1419 based on the fluorescence titration experiment (Figure A3.3).

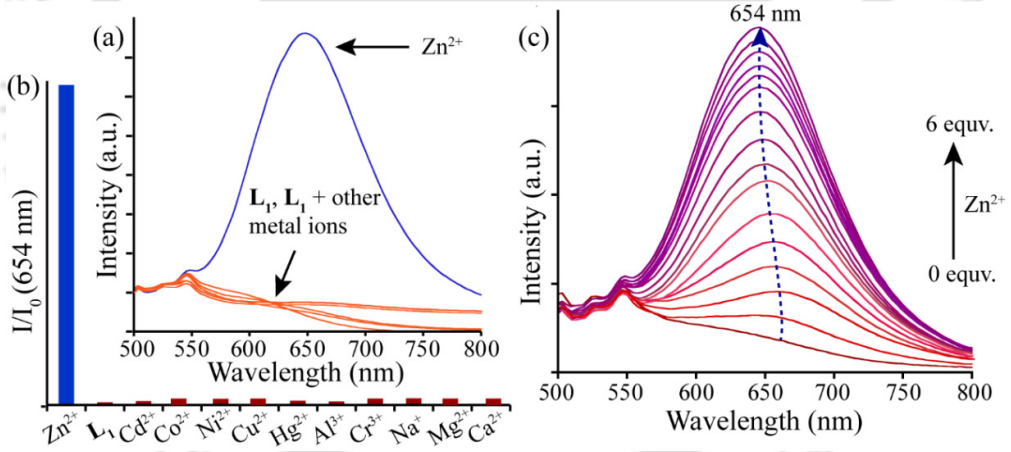

Figure 3.3 Changes in fluorescence emission response of **L1** (10µM) with (a) various metal ions (c = 10^{-4} M) and (b) bar plot presentation of the same. c) Fluorescence titration spectra of **L1** (10µM) upon incremental addition of Zn^{2+} ion in acetonitrile medium (λ_{ex} = 442 nm, slit width = 5 nm/5 nm).

Rapid isomerisation around C=N and photo electron transfer (PET) from N of benzothiazole to quinoxaline fluorophore are the probable reasons for the weak fluorescence of **L1**. While the imine N is essential for the chelation with most metal ions, to understand the importance of benzothiazole group, the metal ion sensing aptitude of the control compound **L1C** is tested under similar experimental conditions. Since **L1C** do not show any selectivity to any of the aforementioned metal ions, it suggests the prominence of the benzothiazole functionality in binding to the Zn^{2+} ion (Figure A3.4). Thus, these experimental results suggest the involvement

of imine N and benzothiazole N/S in the chelation with Zn^{2+} ion,[16] which thereby ceases the isomerisation process and the fluorescence increases as a result of chelation enhanced emission (CHEF) effect.

Further for a realistic appraisal of the chemosensor and for its potential application in the bio-analytical regime, the selectivity of the chemosensor for Zn^{2+} over other competing metal ions in the biological milieu is critical. To that end, fluorescence emissions of the $\mathbf{L_1}$- Zn^{2+} ensembles are also recorded in presence of other metal ions. It is indeed encouraging to observe that except Cu^{2+} ion, the Zn^{2+} induced 'turn-on' fluorescence of $\mathbf{L_1}$ is preserved in most of the cases clearly suggesting the high selectivity and sensitivity of $\mathbf{L_1}$ towards Zn^{2+} even in presence of these metal ions (Figure A3.5a). The paramagnetic nature of copper ion is probably the reason for fluorescence quenching. However, this could be beneficial for the fluorescence based detection of the same, as the fluorescence response of Cu^{2+} ion to $\mathbf{L_1}$ was not visible first. Pandey *et. al.* have used similar approach to report a 'on-off-on' type sensing of Cu^{2+} and Ag^{+} ions with a fluorescent Zn(II) complex.[14] Anyway, the interference from the Cu^{2+} ion can be removed by the addition of S^{2-} ion which restores the fluorescence based on the well-known strong affinity of S^{2-} for Cu^{2+}. However, under similar experimental conditions, interaction of S^{2-} with '$\mathbf{L_1}$-Zn^{2+}' ensemble caused no change in the fluorescence output signal (Figure A3.5b). Finally, considering an environmental application, the fluorescence experiment is also repeated in an optimized mixed aqueous solution. In a buffered acetonitrile (8:2 : acetonitrile : HEPES buffer, pH~7.4) medium, addition of 10 equivalents of Zn^{2+} ion to $\mathbf{L_1}$ has intensified fluorescence emission nearly by 6 fold at the same wavelength (Figure A3.6).

3.6 Binding Mode and Composition of Metal Complex

For detailed understanding of the binding interaction between the Zn^{2+} and $\mathbf{L_1}$, ^{1}H NMR of $\mathbf{L_1}$ is also recorded after addition of Zn^{2+}. However, due to the poor solubility of the probe in CD_3CN, $CDCl_3$ solution has been used. A desired concentration of Zn^{2+} is prepared in DMSO-d_6 and slowly added to the $\mathbf{L_1}$'s solution. The very expected downfield shift of the imine CH(1) from 8.250 ppm to 8.286 ppm suggests the involvement of the imine nitrogen in bonding with the Zn^{2+}. Besides, a highly deshielded singlet peak at 13.46 ppm disappears after the addition of Zn^{2+} ion. Again, CH(2) proton is shifted upfield from 8.151 to 8.132, while CH(3) shifted from 7.991 ppm to 7.961 ppm after addition of 1.3 equivalents of Zn^{2+} (Figure 3.4b). This suggests the involvement of the benzothiazole unit in the binding process which is also supported by control compound $\mathbf{L_{1C}}$. The imine nitrogen from the Schiff base is a very common chelating atom for Zn^{2+} and for other various metals ions. Thus, supporting the 1:1 stoichiometry from the

Job's plot, a quinoxaline N might be the third chelating atom for Zn^{2+} ion. Chelation thereby ceases the isomerization process and hence fluorescence increases.

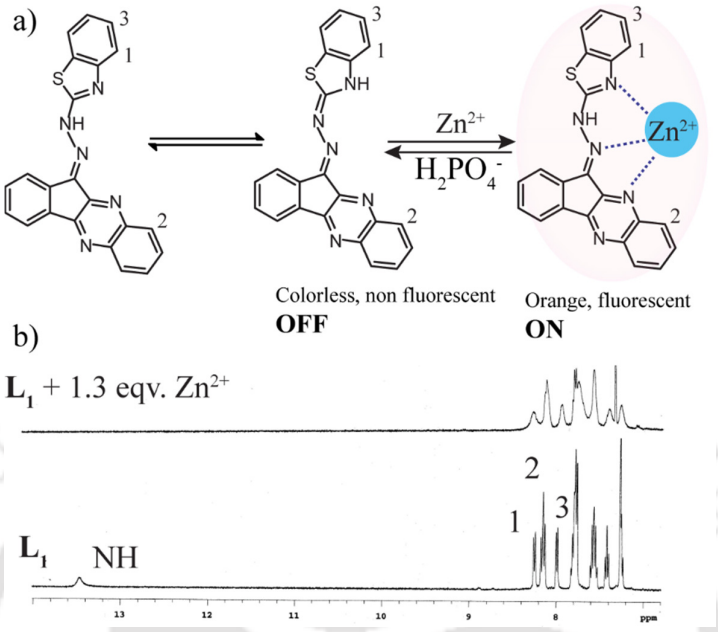

Figure 3.4 a) Plausible binding mechanism of **L1** with Zn^{2+}. b) NMR stack plot with excess concentration of Zn^{2+} in $CDCl_3$ at room temperature.

3.7 Selective $H_2PO_4^-$ sensing by '**L1**-Zn^{2+}' ensemble

After exploring the metal sensing aptitude of the chemosensor, our next aim was to test the anion sensing aptitude of the new Zn^{2+}-chemosensor ensemble. For that, various anions and nucleotides are added to the *in situ* formed '**L1**-Zn^{2+}' ensemble (Figure 3.5a). Among the anions; F^-, Cl^-, Br^-, I^-, HSO_4^- and NO_3^- do not affect the fluorescence emissive property of the '**L1**-Zn^{2+}' ensemble. However, a distinct 'turn-off' fluorescence response is observed with excess $H_2PO_4^-$ while other phosphorylated anionic species such as AMP, ADP, ATP are also insensitive the metal ensemble. To unveil the origin of the 'turn-off' fluorescence, the *in situ* formed '**L1**-Zn^{2+}' ensemble is titrated with increasing concentrations of $H_2PO_4^-$ in similar experimental medium. Now, as seen in titration figure 3.5b, a nonlinear emissive behaviour is recorded with different concentrations of $H_2PO_4^-$. The initial few equivalents of the $H_2PO_4^-$ has blue shifted the emission maximum from 654 nm to 584 nm with intensifying emission intensities. However, on continuing the titration, fluorescence emissions quenches rapidly at 584 nm. The initial fluorescence enhancement is probably due to formation of a $H_2PO_4^-$ complex with the '**L1**-Zn^{2+}' ensemble where the additional hydrogen bonding with the receptor might be helpful for the anion to interact with the '**L1**-Zn^{2+}' complex. Such type of emission enhancement is also described by *Kaur et. al* with a hexaphenylbenzene derivative-Zn^{2+} ensemble.[18]

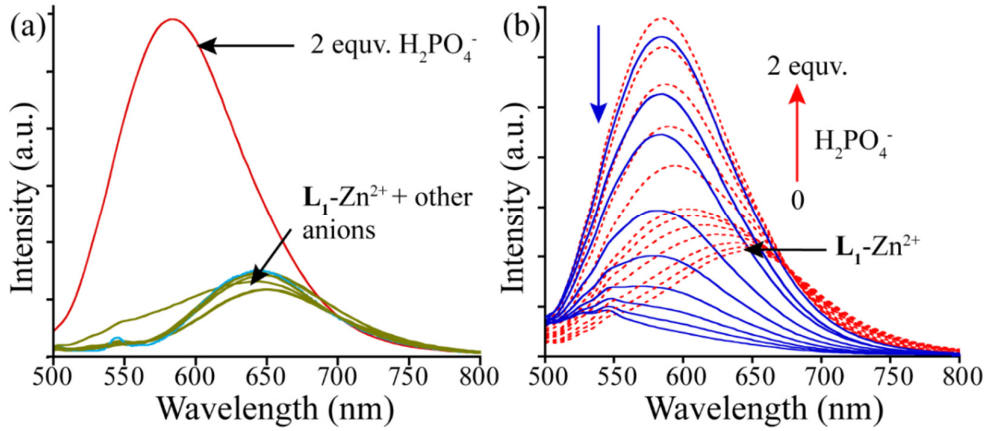

Figure 3.5 Changes in fluorescence intensity of the '**L_1-Zn^{2+}**' ensemble with (a) various anions and nucleotides (c = 10^{-4} M). (b) Fluorescence titration of **L_1** with incremental addition of $H_2PO_4^-$ anion in acetonitrile. The broken red lines refer to the change in emission upto 2 equivalents and the result of excess $H_2PO_4^-$ anion are presented by blue lines (λ_{ex} = 442 nm, slit width = 5 nm/5 nm).

Further addition of $H_2PO_4^-$ anion may result in the de-complexation as manifested by overall quenching of the fluorescence which probably occurred due to strong binding affinity of Zn^{2+} for the $H_2PO_4^-$.

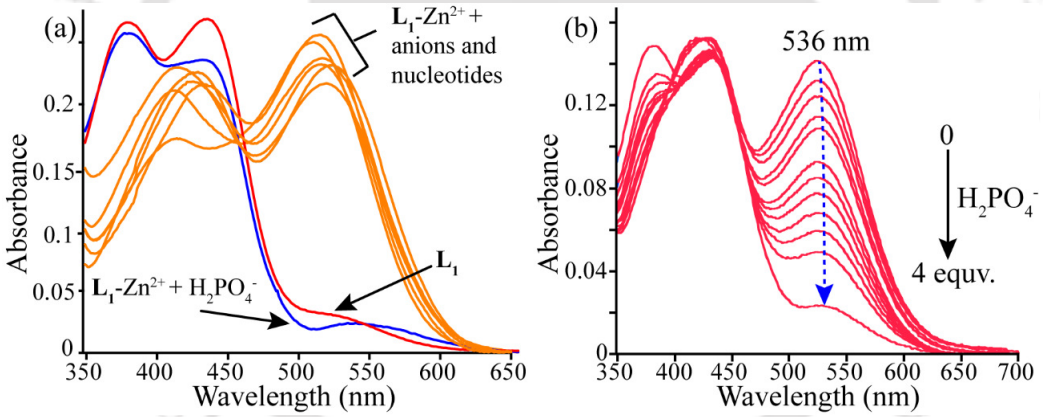

Figure 3.6 UV-Vis response of a) various anions and nucleotides and b) increasing concentrations of $H_2PO_4^-$ towards '**L_1-Zn^{2+}**' ensemble in acetonitrile solution.

Thus, the UV-Vis absorption of this solution is also recorded (Figure 3.6a). As expected, it resembles to the original naked **L_1**'s solution which thereby supports our conjecture of $H_2PO_4^-$ induced decomplexation as the main cause of 'turn-off' fluorescence. Proving the high selectivity of the '**L_1-Zn^{2+}**' ensemble for $H_2PO_4^-$, all other anions are also insensitive to absorption spectra of the ensemble. The absorption titration spectra (Figure 3.6b), revealed a consistent decrease in absorbance of the peak at 536 nm with increasing concentrations of $H_2PO_4^-$. The colour of the solution is also changed from orange to very light yellow, which is the original colour of the naked probe solution.

3.8 Conclusion

A novel benzothiazole functionalized ninhydrin based chemosensor **L_1**, impels excellent colorimetric and 'turn-on' fluorescence response only to Zn^{2+}. The colour of the solution has instantly changed to orange from the original yellowish solution, which enables naked eye detection of the same. The Zn^{2+} solution is highly fluorescent and emits in near infra-red region (NIR). These spectral changes are significant enough to enable naked eye detection of Zn^{2+} ion in physiological medium also. The Job's plot from the titration data suggests a 1:1 (**L_1** : Zn^{2+}) binding stoichiometry and the calculated detection limit is 6 nM. Nature of the Zn^{2+} binding mode with **L_1** is also analysed with ^{1}H NMR titration. Most importantly, the sensitivity of **L_1** for Zn^{2+} ion is also preserved in presence of Cd^{2+} and other heavy transition metals except Cu^{2+}. Finally, the '**L_1**-Zn^{2+}' ensemble responds only to $H_2PO_4^-$ through fluorescence quenching. All other anions such as pyrophosphate, ATP, ADP etc. nucleotides and other common anions are insensitive to the ensemble.

References

1. E. L. Que, D. W. Domailli and C. J. *Chang, Chem. Rev*., 2008, **108**, 1517-1549.
2. (a) R. M. Manez and F. Sancenon, *Chem. Rev*., 2003, **103**, 4419-4476; (b) J. S. Kim and D. T. Quang, *Chem. Rev*., 2007, **107**, 3780-3799.
3. Z. Xu, J. Yoon and D. R. Spring, *Chem. Soc. Rev*., 2010, **39**, 1996-2006.
4. K. P. Carter, A. M. Young and A. E. Palmer, *Chem. Rev*., 2014, **114**, 4564-4601.
5. A. I. Bush, W. H. Pettingell, G. Multhaup, M. d. Paradis, J. P. Vonsattel, J. F. Gusella, K. Beyreuther, C. L. Masters and R. E. Tanzi, *Science*, 1994, **265**, 1464-1467.
6. M. P. Cuajungco and G. J. Lees, *Neurobiol. Dis*., 1997, **4**, 137-169.
7. A. I. Bush and R. E. Tanzi, *Proc. Natl. Acad. Sci. U. S. A*., 2002, **99**, 7317-7319.
8. L. Yuan, W.Lin, K. Zheng, L. He and W. Huang, *Chem. Soc. Rev.,* 2013, **42**, 622-661.
9. J. Wu, B. Kwon, W. Liu, Eric V. Anslyn, P. Wang, and J. Seung Kim, *Chem. Rev*., 2015, **115**, 7893-7943.
10. S. Lee, K. K. Y. Yuen, K. A. Jolliffe and J. Yoon, *Chem. Soc. Rev.*, 2015, **44**, 1749-1762.
11. W. Saenger, *Principles of Nucleic Acid Structure, Springer*, New York, 1988.
12. S. Kondo and R. Takai, *Org. Lett*., 2013, **15**, 538-541.
13. W. Gong, Q. Zhang, F.Wang, B. Gao, Y. Lin and G. Ning, *Org. Biomol. Chem*., 2012, **10**, 7578-7583.
14. J. Cao, C. Zhao, X. Wang, Y. Zhanga and W. Zhu, *Chem. Commun*., 2012, **48**, 9897-9899.
15. J. Wang, Y. Li, E. Duah, S. Paruchuri, D. Zhou and Y. Pang, *J. Mater. Chem. B*, 2014, **2**, 2008-2012.
16. M. Alfonso, A. Tarraga, P. Molina, *J. Org. Chem.*, 2011, **76**, 939-947.
17. R. Pandey, P. Kumar, A. K. Singh, M. Shahid, P. Z. Li, S. K. Singh, Q. Xu, A. Misra and D. S. Pandey, *Inorg. Chem*., 2011, **50**, 3189-3197.
18. V. Bhalla, V. Vij, M. Kumar, P. R. Sharma and T. Kaur, *Org. Lett*., 2012, **14**, 1012-1015.

Appendix 2

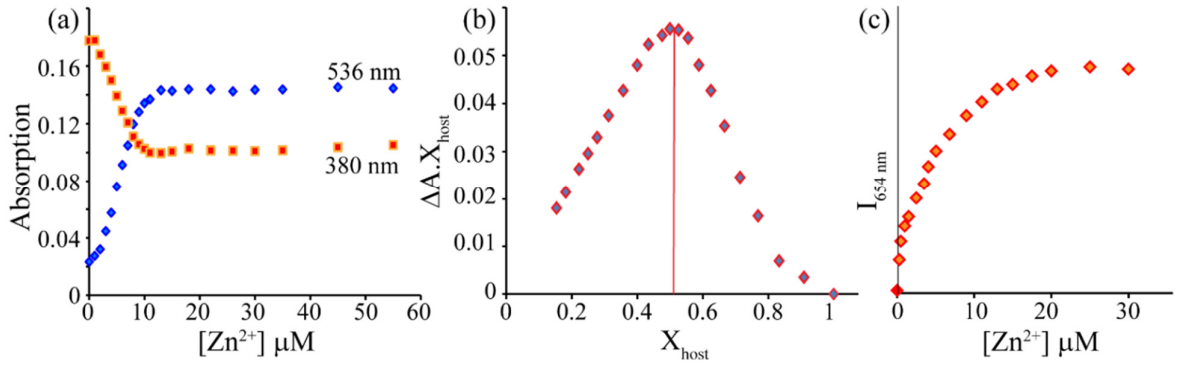

Figure A3.1 a) Spectral curve fitting for the absorption at 536 nm and at 380 nm against Zn^{2+} concentration. b) The Job's plot for the titration of Zn^{2+} with $\mathbf{L_1}$. c) Change of fluorescence emission intensity change with increasing Zn^{2+} concentrations.

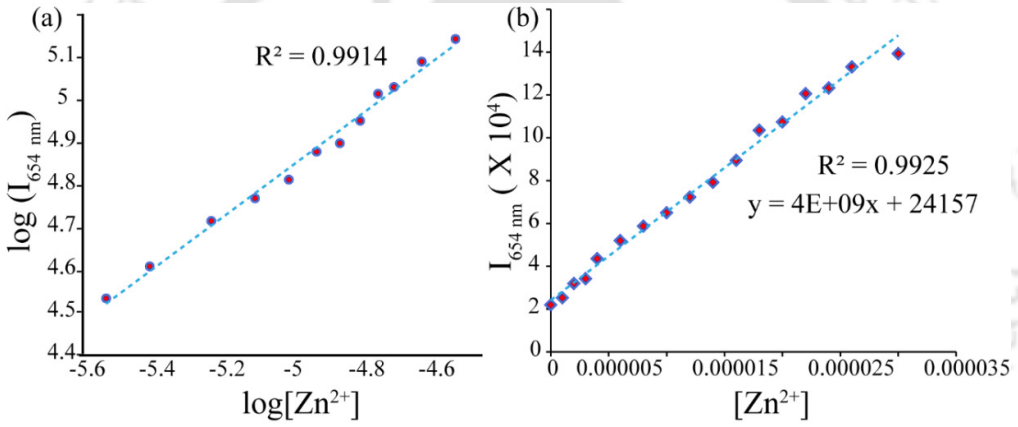

Figure A3.2 a) Plot of log FI (fluorescence intensity) versus log $[Zn^{2+}]$ in the range of 0-6 equiv. of Zn^{2+}. b) Plot of fluorescence intensity versus $[Zn^{2+}](M)$ for the lowest detection limit (LOD) calculation.

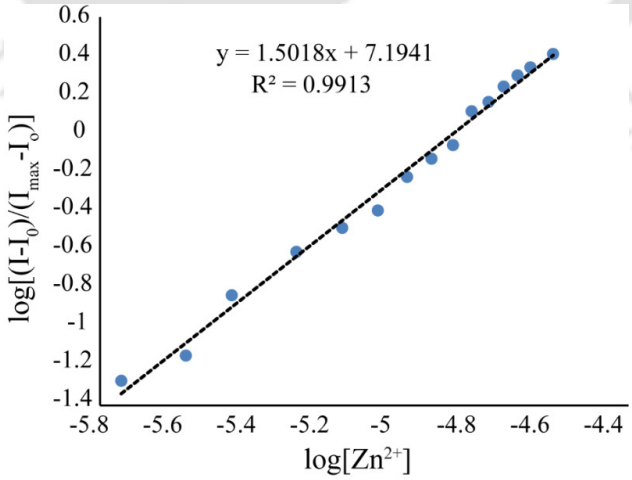

Figure A3.3 The Bensei-Hildebrand plot for the titration of $\mathbf{L_1}$ with Zn^{2+}.

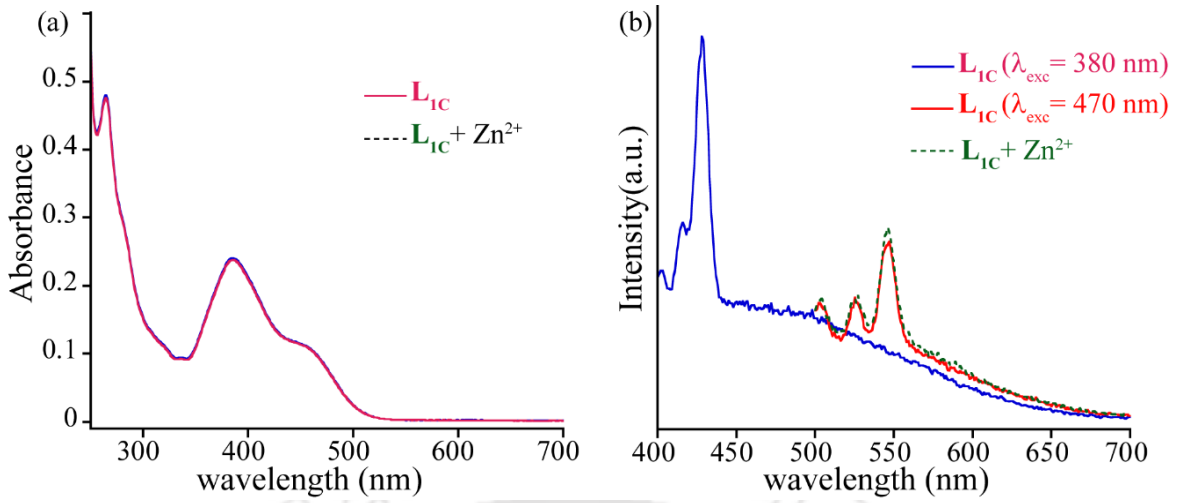

Figure A3.4 a) Absorption spectra and b) the corresponding fluorescence spectra of L_{1C} in the experimental medium.

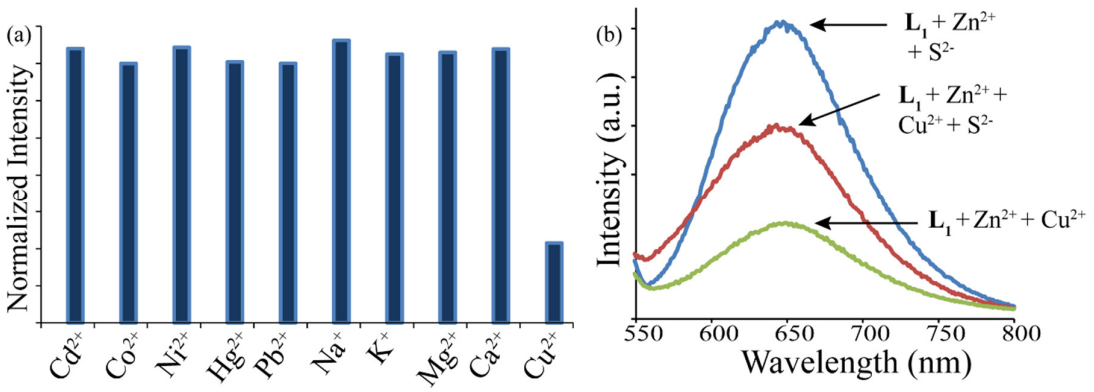

Figure A3.5 a) Bar plot presentation of the fluorescence emission response of 'L_1-Zn^{2+}'ensembles in presence of various metal ions. b) Effect of presence of Cu^{2+} and S^{2-} ions in the signal output of 'L_1-Zn^{2+}' ensembles.

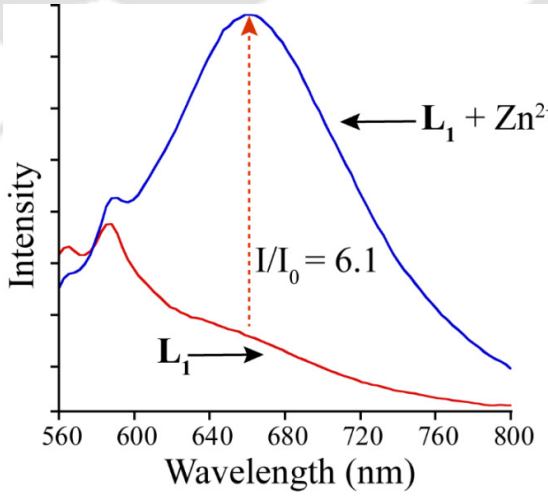

Figure A3.6 The fluorescence response of the receptor L_1 towards Zn^{2+} ion in buffered acetonitrile (8:2 acetonitrile: water) at room temperature.

Table 3.1 Crystallographic parameters and refinement details of $\mathbf{L_1}$

Parameters	L_1
Empirical formula	$C_{22}\ H_{13}\ N_5\ S$
Molecular weight	379.44
Crystal system	Monoclinic
space group	P2(1)/c
a	9.9373(12) Å
b	13.5639(16) Å
c	13.7420(17) Å
α	90°
β	102.302(6)°
γ	90.00°
Volume	1809.73 $Å^3$
T	298(2) K
Z	4
Dx (g/cm^{-3})	1.393
μ	0.197 mm^{-1}
F(000)	784
Reflections collected/unique	25344/4521
R(int)	0.0325
R_1; wR_2 [I > 2sigma(I)]	0.0435; 0.1315
R_1; wR_2 (all)	0.0570; 0.1517
GOF(F2)	0.920
CCDC No.	1000228

Chapter 4

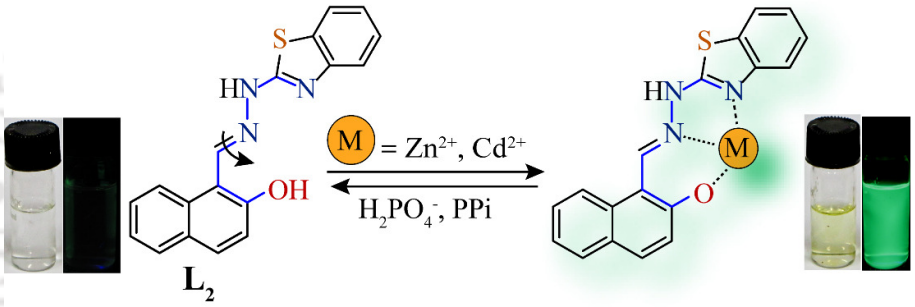

Benzothiazole Functionalized Sensor for Zn(II), Cd(II), PPi and $H_2PO_4^-$: Multi ion sensing platform at Physiological condition

Chapter 4

4.1 Background and Focus of the Chapter

Both zinc and cadmium ions are belong to the same group in the periodic table and possess similar chemical properties due to their identical d^{10} configurations. However, their impact on real biological world is quite opposite to each other. While the zinc ion is known for its indispensable role in human body, the other ion is deleterious to life. Cadmium ion is not even biodegradable, and it is easily accumulated in the environment resulting in contaminated food and water. Electric batteries, pigments in plastics, electroplated steel, are the main sources of cadmium ion. Living organisms can easily absorb and accumulate cadmium ions at cellular level. But a high exposure level of cadmium can damage liver and kidneys, increases risks of cardiovascular diseases, and cancer mortality. Therefore cadmium is listed as number 7 on ATSDR's "CERCLA Priority List of Hazardous Substances" and may cause acute and chronic toxicity. Thus, there is a growing demand for new design and techniques for sensing Cd^{2+} ion.[1-3] Again, among the anions colorimetric and fluorescence based sensing of phosphorylated anions such as pyrophosphate (PPi) and $H_2PO_4^-$ is exceptionally important. The importance of $H_2PO_4^-$ for biological system is already described in chapter 3. PPi is known to be formed by ATP hydrolysis under cellular conditions and it plays a central role in important biochemical pathways such as DNA polymerization and synthesis of cyclic adenosine monophosphate (c-AMP) catalyzed by DNA polymerase and adenylate cyclase respectively. Furthermore, recent studies have highlighted the emerging role of PPi as an important biomarker for several ailments. Consequently, specific recognition and sensing of the PPi anion in physiological conditions is highly desirable. However, owing to its high solvation energy (ΔG^o = - 465 KJ mol^{-1}) in water and low solubility of most of the organic probes designed for PPi sensing, bulk of the studies are confined to organic or mixed aqueous medium.[4-5] At this point, the metal-chemosensor ensemble based displacement approach for sensing anions is superior. This process works well in both organic and aqueous solvent regimes.[6-7] Interaction of the incoming guest anion with the metal-chemosensor ensemble causes distinguishable changes in optical spectra either through complete decomplexation of the chelated metal or by forming a new ensemble where the chemosensor, metal and incoming anion all are present together.

Realizing the metal ion chelating potential of the hydrazinobenzothiazole moiety (chapter 3), it is condensed with 2-hydroxynaphthyl aldehyde to synthesize a new chemosensor **L_2** [(E)-1-((2-(benzo[d]thiazol-2-yl)hydrazono)methyl)naphthalen-2-ol](Scheme 4.1). In this chemosensor

design, the benzothiazole unit is the binding site for metal ion while the naphthol is the signalling unit. The benzothiazole N and S; imine N are already known to bind metal ions. Furthermore, the OH group is expected to increase the number of binding sites as well as water solubility of the chemosensor, which is crucial for a realistic application of the chemosensor.

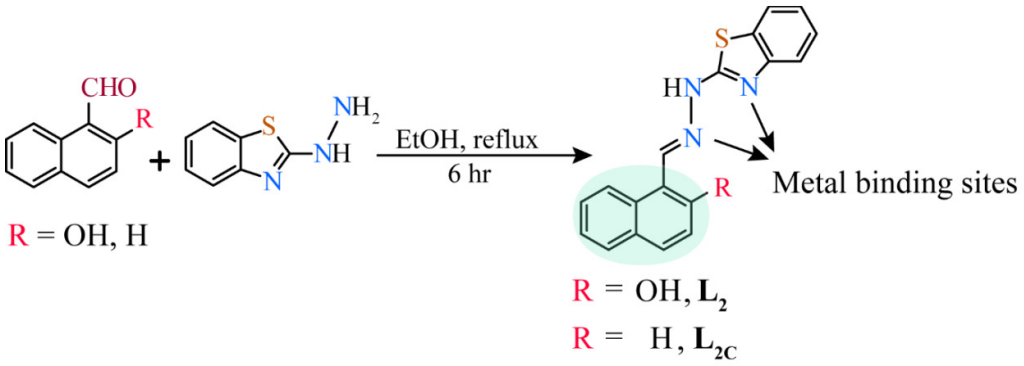

Scheme 4.1 Synthetic scheme of the probes **L2** and **L2C**.

4.2 UV−Vis Spectroscopic Studies Based Metal ions Sensing Aptitude of L2

The photophysical properties of the chemosensor (**L2**) are ascertained by UV-visible absorbance and fluorescence emission changes upon addition of various analytes. Chemosensor **L2** exhibits an absorption maximum at ~ 380 nm in CH_3OH/aqueous HEPES buffer (7:3 v/v) medium, which may be ascribed to the intra-molecular π---π* charge transfer (CT) transition (Figure 4.1a). The metal ion sensing potential of **L2** is analyzed with various metal ions such as Na^+, Mg^{2+}, Cr^{3+}, Hg^{2+}, Cu^{2+}, Pb^{2+}, Zn^{2+}, Fe^{3+}, Co^{2+}, Ni^{2+}, Cd^{2+} and Al^{3+} in the aforesaid buffer medium. It is interesting to observe that among the tested metal ions, addition of Zn^{2+}, Cd^{2+} and Cu^{2+} ions display notable changes in UV-Vis spectral pattern of **L2** (Figure 4.1a). Upon addition of 10 equivalents of Zn^{2+} ion to the buffer solution, there is new absorption maximum at 422 nm with the concurrent disappearance of the absorbance peak at 380 nm. Concomitantly, the visual colour of the studied solution is also changes from colourless to yellowish green type. Further, to get a quantitative appraisal of the specific interaction between Zn^{2+} and **L2**, a fresh solution of **L2** is titrated with varying concentrations of Zn^{2+} ion (0 to 4 equivalents) (Figure 4.1b). During this titration experiment, the absorbance peak at 380 nm decreases and simultaneously the 442 nm peak got intensified. Two prominent isosbestic points at 405 nm and 324 nm can be identified in the titration spectra which might be hinting toward a possible chelation between **L2** and Zn^{2+}. Again, due to the identical chemical behaviour also shown by Cd^{2+} ion, **L2** is also titrated with increasing concentrations of Cd^{2+} ion under the same experimental condition (Figure A4.1a). It exhibits a decrease in absorbance intensity at 380 nm with the increasing concentrations of Cd^{2+} ions under similar experimental conditions. Furthermore, the absorption spectra of the coloured **L2**-Cu^{2+} solution exhibits with two new absorption peaks at 423 nm and at 451 nm. This

suggests the formation of a new UV-active copper complex with **L2**. Subsequently, fluorescence emission and NMR changes are also recorded under similar experimental conditions.

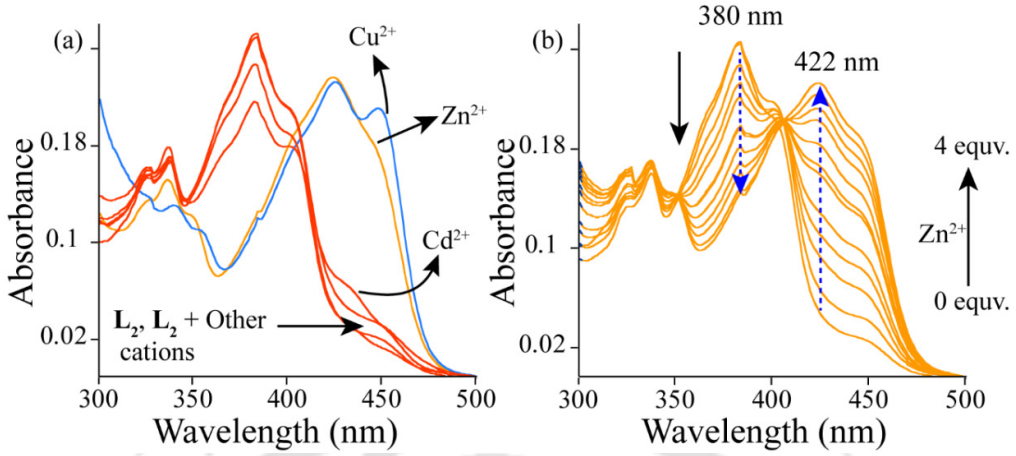

Figure 4.1 a) The UV-Visible changes of the receptor **L2** with various cations in the in a MeOH/aqueous HEPES buffer (5 mM, pH 7.3; 7:3, v/v) buffered solution. b) The titration spectra of **L2** with an incremental addition of Zn^{2+} ion.

4.3 Fluorescence Spectroscopic Changes of L2 in Presence of Metal ions

The naked chemosensor **L2** is weakly fluorescent when excited at 380 nm under the aforementioned experimental medium. But, the emission spectra exhibits dual emission peaks nearly at 426 nm and at 495 nm which are attributed to the possible keto-enol tautomerism in the system originating from the formation of a six membered ring. The lower wavelength band is for the enol form of the receptor whereas the keto tautomer is responsible for the higher energy emission.[8-9] Concerning the UV-Vis responses of Zn^{2+}, Cd^{2+} and Cu^{2+} ions towards **L2**, the aforementioned ions are first treated with **L2**. Likewise the UV-Vis spectra, addition of excess of Zn^{2+} (10 equivalents) to the **L2** solution renders a remarkable enhancement in the fluorescence intensity of **L2** along with the generation of a new 15 nm red shifted emission maximum at 510 nm (quantum yield = 0.13) as shown in figure 4.2a. The solution thus emits a yellowish green light from a completely dark solution under the 365 nm UV light chamber (Figure 4.2c). Thus, the present chemosensor also enables naked eye detection of Zn^{2+}. Owing to similar electronic configurations, cadmium ion also triggered the emission at 510 nm. However, the increment in the emission intensity is comparatively less than that of Zn^{2+} (Figure 4.2b). Although Cu^{2+} has shown some colorimetric responses, the addition of Cu^{2+} solution fail to induce any change in emission spectra of **L2** (Figure 4.2a). Similarly, the emission spectra of **L2** is not affected by the presence of other metal ions such as Na^{+}, Mg^{2+}, Cr^{3+}, Hg^{2+}, Pb^{2+}, Fe^{3+}, Co^{2+}, Ni^{2+} and Al^{3+} (Figure 4.2a).

Subsequently, to understand the binding mechanism more precisely we have pursued titration experiments of the chemosensor with the sequentially added Zn^{2+} and Cd^{2+} ion under similar

experimental conditions. These titration spectra explain a linear enhancement in the emission intensity of **L2** at 510 nm with the gradual increase in concentrations of Zn^{2+} and Cd^{2+} ions (Figure 4.3a and A4.1b). Job's plots are derived from these titration data and this suggest 1:1 host-guest binding in both the cases (Figure A4.2). The corresponding binding constants are calculated using Benesi-Hildebrand equation and found to be 1.11×10^5 M^{-1} and 1.0×10^5 M^{-1} for Zn^{2+} and Cd^{2+} respectively (Figure A4.2). The detection limits are determined using the $3\sigma/K$ method, and found to be 5.8×10^{-8} M and 4.7×10^{-8} M for Zn^{2+} and Cd^{2+} ions respectively (Figure A4.3).

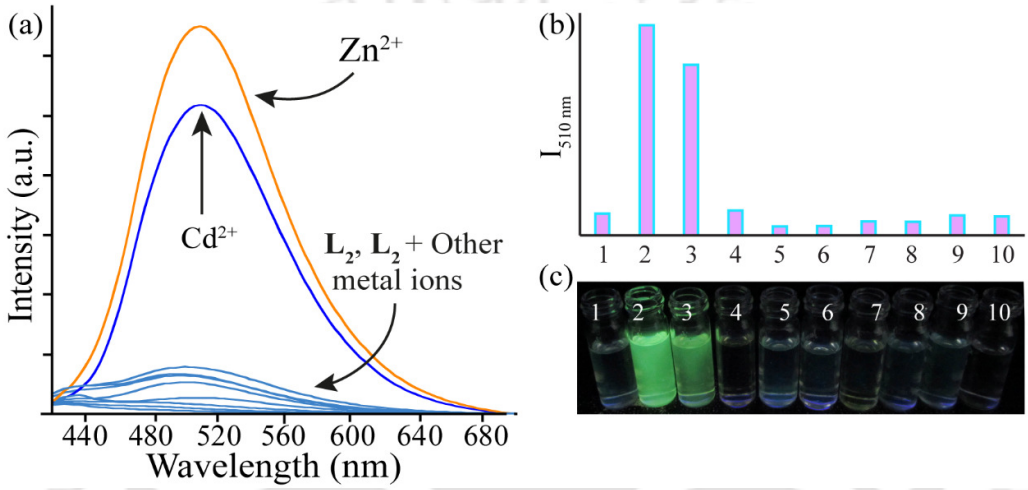

Figure 4.2 a) Variation in fluorescence emissions of **L2** with different metal ions and b) bar plot presentation of the same at λ_{em} = 510 nm. c) The visual colour change experiment of **L2** with various metal ions under the UV chamber (λ_{ex} = 365 nm). (1= **L2**, 2 = **L2** + Zn^{2+}, 3 = **L2** + Cd^{2+}, 4 = **L2** + Al^{3+}, 5 = **L2** + Cu^{2+}, 6 = **L2** + Co^{2+}, 7 = **L2** + Ni^{2+}, 8 = **L2** + Fe^{3+}, 9 = **L2** + Pb^{2+}, 10 = **L2** + Hg^{2+}) (λ_{ex} = 380 nm, slit = 3 nm/ 3 nm).

For the selective 'turn-on' fluorescence with red shifting of λ_{max} upon Zn^{2+} and Cd^{2+} ions chelation with **L2**, several factors can be listed to rationalize the findings. PET (photo induced electron transfer) from nitrogen of benzothiazole to the naphthyl fluorophore and the cis-trans isomerization around the C=N bond of **L2** may be accountable for the initial weak fluorescence of **L2**. The hydroxyl group seems to play an important role in the recognition and sensing of the Zn^{2+} and Cd^{2+} ions, as the control receptor **L2c**, which devoid of OH group is fails to show any selectivity towards the aforementioned cations (Figure A4.4). Thus, the OH group probably strengthens the ultimate metal-chemosensor complexes. Further to validate this binding process, we have also carried out the ^1H NMR titrations with Zn^{2+} and Cd^{2+} ions, and the results thus obtained are discussed later in the NMR binding section.

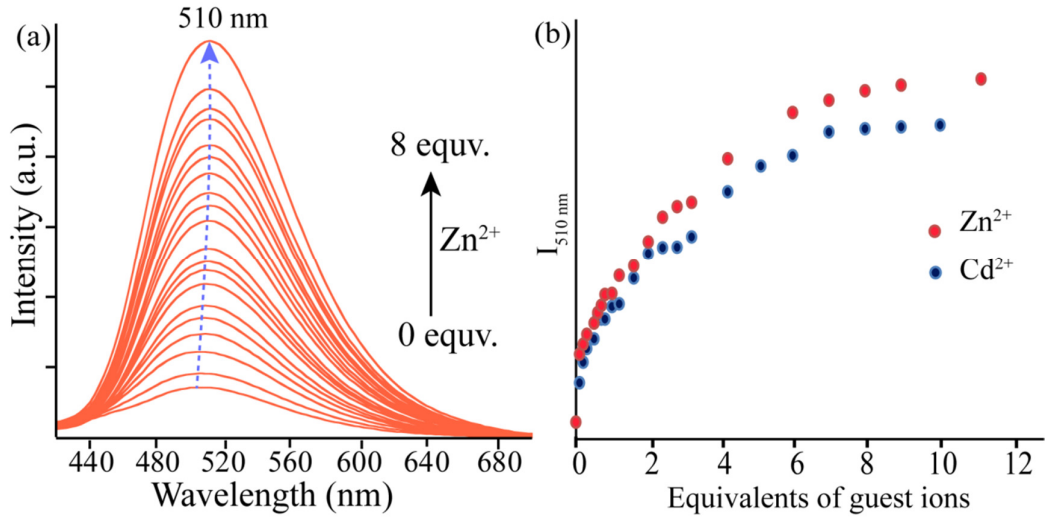

Figure 4.3 a) Fluorescence titration experiment of **L2** with increasing concentrations of Zn^{2+} ions. b) Correlation of fluorescence emission intensity at 510 nm versus the equivalents of guest metal ions (λ_{ex} = 380 nm, slit = 3 nm/3 nm).

Again, the fluorescence emission intensity also increases upon addition of Zn^{2+} to the already flourish Cd^{2+} added **L2** solution. Similarly, the emission intensities of the '**L2**-Zn^{2+}' ensembles do not vary much upon addition of other competitive metal ions except Cu^{2+} (Figure A4.5). Most importantly, higher concentrations (1 mM) of Ca^{2+}, Mg^{2+}, Na^{+} and K^{+} which generally coexist with Zn^{2+} in the biological systems did not interfere in the sensing of Zn^{2+} under the same physiological conditions. Again, the intracellular Zn^{2+} sensing behaviour of **L2** will not be interfered by Cd^{2+} due to its extremely low intracellular concentration level. Thus, all these experimental results recommends the present chemosensor as a potential Zn^{2+} sensor.

4.4 NMR Binding study

We have also recorded ^{1}H NMR of **L2** with varying concentrations of Zn^{2+} and Cd^{2+} ions in mixed $CDCl_3$-DMSO(d_6) solutions for further insight into the binding events of **L2** with the aforementioned cations. Subsequently, some changes in the positions of NMR peaks are recorded. It is the imine proton CH(b) and benzothiazole proton CH(c), which exhibit small but significant downfield shifts after addition of Zn^{2+} ion. Similarly, a distinguishable broadening and downfield movement of OH proton CH(a) is also recorded after addition of Zn^{2+} ion. This occurs probably due to the decrease in electron density at these positions due to cation coordination, which suggests the involvement of hydroxyl, imine and benzothiazole functionalities of **L2** in Zn^{2+} complexation (Figure A4.6). Thus, this chelation mode inhibits the C=N isomerisation and PET process, and fluorescence intensity increases as a result of CHEF mechanism (Scheme 4.2). Similarly, after addition of more than one equivalent Cd^{2+} ion to **L2**, the OH peak becomes broad, imine proton and aromatic protons of benzothiazole group exhibit

small but significant downfield shifts. Thus, probably the Cd^{2+} ion is also coordinated to the **L2** in the same tridentate fashion. However, the respective chemical shifts for the Cd^{2+} titration are smaller than that of Zn^{2+}, which reflects the relatively weaker binding of Cd^{2+} than Zn^{2+} ion.

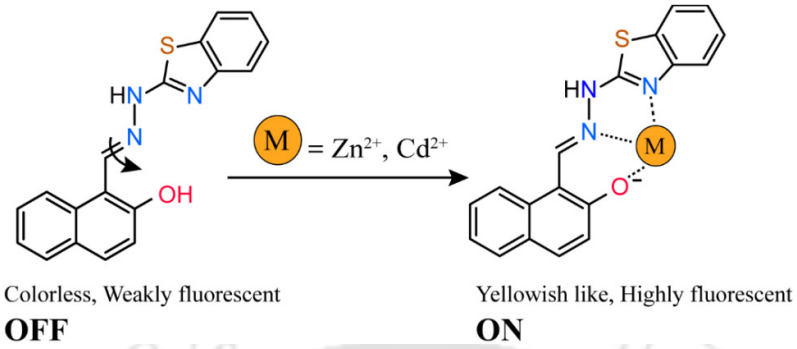

Scheme 4.2 Plausible binding mechanism of **L2** with Zn^{2+} and Cd^{2+}.

4.5 Fluorescence Based Selectivity of the 'L2-Zn^{2+}/Cd^{2+}' Ensembles towards Anions

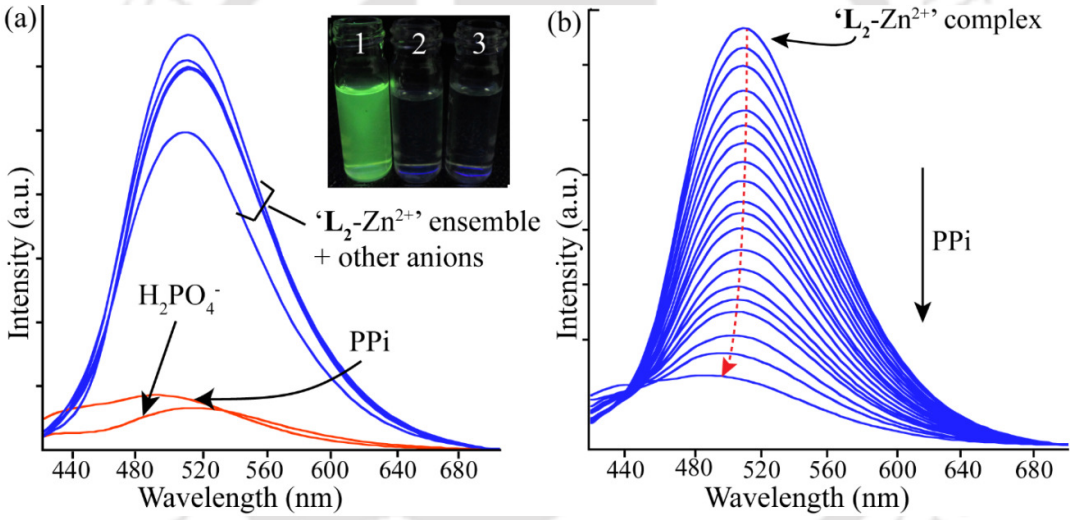

Figure 4.4 a) Fluorescence emission responses of '**L2**-Zn^{2+}' ensembles with various anions. **Inset**: Visual Colour change experiment of (1) '**L2**-Zn^{2+}' ensemble with (2) PPi and (3) $H_2PO_4^-$ (λ_{ex} = 365 nm). b) Fluorescence emission titration of '**L2**-Zn^{2+}' ensembles with incremental addition of PPi in methanolic buffer solution (λ_{ex} = 380 nm, slit = 3 nm/ 3 nm).

Finally, the anion sensing aptitude of the chemosensor is checked with F^-, Cl^-, Br^-, I^-, CN^-, CO_3^{2-}, HCO_3^-, CH_3COO^-, NO_3^-, SO_4^{2-}, $H_2PO_4^-$, ATP, ADP, PPi etc. anions in the same experimental medium. At first, the naked chemosensor fails to produce any distinguishable change with any of those aforementioned anions (Figure A4.7), thus metal-chemosensor ensembles are next tested. As depicted in figure 4.4a, among the anions only PPi and $H_2PO_4^-$ produce a distinguishable change in the fluorescence emission intensity of '**L2**-Zn^{2+}' ensemble. Both the anions display 'turn-off' fluorescence character to the metal ensembles while all other anions are insensitive to the ensembles. Hereafter to unveil the binding interactions between the guest

anion and the ensemble, the '**L**$_2$-Zn^{2+}' ensemble is titrated with of each of $H_2PO_4^-$ and PPi. The ensembles quickly response to the presence of those anions as the fluorescence emission intensities at 510 nm decrease rapidly (Figure 4.4b and A4.8a). Further, a plot of fluorescence emission intensity at 510 nm against the number equivalents of the guest anions ($H_2PO_4^-$ and PPi), represent nearly a straight line after 2 equivalents of $H_2PO_4^-$ and PPi (Figure A4.8b). The binding stoichiometry is calculated using Job's plot analysis and found to be 1:1 host-guest binding in every cases (Figure A4.9). The calculated binding constants from these titration experiments for PPi and $H_2PO_4^-$ are 2×10^5 M^{-1} and 3.3×10^5 M^{-1} respectively (Figure A4.9). Again, the lowest detection limit for PPi and $H_2PO_4^-$ detection with the '**L**$_2$-Zn^{2+}' ensembles are 1.547×10^{-7} M and 1.083×10^{-7} M respectively based on 3σ/K method. Further, to understand the sensitivity of the ensemble in detecting PPi and $H_2PO_4^-$, fluorescence of the ensembles are also recorded in a mixed anionic environment where all the anions are also present. Much to our delight, the '**L**$_2$-Zn^{2+}' ensemble can detect PPi and $H_2PO_4^-$ in these competitive environment also (Figure A4.8c). Similarly, the Cd^{2+} ensemble of **L**$_2$ also responds to $P_2O_7^{4-}$ and $H_2PO_4^-$ anions as 'turn-off' sensor. From the titration experiments of the flourish Cd^{2+} ensemble with PPi and $H_2PO_4^-$ (Figure A4.10), the calculated binding constants are 1.6×10^5 M^{-1} and 5×10^3 M^{-1} respectively with 1:1 stoichiometry in every cases (Figure A4.11). Other tested anions which include F^-, Cl^-, Br^-, I^-, CN^-, CO_3^{2-}, HCO_3^-, CH_3COO^-, NO_3^-, SO_4^{2-}, ATP and ADP; could not change the fluorescence intensity even at higher mole ratios. Furthermore, to understand the reason behind the fluorescence quenching behaviour of the ensemble towards $P_2O_7^{4-}$ and $H_2PO_4^-$, UV-Vis changes of the solutions are also recorded.

4.6 Absorbance Studies of the 'L$_2$-Zn^{2+}' Ensembles with Anions

The UV-vis pattern of the PPi ($P_2O_7^{4-}$) and $H_2PO_4^-$ added solutions are different from that of the '**L**$_2$-Zn^{2+}' ensemble (Figure A4.12). Apart from that, we have also noticed visual colour changes of the solutions. The yellowish like Zn^{2+} containing solutions of the **L**$_2$ are instantly changed into colourless solutions after addition of PPi and $H_2PO_4^-$ (Inset figure A4.12b). During the incremental addition of PPi to the '**L**$_2$-Zn^{2+}' ensemble, the absorbance values at 422 nm are constantly decreases but a new peak at 380 nm get intensified. The resulting spectra is reminiscent to the free **L**$_2$ (Figure A4.12), which suggests the possibility of PPi induced dissociation of coloured zinc complex triggering the free chemosensor **L**$_2$ into the solution. The higher stability of the resulting Zn^{2+}-PPi complex could be the driving force for this decomplexation process. We anticipate the same process to occur after the addition of $H_2PO_4^-$ ion to the coloured '**L**$_2$-Zn^{2+}' ensemble, as the resulting absorption spectra of the colourless solution reinstate to the free receptor with the characteristic peak at 380 nm (Figure A4.12).

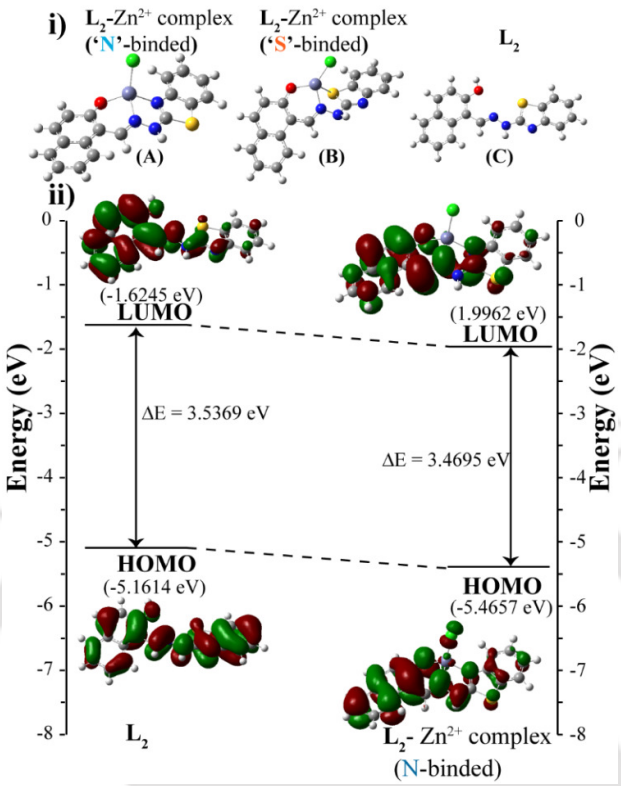

Figure 4.5 (i) Optimized structure of **L2** and its Zn^{2+} complexes (both 'N' and 'S' coordinated). (ii) Energy diagrams of HOMO and LUMO orbitals of **L2** and the **L2**-Zn^{2+} ('N'-coordinated) complex calculated at the DFT level using a B3LYP/6-31+G(d,p) basis set.

4.7 Theoretical Calculations

To understand the relationship between the structural changes of **L2** on its complexation with Zn^{2+} and the optical response of **L2** to Zn^{2+}, we carried out density functional theory (DFT) calculations with the B3LYP/6-31+G(d,p) method basis set using the Gaussian 03 program. Selected orbitals and their energies for **L2** are presented in the supporting information (Figure A4.14). It is evident from the Job's plot, NMR titration and mass spectra that **L2** is forming a 1:1 complex with Zn^{2+}. As there are two potential chelating sites in the benzothiazole group of **L2**, one through 'N' and other through 'S', it is important to find out which one of them is actually coordinating to the zinc ion. We have explored both the structural possibility with the DFT optimization using B3LYP/6-31+G(d,p) method basis set implemented on the Gaussian 03.[10] In the first proposed structure (structure A of the Figure 4.5), the coordination of Zn^{2+} is through benzothiazole nitrogen while in the second proposed structure (structure B of the Figure 4.5) metal ion is coordinated to the sulphur of benzothiazole. In both the cases the other binding units are Schiff base N and phenolic OH which mostly bind as phenoxide anion. The calculated lower in energy (10.96 kcal/mol) of structure A than B strongly favored the zinc ion coordination to

nitrogen of benzothiazole of **L2** (Table A4.1). Also the bond length in the case of structure A is shorter than structure B. The optimized geometry and the highest occupied molecular orbital (HOMO) and the lowest unoccupied molecular orbital (LUMO) of **L2** and its Zn^{2+} complexes are presented in Figure 4. There is a small lowering in the HOMO to LUMO energy gap from **L2** to its Zn^{2+} complex, which probably assists the small red shift in the fluorescence spectra of **L2** upon Zn^{2+} complexation. Selected orbitals and their energies for **L2**-Zn^{2+} complex are presented in the supporting information which are associated with the key electronic transitions and there by displaying these selective spectral outcomes (Figure A4.15).

4.8 Reversible Binding and Interpretation of Related Logic Gates

The chemosensor **L2** has been found to be reversible and recyclable towards Zn^{2+} and PPi ions over more than six cycles (Figure 4.6) which minimum loss in fluorescence intensities. Such distinct chemical behaviour (output) of intelligent molecules upon addition of different chemicals (input) are further useful to construct various fluorescent logic gates such as the AND, OR, NOR, INHIBIT, XOR, YES, NOT, and XNOR.[11-13] The output states (0 or 1) of such molecular switches are dependent on the inputs only (0 or 1). Such basic logic gates, programmed in a single molecular chemosensor, are interesting in the development of electronic and photonic devices. Thus, we focus on the fluorescence signal output at 510 nm after addition of the inputs Zn^{2+} and $P_2O_7^{4-}$ to **L2**.

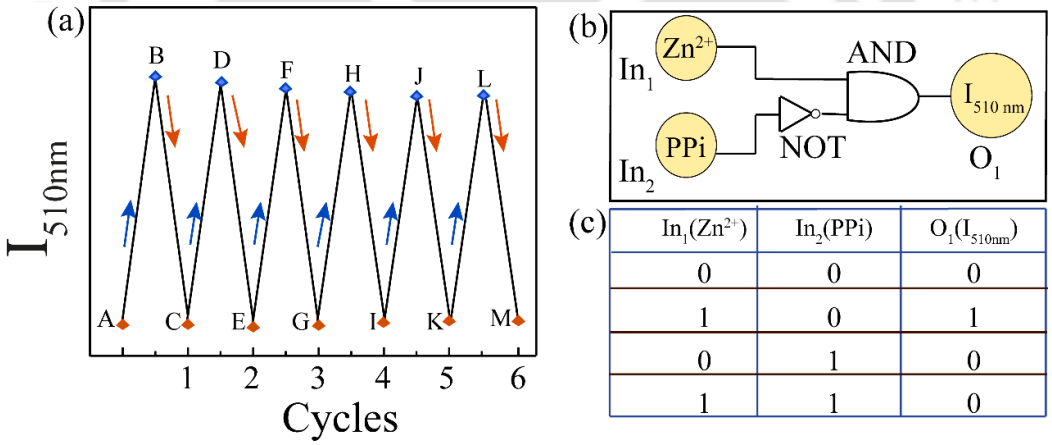

$In_1(Zn^{2+})$	$In_2(PPi)$	$O_1(I_{510nm})$
0	0	0
1	0	1
0	1	0
1	1	0

Figure 4.6 (a) Reversible and recyclable behaviour of **L2** for Zn^{2+} and PPi (A = **L2**, B = [A + Zn^{2+}], C = [B + PPi], D = [C + Zn^{2+}], E = [D + PPi], F = [E + Zn^{2+}], G = [F + PPi], H = [G + Zn^{2+}], I = [H + PPi], J = [I + Zn^{2+}], K = [I+ PPi], L = [K+ Zn^{2+}], M = [L+ PPi]). (b) Representation of a two-state molecular switch based on INHIBIT logic function. (c) The truth table with the inputs Zn^{2+} and PPi.

For the 'turn-on' fluorescence at 510 nm the output is '1' and for the 'turn-off' nature it is '0'. Again when both the inputs Zn^{2+} and PPi are absent, then they are read as '0' and for their presence the inputs are '1'. When both the inputs are '0', the output signal is also '0' and the gate is OFF. PPi alone does not show any fluorescence change and thus the output signal is '0'.

On the other hand Zn^{2+} alone enhances the fluorescence significantly, and the output signal is read out as '1' and the gate is ON. However, when both the inputs are present together, then the output was '0' and the gate was OFF. These studies clearly demonstrate a INHIBIT logic gate for these ions at 510 nm (Figure 4.6b).

4.9 Paper Strip with Zn^{2+}

Encouraged by the positive response of **L_2** towards Zn^{2+}, we have developed a test kit for the practical application of the sensor.[14] At first ligand-coated filter paper strips are prepared by immersing them into a **L_2** solution (2.0 mM) in methanol and air-dried. After that the strips are dipped directly into aqueous methanolic solutions containing Zn^{2+} ions which are carried upward by capillary action of the solvent. After the solvent front reached a certain height, the strips are taken out, dried with a blow-drier, and the paper held under 365 nm fluorescent light. In presence of Zn^{2+}, we envision that the formed complex with **L_2** moved further up and display a bluish green fluorescence (Figure A4.16).

4.10 Conclusion

In conclusion, the present chemosensor can selectively sense both biologically important Zn^{2+} and deleterious Cd^{2+} ion though 'turn-on' fluorescence emissions, which thus enable rapid naked eye detection of the ions. Compared to the **L_1** in chapter 3, the present chemosensor (**L_2**) is more potent Zn^{2+} sensor with higher binding constant even in the mixed buffer medium. Again, proving the higher affinity of **L_2** for Zn^{2+} ion, fluorescence also increases after addition of Zn^{2+} to an already flourish Cd^{2+}-**L_2** solution. The sensitive sensing of Zn^{2+} is also possible in presence of other biologically important cations except copper. ^{1}H NMR titration and theoretical calculations suggest the involvement of benzothiazole N, Schiff base N and phenolic OH, in binding with Zn^{2+} ion. The calculated lowest limit of Zn^{2+} and Cd^{2+} detection by **L_2** is 5.8×10^{-8} M and 4.7×10^{-8} M respectively. Further, both the zinc and cadmium ensembles of **L_2** respond to $H_2PO_4^-$ and PPi anions in the same buffered medium as 'turn-off' sensors. Chemosensor **L_2** is also reversible and recyclable towards Zn^{2+} and pyrophosphate ions over more than six cycles and responds to a INHIBIT logic gate. In addition, the present study demonstrates the utility of solution-coated dip paper strips of **L_2** for rapid and easy detection of Zn^{2+} ion.

References

1. H. N. Kim, W. X. Ren, J. S. Kim and Juyoung Yoon, *Chem. Soc. Rev.*, 2012, **41**, 3210-3244.
2. G. F. Nordberg, R. F. M. Herber and L. Alessio, Cadmium in the Human Environment, Oxford University Press, Oxford, UK, 1992.
3. Agency for Toxic Substances and Disease Registry, 4770 Buford Hwy NE, Atlanta, GA 30341. http://www.atsdr.cdc.gov/cercla/07list.html.
4. S. K. Kim, D. H. Lee, J. I. Hong, J. Yoon, *Acc. Chem. Res*., 2009, **42**, 23-31.
5. S. Xu, M. He, H. Yu, X. Cai, X. Tan, B. Lu, B. Shu, *Anal. Biochem*., 2001, **299**, 188-193.
6. N. Busschaert, C. Caltagirone, W. V. Rossom and P. A. Gale, *Chem. Rev.,* 2015, **115**, 8038-8155.
7. X. Lou, D. Ou, Q. Li and Z. Li, *Chem. Commun.,* 2012, **48**, 8462-8477.
8. V. Bhalla, M. Kumar, *Org. Lett*., 2012, **14**, 2802-2805.
9. W. H. Ding, W. Cao, X. J. Zheng, D. C. Fang, W. T. Wong and L. P. Jin, *Inorg. Chem*. 2013, **52**, 7320-7322.
10. M. J. Frisch, G. W. Trucks, H. B. Schlegel, G. E. Scuseria, M. A. Robb, J. R. Cheeseman, J. A. Montgomery, Jr., T. Vreven, K. N. Kudin, J. C. Burant, J. M. Millam, S. S. Iyengar, J. Tomasi, V. Barone, B. Mennucci, M. Cossi, G. Scalmani, N. Rega, G. A. Petersson, H. Nakatsuji, M. Hada, M. Ehara, K. Toyota, R. Fukuda, J. Hasegawa, M. Ishida, T. Nakajima, Y. Honda, O. Kitao, H. Nakai, M. Klene, X. Li, J. E. Knox, H. P. Hratchian, J. B. Cross, V. Bakken, C. Adamo, J. Jaramillo, R. Gomperts, R. E. Stratmann, O. Yazyev, A. J. Austin, R. Cammi, C. Pomelli, J. W. Ochterski, P. Y. Ayala, K. Morokuma, G. A. Voth, P. Salvador, J. J. Dannenberg, V. G. Zakrzewski, S. Dapprich, A. D. Daniels, M. C. Strain, O. Farkas, D. K. Malick, A. D. Rabuck, K. Raghavachari, J. B. Foresman, J. V. Ortiz, Q. Cui, A. G. Baboul, S. Clifford, J. Cioslowski, B. B. Stefanov, G. Liu, A. Liashenko, P. Piskorz, I. Komaromi, R. L. Martin, D. J. Fox, T. Keith, M. A. Al-Laham, C. Y. Peng, A. Nanayakkara, M. Challacombe, P. M. W. Gill, B. Johnson, W. Chen, M. W. Wong, C. Gonzalez, and J. A. Pople, Gaussian 03, Revision E.01,Gaussian, Inc., Wallingford CT, 2004.
11. P. Mahato, S. Saha and A. Das, *J. Phys. Chem. C,* 2012, **116**, 17448-17457.
12. Y. Xianyu, K. Zhu, W. Chen, X. Wang, H. Zhao, J. Sun, Z. Wang and X. Jiang, *Anal. Chem*., 2013, **85**, 7029-7032.
13. A. K. Mandal, P. Das, P. Mahato, S. Acharya and A. Das, *J. Org. Chem*., 2012, **77**, 6789-6800.
14. J. Hatai, S. Pal, G. P. Jose and S. Bandyopadhyay, *Inorg. Chem*., 2012, **51**, 10129-10135.

Appendix 3

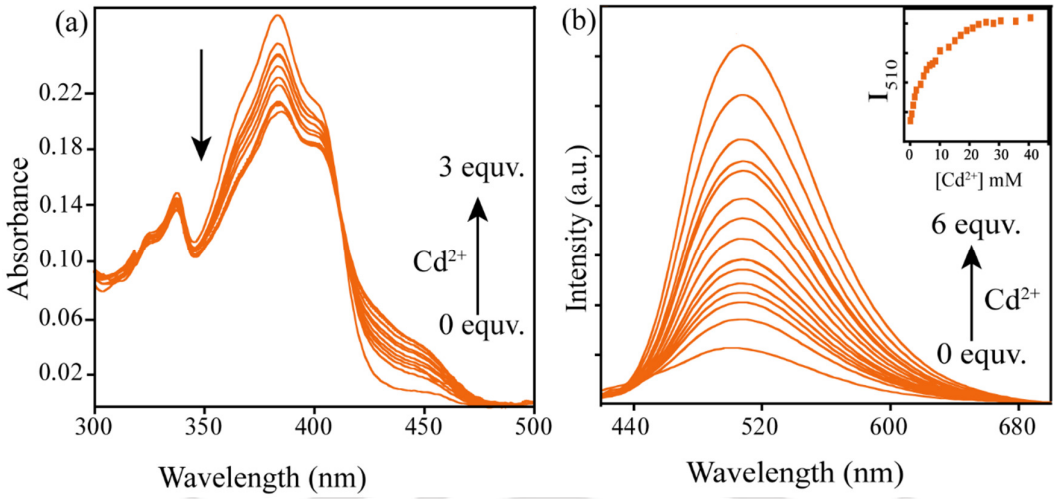

Figure A4.1 The UV-Visible and b) fluorescence titration spectra of **L₂** with increasing concentrations Cd^{2+} ions in the buffered experimental medium.

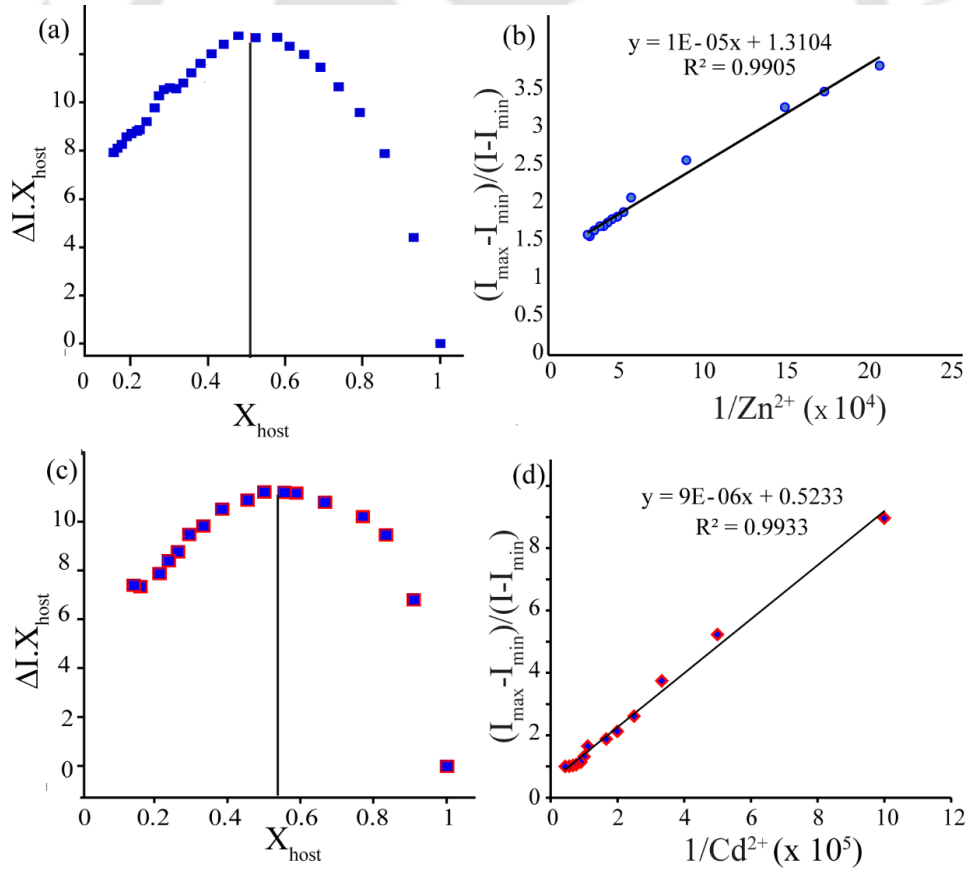

Figure A4.2 Job's plots for the binding of **L₂** with (a) Zn^{2+} and (c) Cd^{2+}. The corresponding Bensei-Hildebrand plots are b) and d) for Zn^{2+} and Cd^{2+} respectively.

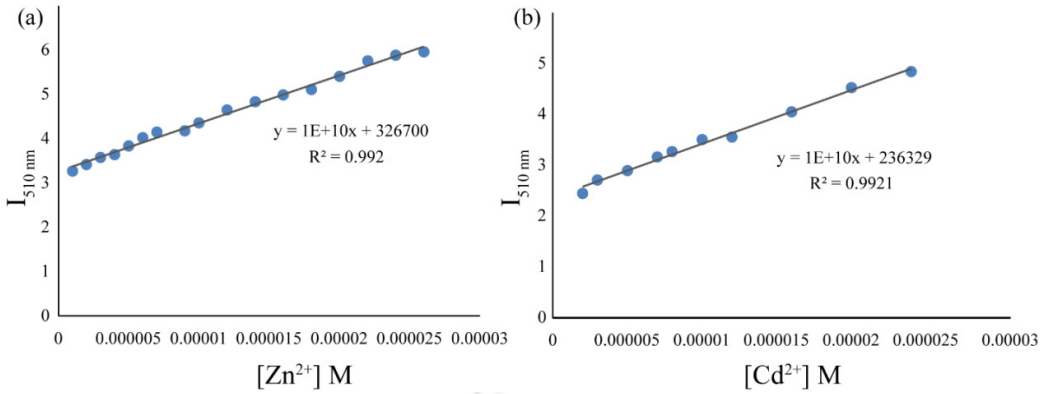

Figure A4.3 Intensity versus concentration (in molar) plots for LOD calculation for a) Zn^{2+} and b) Cd^{2+} ions.

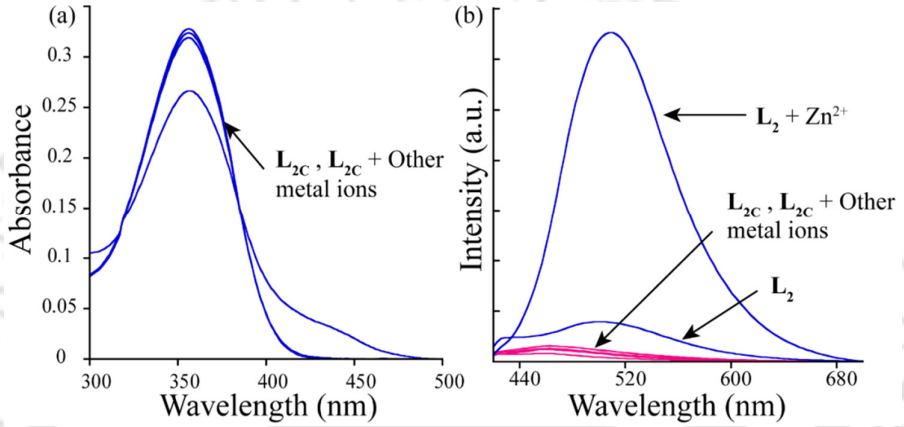

Figure A4.4 The a) UV-vis and b) fluorescence emission changes to $\mathbf{L_{2C}}$ with various metal ions in the same experimental medium.

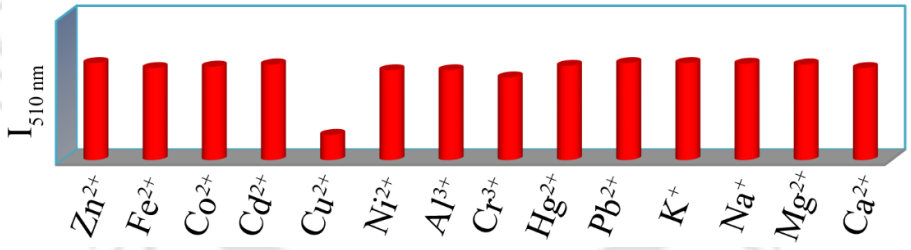

Figure A4.5 Zn^{2+} binding potential of $\mathbf{L_2}$ in a competitive environment of metals.

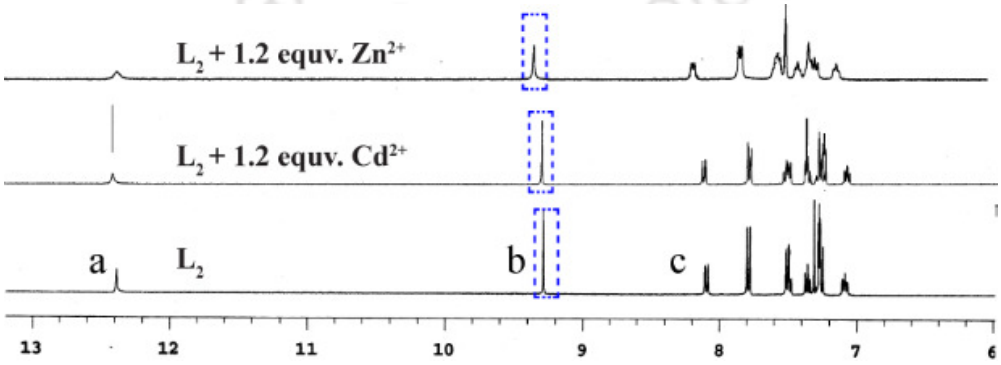

Figure A4.6 ^{1}H NMR stack plots of $\mathbf{L_2}$ with Zn^{2+} and Cd^{2+} ions in DMSO-d_6 at room temperature.

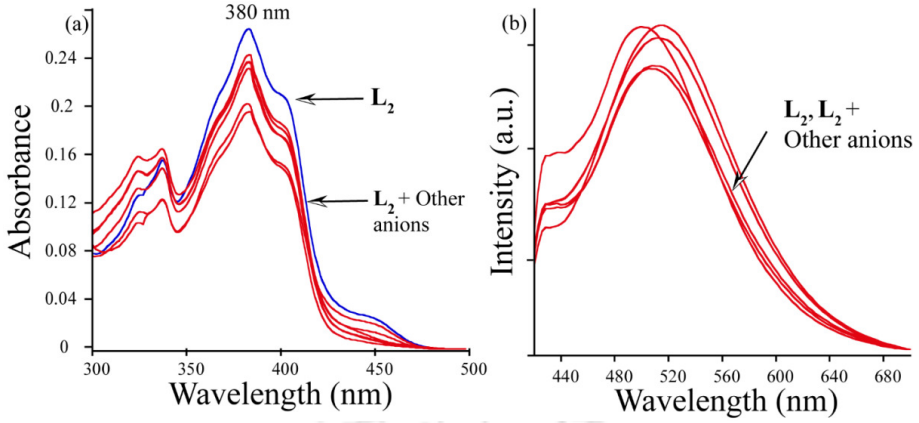

Figure A4.7 a) UV-Vis and b) fluorescence emission changes of chemosenor **L2** upon addition of various anions in the methanolic buffer medium.

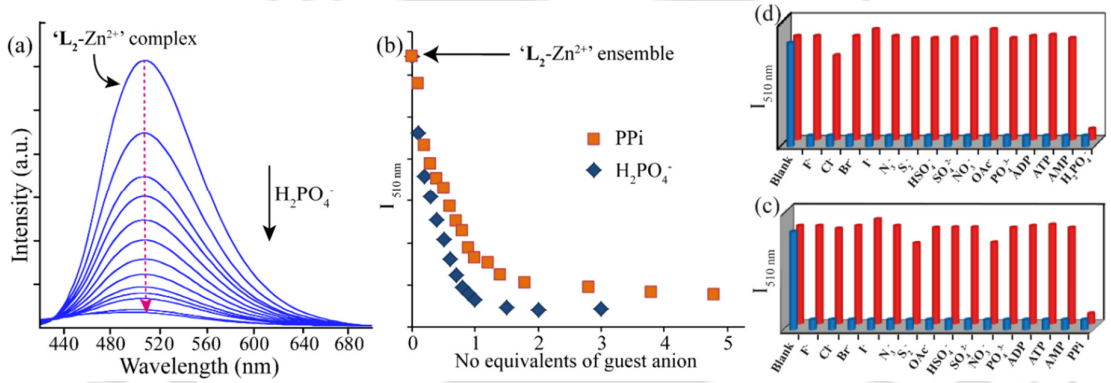

Figure A4.8 a) Fluorescence emission titration of '**L2**-Zn^{2+}' ensemble with increasing concentrations of $H_2PO_4^-$. b) Comparison of variation in fluorescence intensity changes at 510 nm against the guest anion concentrations (in equivalents). c) PPi and d) $H_2PO_4^-$ sensing potential of the '**L2**-Zn^{2+}' ensembles in a competitive medium when other anions are also present (Red bars represents the individual fluorescence emission intensities of the '**L2**-Zn^{2+}' ensembles with various anions at 510 nm while the changes in presence of PPi/ $H_2PO_4^-$ are presented by blue bars).

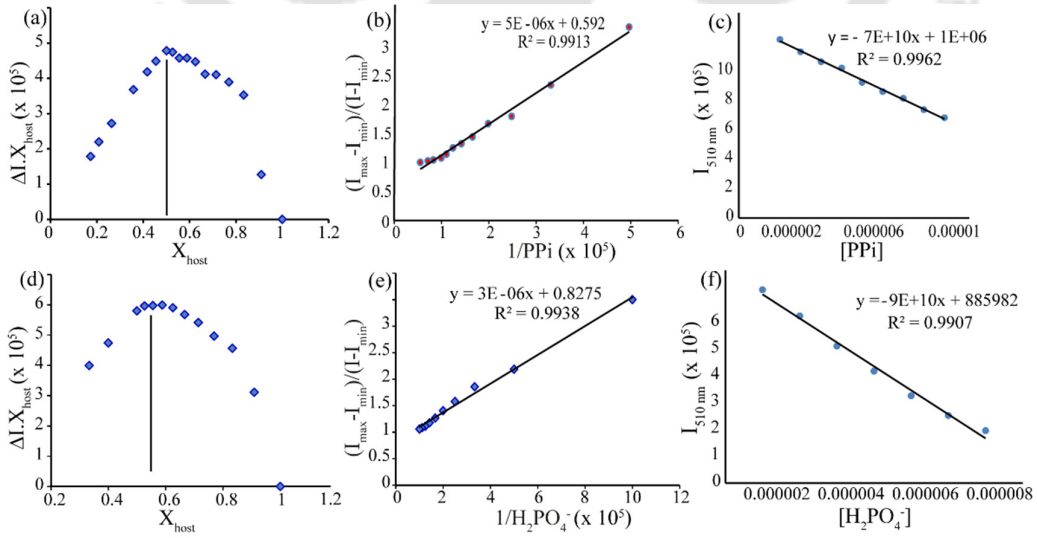

Figure A4.9 a) The Job's plot and the corresponding b) B. H. plot for the titration of PPi with '**L2**-Zn^{2+}' ensemble. The d) Job's plot and e) B.H. plot for the titration of $H_2PO_4^-$ with '**L2**-Zn^{2+}' ensemble. Intensity versus concentration (molar) plots for LOD calculations of c) PPi and f) $H_2PO_4^-$ with '**L2**-Zn^{2+}' ensembles.

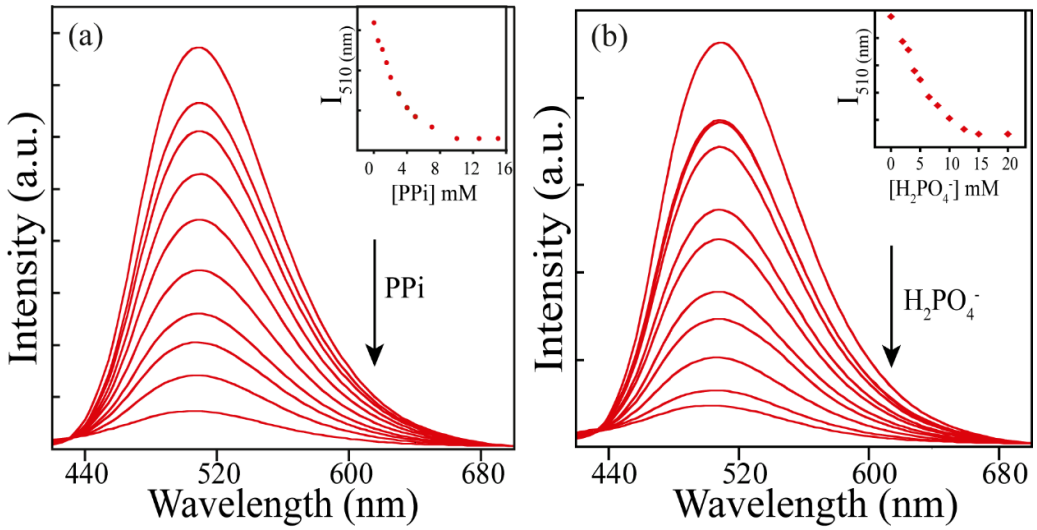

Figure A4.10 Fluorescence titrations of '**L**$_2$-Cd^{2+}' ensemble with increasing concentrations of a) PPi and b) $H_2PO_4^-$.

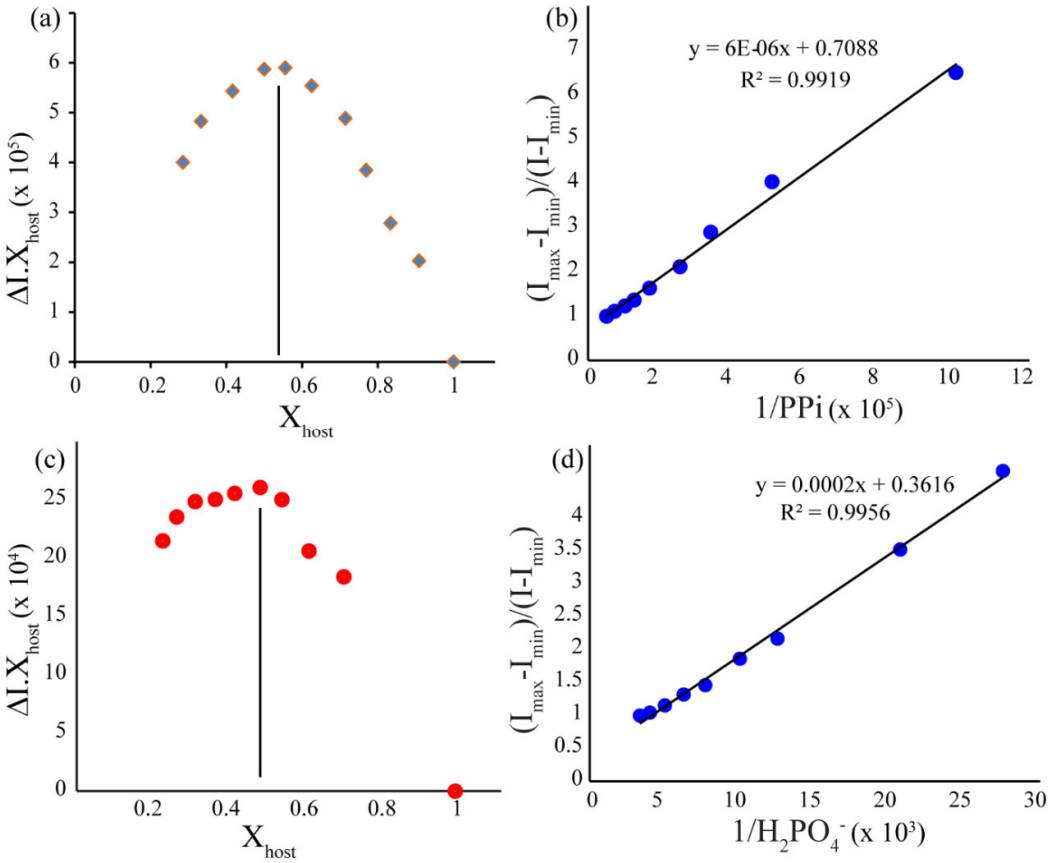

Figure A4.11 a) The Job's plot and the corresponding b) for the titration of PPi with '**L**$_2$-Cd^{2+}' ensemble. The c) Job's plot and d) B.H. plot for the titration of '**L**$_2$-Cd^{2+}' ensembles with $H_2PO_4^-$.

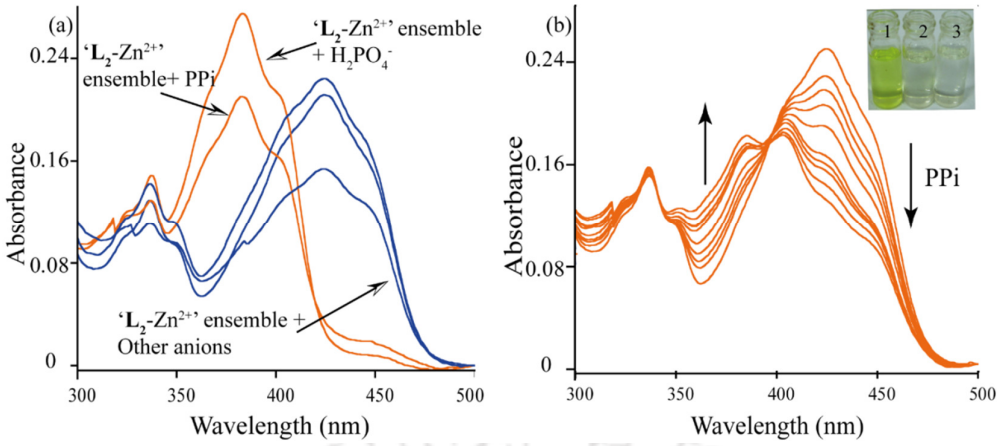

Figure A4.12 a) UV-vis changes of '$\mathbf{L_2}$-Zn^{2+}' ensemble with few selected anions. b) UV-Vis titration of '$\mathbf{L_2}$-Zn^{2+}' ensemble with increasing concentrations of PPi. Inset: Colour change after addition of PPi (2) and $H_2PO_4^-$(3) to '$\mathbf{L_2}$-Zn^{2+}' ensemble (1).

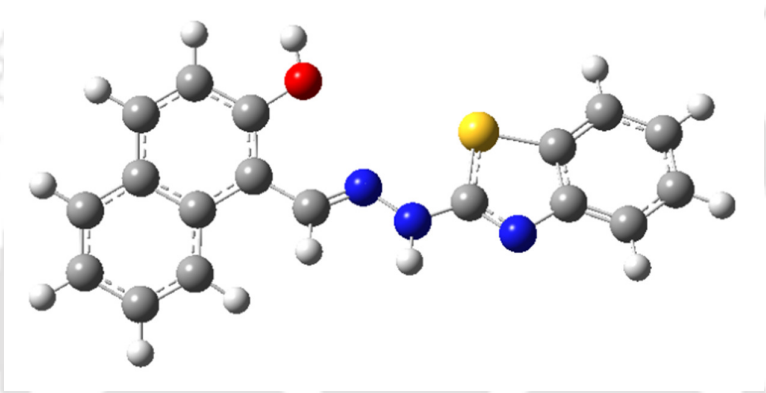

Figure A4.13 Optimized structure of $\mathbf{L_2}$ at B3LYP/6-31+G(d,p).

Occupied Orbitals	Energy (eV)	Vacant Orbitals	Energy (eV)
HOMO -2 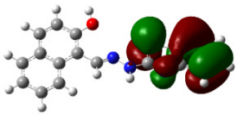	-6.0610	LUMO 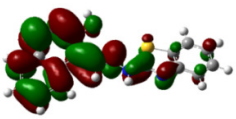	-1.6245
HOMO -1 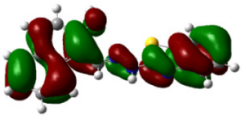	-5.9979	LUMO+1 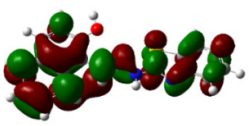	-0.5303
HOMO 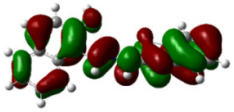	-5.1614	LUMO+2 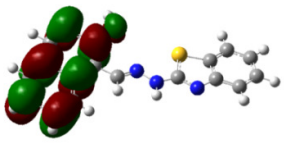	-0.2609

Figure 4.14 Selected orbitals and their energies of $\mathbf{L_2}$ at B3LYP/6-31+G(d,p).

Occupied Orbitals	Energy (eV)	Vacant Orbitals	Energy (eV)
HOMO -2 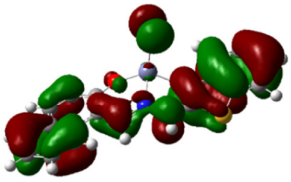	-6.5465	LUMO 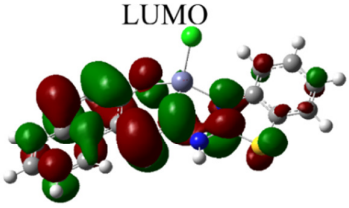	-1.9962
HOMO -1 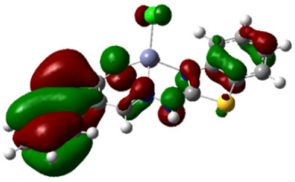	-6.2417	LUMO+1 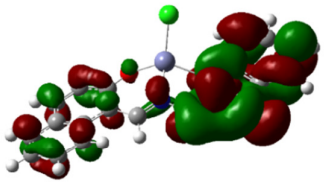	-1.0364
HOMO 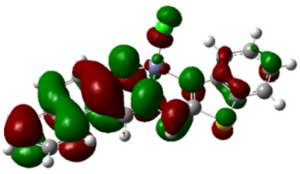	-5.4657	LUMO+2 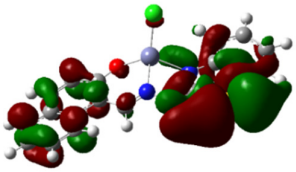	-0.8542

Figure 4.15 Selected orbitals and their energies of L_2-Zn^{2+}complex ('N'- coordinated) at B3LYP/6-31+G(d,p).

Molecule	Total Energy (a.u.)
L_2	-1331.41667814
L_2-Zn^{2+} Complex (N-Coordinated) [Structure(A)]	-3570.27462417
L_2-Zn^{2+} Complex (S-Coordinated) [Structure(B)]	-3570.25729119

(Structure A is more stable by 10.96 kcal/mole than the structure B.)

Table A4.1 Calculated absolute energies in a.u. B3LYP/6-31+G(d,p).
Coordinates for optimized geometry of L_2 at B3LYP/6-31+G(d,p).

Center Number	Atomic Number	Atomic Type	Coordinates (Angstroms) X	Y	Z
1	6	0	5.164225	-2.360806	0.336154
2	6	0	3.914917	-1.797543	0.188252
3	6	0	3.744554	-0.393641	0.024542
4	6	0	4.928980	0.415211	0.058776
5	6	0	6.201619	-0.194295	0.211090
6	6	0	6.326009	-1.557623	0.340870
7	1	0	5.253482	-3.436052	0.460840

8	1	0	3.050168	-2.449013	0.225077
9	6	0	2.452727	0.228369	-0.149739
10	6	0	4.805095	1.823608	-0.049491
11	1	0	7.080767	0.444645	0.228313
12	1	0	7.303817	-2.014307	0.457943
13	6	0	3.572950	2.409716	-0.179470
14	6	0	2.394825	1.625266	-0.230614
15	1	0	5.701469	2.436562	-0.020831
16	1	0	3.483804	3.491640	-0.254438
17	6	0	1.266751	-0.610232	-0.300096
18	1	0	1.437806	-1.648391	-0.604177
19	6	0	-2.243795	-0.713636	-0.188415
20	6	0	-4.434807	-0.890599	-0.149396
21	6	0	-4.338558	0.472733	0.224625
22	6	0	-5.700232	-1.481300	-0.261034
23	6	0	-5.471330	1.240810	0.485062
24	6	0	-6.832486	-0.714429	-0.001450
25	1	0	-5.774358	-2.525195	-0.547416
26	6	0	-6.722426	0.634041	0.368294
27	1	0	-5.386979	2.284378	0.771892
28	1	0	-7.815944	-1.167131	-0.086391
29	1	0	-7.618023	1.214796	0.566825
30	7	0	-0.936848	-1.081133	-0.345347
31	1	0	-0.758445	-2.041501	-0.633367
32	7	0	0.058043	-0.195194	-0.125856
33	7	0	-3.228556	-1.537300	-0.376683
34	16	0	-2.639949	0.952447	0.287255
35	8	0	1.190808	2.233608	-0.386634
36	1	0	1.332572	3.183049	-0.499837

Rotational constants (GHZ): 0.8216729 0.0891019 0.0810162

Coordinates for optimized geometry of **L_2+Zn^{2+}** complex of **structure A** [main text figure 4.5(i)] at B3LYP/6-31+G(d,p).

Center Number	Atomic Number	Atomic Type	Coordinates (Angstroms) X	Y	Z
1	6	0	5.763891	2.048215	0.587486
2	6	0	4.421969	1.707742	0.579233
3	6	0	3.966083	0.514654	-0.032444
4	6	0	4.949891	-0.350652	-0.596965
5	6	0	6.313842	0.014078	-0.569769
6	6	0	6.723728	1.201935	0.004498
7	1	0	6.077571	2.971320	1.066475
8	1	0	3.719456	2.360984	1.086661
9	6	0	2.564098	0.134763	-0.085921
10	6	0	4.526336	-1.590765	-1.173733
11	1	0	7.040998	-0.664300	-1.008750
12	1	0	7.774718	1.472565	0.021834
13	6	0	3.220098	-1.971877	-1.181193
14	6	0	2.182319	-1.151053	-0.610790
15	1	0	5.283495	-2.242194	-1.603813
16	1	0	2.903539	-2.918648	-1.605257

17	6	0	1.572436	1.114591	0.191109
18	1	0	1.865703	2.167444	0.158060
19	6	0	-1.889615	1.462509	0.099980
20	6	0	-3.535569	0.030254	-0.393281
21	6	0	-4.300010	1.212217	-0.323132
22	6	0	-4.166110	-1.185811	-0.669822
23	6	0	-5.675435	1.213081	-0.536487
24	6	0	-5.541928	-1.190414	-0.881710
25	1	0	-3.585041	-2.101082	-0.694903
26	6	0	-6.290116	-0.006540	-0.820534
27	1	0	-6.253647	2.129362	-0.481202
28	1	0	-6.042938	-2.129574	-1.092995
29	1	0	-7.361663	-0.035262	-0.989654
30	7	0	0.313723	0.831836	0.411038
31	7	0	-0.619768	1.858769	0.354821
32	1	0	-0.406487	2.774670	0.729808
33	16	0	-3.247233	2.584982	0.068521
34	8	0	0.976631	-1.611919	-0.666755
35	7	0	-2.171937	0.204459	-0.160685
36	30	0	-0.548075	-1.021196	0.360558
37	17	0	-1.289431	-2.418869	1.887018

Rotational constants (GHZ): 0.4238135 0.0900247 0.0798769

Coordinates for optimized geometry of **L_2+Zn^{2+}**complex of **structure B** [main text figure 4.5(i)] at B3LYP/6-31+G(d,p).

Center Number	Atomic Number	Atomic Type	Coordinates (Angstroms) X	Y	Z
1	6	0	5.148193	-2.773554	-0.592102
2	6	0	3.950269	-2.084693	-0.671732
3	6	0	3.785284	-0.811741	-0.074213
4	6	0	4.919654	-0.257029	0.591010
5	6	0	6.133316	-0.977999	0.658397
6	6	0	6.253928	-2.225231	0.080671
7	1	0	5.231625	-3.748273	-1.063662
8	1	0	3.139921	-2.547082	-1.223335
9	6	0	2.539581	-0.042659	-0.116886
10	6	0	4.816435	1.043358	1.178963
11	1	0	6.975676	-0.525769	1.175124
12	1	0	7.189177	-2.772867	0.136219
13	6	0	3.670443	1.774192	1.117949
14	6	0	2.495568	1.268815	0.467150
15	1	0	5.691343	1.449331	1.680938
16	1	0	3.594457	2.762559	1.557468
17	6	0	1.387824	-0.646057	-0.678047
18	1	0	1.447468	-1.689605	-0.977102
19	6	0	-1.981164	-0.995828	-0.774296
20	6	0	-4.136865	-1.257475	-0.427622
21	6	0	-3.778119	-0.882708	0.890126
22	6	0	-5.478078	-1.536950	-0.716858
23	6	0	-4.722912	-0.778363	1.908609
24	6	0	-6.423503	-1.436733	0.298826

25	1	0	-5.754585	-1.821747	-1.726274
26	6	0	-6.052619	-1.061027	1.598717
27	1	0	-4.436749	-0.485397	2.913383
28	1	0	-7.465571	-1.650322	0.081701
29	1	0	-6.807643	-0.986725	2.375010
30	7	0	0.205400	-0.093060	-0.877099
31	7	0	-0.754249	-0.995426	-1.421026
32	1	0	-0.875599	-0.869860	-2.424146
33	7	0	-3.095846	-1.299391	-1.347152
34	16	0	-2.036536	-0.611998	0.967458
35	30	0	-0.221387	1.736931	-0.332892
36	8	0	1.454335	2.042856	0.471826
37	17	0	-1.764033	3.119540	-0.863974

Rotational constants (GHZ): 0.3520898 0.0906042 0.0793889

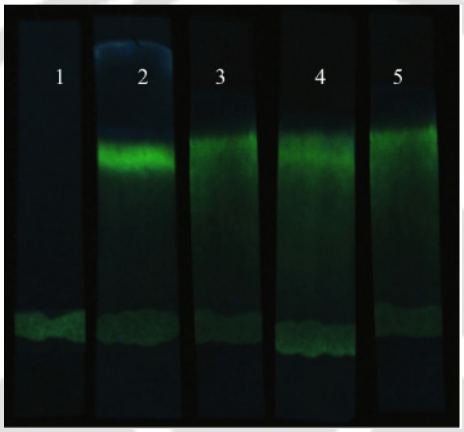

Figure A4.16 Photographs of the paper strip based sensing with $Zn(ClO_4)_2$ solutions (left to right): (1) no Zn^{2+}, (2) 300 μM, (3) 200 μM, (4) 100 μM and (5) 50 μM Zn^{2+} in methanol.

Chapter 5

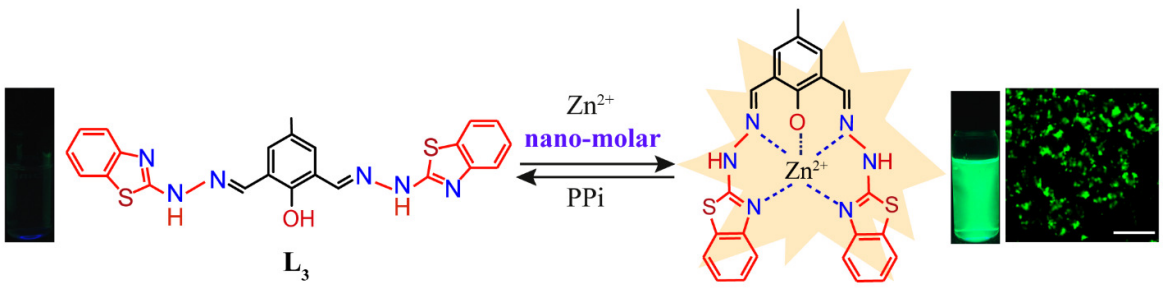

Benzothiazole Functionalized Sensor for Zn(II) and PPi: Nano-molar sensing in Physiological condition and in Live Cells

Chapter 5

5.1 Background and Focus of the Chapter

Sensing of Zn^{2+} and Cd^{2+} ions are equally important because of their vital biological and environmental impacts. However, owing to their identical chemical properties most chemosensors could not to distinguish them and produce similar optical outputs. Thus, chemosensors are redesigned with new functionalities to overcome this problem. In this regard, Jiang *et. al.* had shown the role of a carbonyl group from amide functionality in differentiating Cd^{2+} from Zn^{2+} through two different coordination modes.[1] Yoon et. *al.* was also focused with the amide group and had reported that the amide tautomerization could be a possible tool in distinguishing Zn^{2+} and Cd^{2+} ions.[2] In an another approach, Pang *et. al.* has described a synthetically control receptor design to switch the selectivity between Zn^{2+} and Cd^{2+}.[3] Apart from these, the size differences between the Zn^{2+} and Cd^{2+} can also be utilize to design a chemosensor selective to either of the metal ion.

In the previous chapter, the chemosensor **L_2** was a monopodal acyclic receptor which could bind to both Zn^{2+} and Cd^{2+} ions. Thus, modifications are essential to improve the selectivity and sensitivity of the chemosensor. Again, for the *in vitro* and *in vivo* sensing of Zn^{2+} ion, the new probe should also have good selectivity for Zn^{2+} ion in presence of other interfering ions. Based on this, an attempt was made to design a cleft like chemosensor for Zn^{2+} ion. To that end, 2-hydroxy-5-methylisophthalaldehyde is condensed with 2 equivalents of 2-hydrazinylbenzo[d]thiazole to give a new chemosensor **L_3** (2,6-bis((E)-(2-(benzothiazol-2-yl)hydrazono)methyl)-4-methylphenol) (Scheme 5.1). This new probe has two imine bonds, two benzothiazole units and a hydroxyl group, which are in well positioned for bonding with the guest metal ion. Careful observation also reveals that the probe has a cavity inside which would allow only the metals of definite sizes to come and bind with the probe. A control compound **L_{3C}** which devoid of hydroxyl functionality was also synthesized to understand the role played by OH in metal ion chelation.

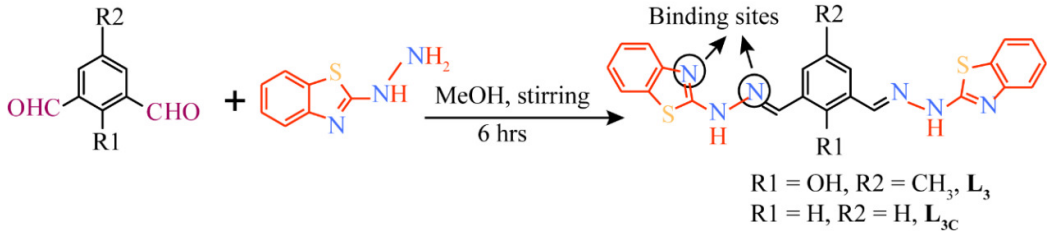

Scheme 5.1 Synthetic procedure of the probes.

5.2 Selective Sensing of Zn(II) in Aqueous Medium by L_3

The photophysical properties of the chemosensor (L_3) are elucidated by UV-visible absorbance and fluorescence emission changes upon addition of various analytes. Absorption spectrum of naked L_3 (10 μM) in buffered ethanol (1:1 EtOH : 10 mM HEPES, pH~7.2) exhibits an intense band at 333 nm and a weak band around 386 nm, which may be ascribed to intramolecular π–π* transitions (Figure 5.1a). However, addition of Zn^{2+} ion resulted in the formation of new red shifted absorption peaks at 376 nm and at 431 nm with a distinct change in the colour of the solution from colorless to yellowish type (Inset, Figure 5.1a). Incremental addition of Zn^{2+} ion (0-70 μM) to L_3 resulted in a decrease in intensity at 333 nm accompanied by blue shifting of the 386 nm peak to 376 nm, which emerged with increasing intensity (Figure 5.1b). Furthermore, higher Zn^{2+} concentrations also lead to the manifestation of a broad peak at 431 nm. The isosbestic points at 297 nm, 355 nm and 414 nm indicates the formation of a new zinc complex. Interestingly, none of the other tested metal ions, which included biologically relevant metal ions like Na^{+}, Mg^{2+} and Ca^{2+}, toxic heavy metal ions like Hg^{2+} and Cd^{2+} affected the absorption spectra of L_3. Similarly, L_3 remained unaffected even after addition Cu^{2+} ion and extending this list further other cations such as K^{+}, Mn^{2+}, Fe^{2+}, Co^{2+}, Ni^{2+}, Ag^{+}, Pb^{2+} and Al^{3+} also produce no distinguishable change (Figure 5.1a).

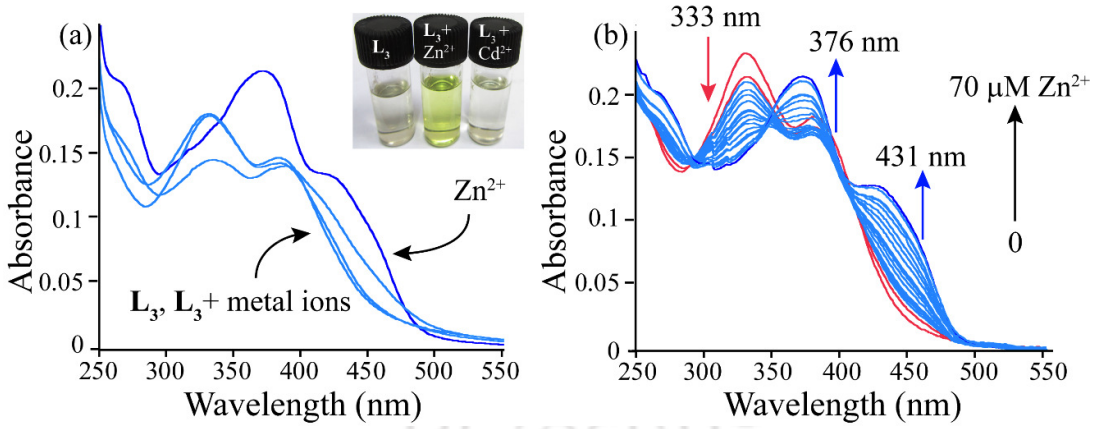

Figure 5.1 (a) Change in absorption spectra of L_3 (10 μM) with different metal ions (50 μM) in ethanol mixed buffered solution (1:1 EtOH : 10 mM HEPES, pH~7.2). **Inset**: Change in the colour of L_3 solution after the addition of Zn^{2+} and Cd^{2+}. (b) UV-Vis titration spectra of L_3 with increasing Zn^{2+} ion concentrations.

To acquire a nuance understanding of the binding mechanism, we have also performed fluorescence emission studies and ^{1}H NMR titration in presence of Zn^{2+} ions.

The naked probe L_3 (10 μM) is weakly fluorescent at 510 nm (λ_{ex} = 430 nm, slit = 3/3 nm) which can be attribute to two different mechanism- i) perhaps due to rapid rotation around single bond adjacent to azo methine group and ii) photo-induced electron transfer from N to the

fluorophore. However, interaction with Zn^{2+} resulted in a remarkable enhancement ($I/I_0 = 90$) of the fluorescence emission peak at around 510 nm (Figure 5.2a). Additionally, under a UV lamp ($\lambda = 365$ nm) the coloured **L_3-Zn^{2+}** solution display a strong yellowish green fluorescence (Inset, Figure 5.2a) and thus renders rapid naked eye detection of Zn^{2+}. However, interaction of **L_3** with the other tested metal ions fail to impart any change in the fluorescence emission of the probe (Figure 5.2a and 5.2b). Thus, there is no interference from Cd^{2+} ion as encountered in chapter 4. Also, the fold of fluorescence emission enhancement in case of **L_3** after Zn^{2+} addition is much more than that of **L_2-Zn^{2+}** complex (Figure 5.2c) and this resulted in improved quantum yields (ϕ = 0.37). Collectively the results are encouraging as chemosensor, which exhibit large stokes shift and manifold enhancement in fluorescence upon binding of target analyte are envisaged as potential candidates for fabrication of sensing devices.

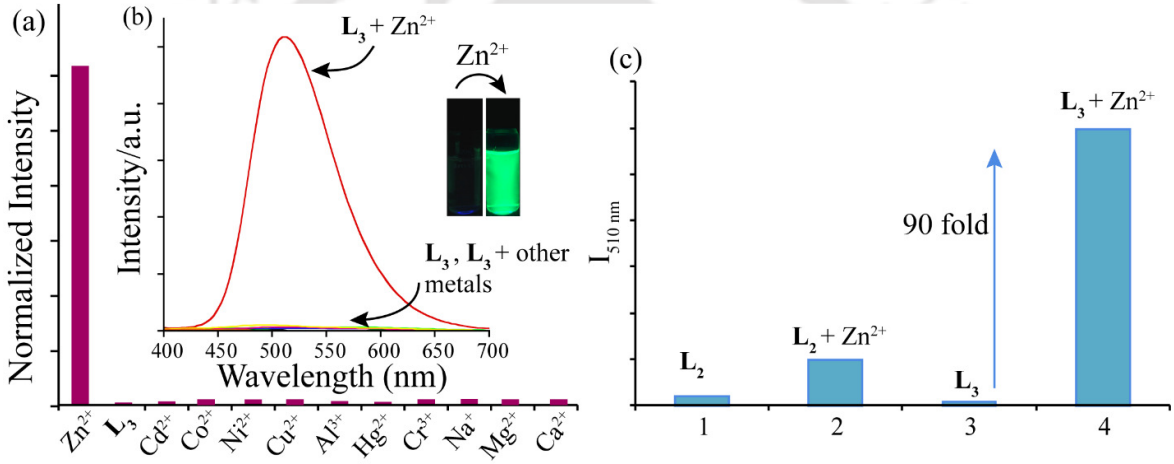

Figure 5.2 (a) Emission intensities of **L_3** (10 µM) in presence of various metal ions in mixed buffered solution and b) bar plot presentation of the same (λ_{ex} = 430 nm, slit = 3/3 nm). **Inset**: Change in colour of **L_3** solution observed under a UV lamp following addition of Zn^{2+}. c) Comparison of fluorescence emissions of **L_2** and **L_3** at 510 nm after addition Zn^{2+}.

To explore the binding mechanism, we have titrated a fixed concentration of the probe (10 µM) with varying concentrations of Zn^{2+} ion. With increasing concentrations of Zn^{2+} there is a systematic enhancement in the fluorescence emission at 510 nm. Following addition of 0.1 equivalent of Zn^{2+} (1.0 µM of Zn^{2+}), there is nearly 26 fold increase in the fluorescence intensity of the probe (Figure 5.3a). It may also be mentioned that a noticeable enhancement in the fluorescence intensity of **L_3** is even observed with 1.0 nM Zn^{2+}, which indicate the excellent sensitivity of the probe (Figure 5.3b). On contratory to the normal 1:2 host-guest binding the Job's plot from the fluorescence titration data suggests a 1:1 complexation (Figure A5.1). The binding constant for Zn^{2+} ion is 1.25×10^5 M^{-1} as calculated by Benesi- Hildebrand equation using the fluorescence titration reading (Figure A5.2a). The calculated lowest detection limit for

Zn^{2+} is 71 ppb on the basis of signal: noise = 3:1 (Figure A5.4b). In comparison with the reported examples of fluorescent sensors for Zn^{2+} (Table A5.1, A5.2), we have achieved better detection limit. Again, such level of detection limit bears significant implications to sense Zn^{2+} in biological systems.

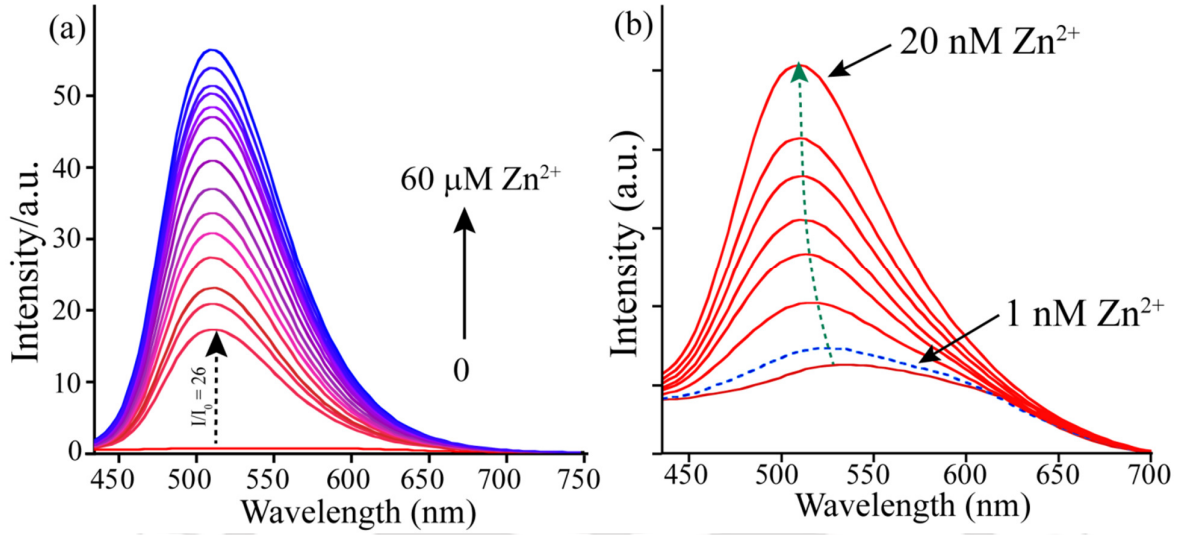

Figure 5.3 a) Fluorescence titration of **L3** with varying Zn^{2+} concentrations of Zn^{2+} and b) with lower concentrations of Zn^{2+} ion (0-20 nM) (λ_{ex} = 430 nm, slit = 3/3 nm).

Subsequently, interference studies are conducted to ascertain the affinity of **L3** for Zn^{2+} in presence of other competitive metal ions. For this, fluorescence emission spectra are recorded after the addition of different metal ion solutions to a mixture of 1:1 **L3** and Zn^{2+}. Interestingly, the sensing capability of **L3** for Zn^{2+} is not affected in presence of any of the competing species (Figure A5.3).

5.3 Plausible Mechanism of Zn^{2+} Sensing

To gain an insight of the chelation mode of zinc ion to **L3**, ^{1}H NMR titration is conducted. However, due to the poor solubility of the probe in CD_3OD, titration is performed in DMSO-*d*$_6$ (Figure 5.4). There are three possible binding sites in **L3** viz. OH, Schiff base N and N of benzothiazole group; and Zn^{2+} coordination through this functionalities are expected to change the nearby electronic environment. Just following addition of the first aliquot of Zn^{2+} ion, the OH peak is obliterated, which suggest the strong involvement of the OH functionality in the binding event. Interaction with the Zn^{2+} ion also caused de-shielding of the Schiff base CH(Hb) and the aromatic CHs of the benzothiazole ring. The control receptor **L3C** also reveals the importance of the same, as it fails to produce any selectivity under the same experimental condition (Figure A5.4). Further, the experimental 1:1 Job's plot is also corroborated by 1:1

mass of complex ($\mathbf{L_3}$+Zn^{2+}+NO_3^- = 584.0234, Figure A5.5) which also suggests the involvement of OH in bonding to Zn^{2+}.

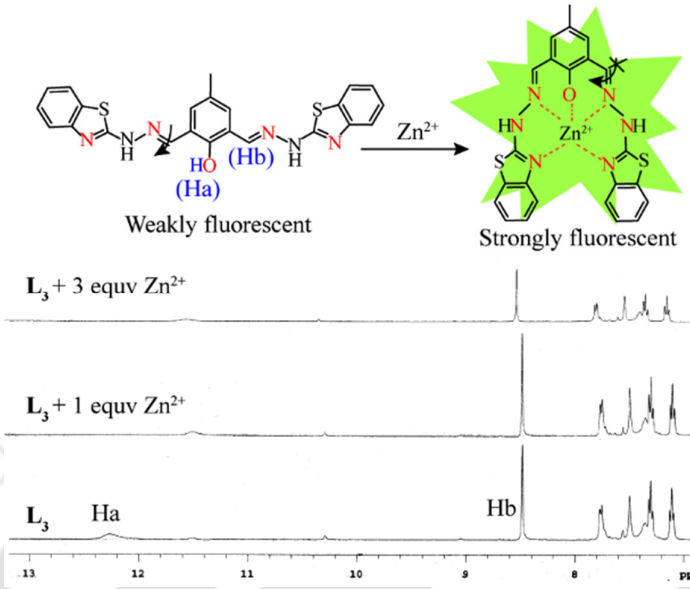

Figure 5.4 ^{1}H NMR stack plot of $\mathbf{L_3}$ with different concentrations of Zn^{2+} in DMSO-d_6 and the plausible Zn^{2+} binding on top.

Thus, guided by the phenoxide oxygen, Schiff base N and benzothiazole N are also coordinated to Zn^{2+} ion, and thereby rigidify the molecular assembly by restricting the free rotation of the azomethine carbon, which resulted in significant fluorescent enhancement through the process of chelation-enhanced fluorescence (CHEF).

To test the sensing potential of the developed probe in biological system, it is important to ascertain the performance of the probe in presence of serum proteins such as albumin.[4] Thus, the Zn^{2+} sensing by $\mathbf{L_3}$ is analysed in presence of human serum albumin (HSA) and bovine serum albumin (BSA) in mixed solvent system as well as in simulated body fluid (SBF) by tracking the fluorescence emission at 510 nm (Figure 5.5). Interestingly, even in presence of higher concentrations of HSA, BSA and SBF the fluorescence emission intensity of $\mathbf{L_3}$-Zn^{2+} at 510 nm remain unaffected. These results reiterated the selectivity of the developed probe and demonstrated its application potential in a physiologically relevant milieu.

Given that chemosensors can exhibit proton-induced fluorescence, the zinc ion induced 'turn-on' fluorescence of $\mathbf{L_3}$ is also checked in a wide pH range. Importantly, $\mathbf{L_3}$ renders Zn^{2+} sensing in the pH range 5.0 to 11 (Figure A5.6). In the pH range <5.0, there is no fluorescence response to Zn^{2+} which may perhaps be attributed to the weak coordination capability of zinc ions due to the protonation of the co-ordination sites of $\mathbf{L_3}$.

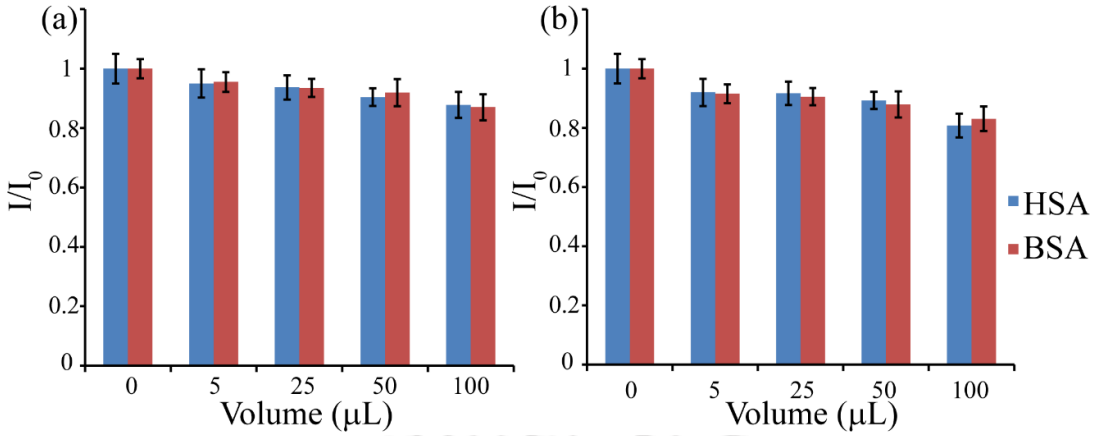

Figure 5.5 Histogram showing the fluorescence response of **L3**-Zn^{2+} ensemble towards various concentrations of BSA and HSA in (a) buffered ethanol (1:1:: EtOH: :10mM HEPES, pH~7.2) and (b) simulated body fluid (SBF).

For practical application of the chemosensor, paper test strips are used for facile and rapid qualitative detection of Zn^{2+} ion. The ligand coated test strips are prepared by immersing the filter papers into a DCM solution of **L3** and then air dried. An intense 'turn-on' fluorescence could be observed under the UV lamp (λ = 365 nm) on spraying a Zn^{2+} solution over the test strips (Figure A5.7).

5.4 Selective PPi sensing by 'L3-Zn^{2+}' ensemble

The next endeavour is to ascertain the anion sensing aptitude of the **L3**-Zn^{2+} ensemble. To this end, the **L3**-Zn^{2+} ensemble is treated with various anions such as F^-, Cl^-, Br^-, I^-, CN^-, CO_3^{2-}, HCO_3^-, $CH_3CO_2^-$ (OAc^-), NO_3^-, PPi, SO_4^{2-}, PO_4^{3-}, $H_2PO_4^-$, AMP, ADP and ATP etc. Among the aforesaid anions, only PPi induced a conspicuous change in the emissive behaviour of the ensemble (Figure 5.6a). Again, the addition of dNTP (N = A, G, C, T) also produce no change in the emissive behavior of the ensemble. Addition of 1.0 equivalent of PPi (10 µM) solution resulted in complete quenching of the initial fluorescence emission of the **L3**-Zn^{2+} ensemble. Titration of the metal ensemble with sequentially added PPi solution lead to a continuous decrease in emission intensity at 510 nm (Figure 5.6b). The 'turn-off' fluorescence behaviour of the **L3**-Zn^{2+} ensemble could be explained by considering the strong binding affinity of PPi towards Zn^{2+}. The sequestration of Zn^{2+} ions by PPi and formation of stable Zn-PPi adduct releases the free probe in the solution, which renders the strong emission of the **L3**-Zn^{2+} ensemble.

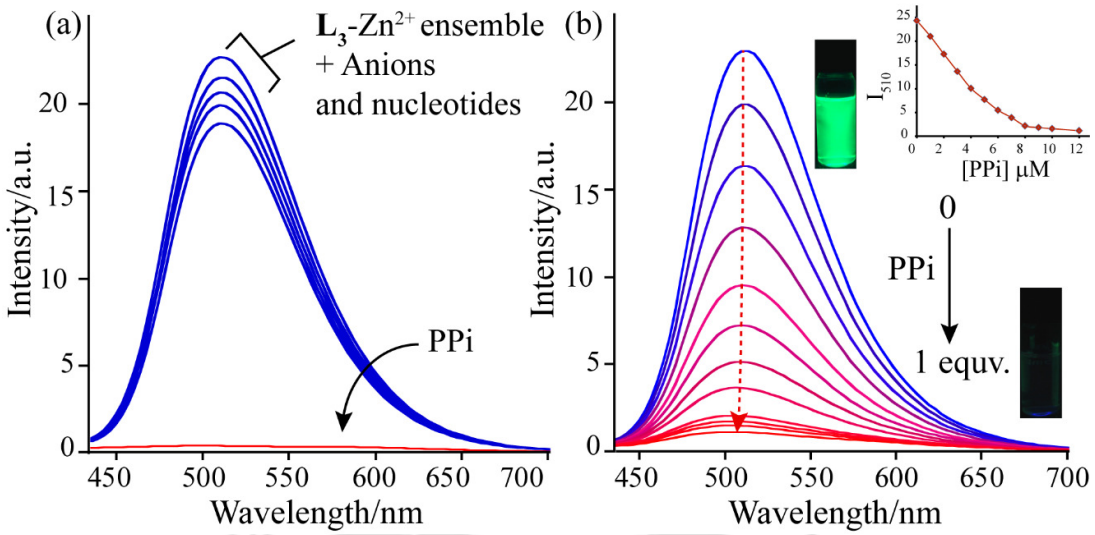

Figure 5.6 Change in fluorescence emission upon addition of (a) different anions and (b) increasing concentrations of PPi (0 – 10 μM) to the '$\mathbf{L_3}$-Zn^{2+}' ensemble ion in mixed buffered solution (λ_{ex} = 430 nm, slit = 3/3 nm). **Inset**: Change of fluorescence emission intensity of the '$\mathbf{L_3}$-Zn^{2+}' ensemble at 510 nm with increasing concentrations of PPi.

The UV-Vis spectral pattern further validate our conjecture, as absorption maximum at 380 nm for naked $\mathbf{L_3}$ is regained and the characteristic 431 nm peak for the zinc ensemble diminished after PPi addition (Figure A5.8). Concurrently, the yellowish color solution is also transformed to the original colourless solution. However, neither any visual colour change nor any development of new peak around 380 nm is observed in the UV-visible absorbance spectra after addition of any of the anions viz. F^-, Cl^-, Br^-, I^-, CO_3^{2-}, HCO_3^-, OAc^-, NO_3^-, SO_4^{2-}, PO_4^{3-}, $H_2PO_4^-$ even at higher mole ratios. This indicates the high selectivity of the $\mathbf{L_3}$-Zn^{2+} ensemble for PPi ion in the physiological pH. It may also be mentioned that the aforementioned anions could not be detected by the free probe $\mathbf{L_3}$ (Figure A5.9). Thus the $\mathbf{L_3}$-Zn^{2+} ensemble can be employed both as colorimetric as well as fluorescence based sensing of PPi.

The Job's plot obtained from the titration experiment suggests a 1:1 binding of PPi with metal ensemble and the calculated binding constant is 1.4×10^5 M^{-1} (B-H equation, Figure A5.10). The LOD of the zinc ensemble for PPi anion is 480 pM (Figure A5.11). To establish the practical applicability of the $\mathbf{L_3}$-Zn^{2+} ensemble as selective PPi sensor, competitive fluorescence experiment is carried out with the competing anions. Addition of PPi caused a prominent fluorescence quenching in every case (Figure A5.12), which suggested excellent selectivity and sensitivity of $\mathbf{L_3}$-Zn^{2+} ensemble towards PPi in the buffer medium even in the presence of other interfering anions.

5.5 Fabrication of logic gates with Zn^{2+} and PPi as inputs

The chemosensor **L3** has been found to be reversible and recyclable towards Zn^{2+} and PPi ions over more than six cycles (Figure 5.7a). We further focused to demonstrate the logic operation by monitoring the fluorescence output response of **L3** in presence of different chemical inputs. For the inputs Zn^{2+} and PPi in methanolic buffered solution, the fluorescence output change is monitored at 510 nm (O1). For turn-on fluorescence at 510 nm the output is '1', i.e. O1 = 1 and for the turn-off nature it is '0'. Similarly, for the absence of the inputs Zn^{2+} and PPi i.e. I1 = I2 = 0, O1is also '0' and the gate is OFF. Again, for the nonchalant behaviour of PPi, the O1=0 but for the turn-on fluorescence of Zn^{2+} ion O1=1 and the gate-on. When I1=I2=1, O1 is also '0' and the gate is OFF. These studies clearly demonstrate a INHIBIT logic gate for these ions at 510 nm (Figure 5.7b and figure 5.7c).

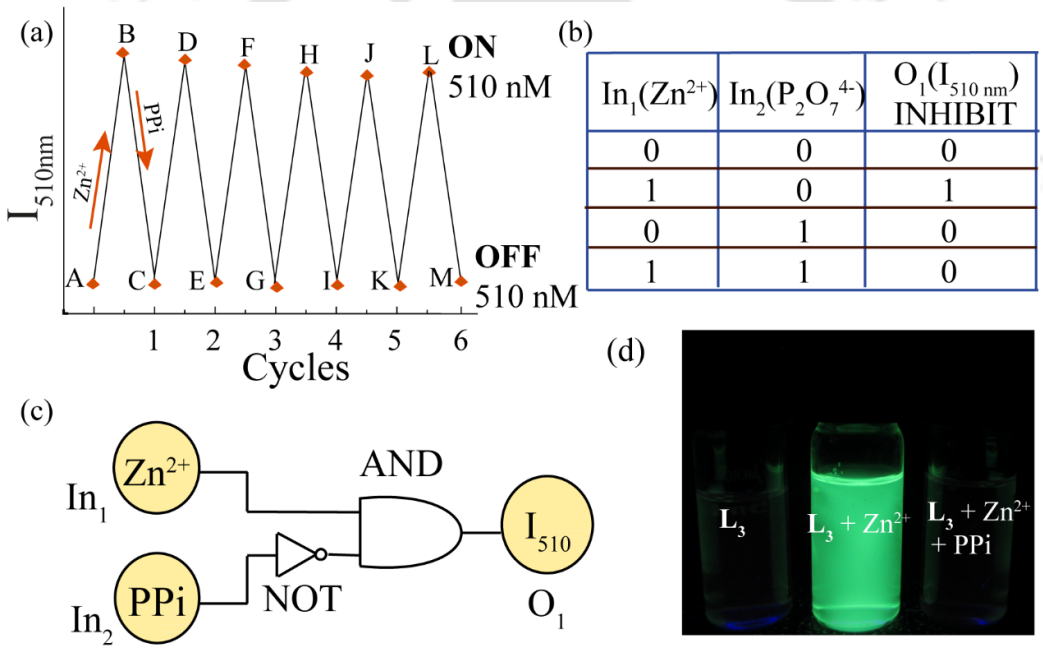

Figure 5.7 (a) Relay recognition of Zn^{2+} and PPi with **L3**. (b) Truth table with the inputs Zn^{2+} and PPi and the (c) logic gate representation of the same. (d) Change in colour of **L3** solution observed under a UV lamp after addition of Zn^{2+} and PPi.

5.6 Detection of Zn^{2+} in Live Cells

Zn^{2+} related physiology and pathology has attracted considerable interest in recent days. Again, photoluminescence (PL) imaging has become a powerful tool for the real time monitoring of Zn^{2+} distribution, uptake, and trafficking, as it possesses distinct advantages, such as high sensitivity and non-invasiveness, and excellent temporal and spatial resolution.

The results obtained from the fluorescence experiments are encouraging and we sought to investigate the potential of **L**$_3$ as a probe for detection of intracellular Zn^{2+}. However, prior to **L**$_3$- mediated zinc detection in live cells, it is important to determine its cytotoxic potential. To that end, a MTT assay is performed. It is observed that that probe alone fails to impart any adverse effect on the viability of HeLa cells at a concentration of 60 μM (Figure A5.13). Even at high concentrations of 90 μM and 120 μM, cell viability is around 80%. Akin to the results obtained with **L**$_3$, HeLa cells treated with **L**$_3$-Zn^{2+} and **L**$_3$-Zn^{2+}-PPi ensembles also displayed significant viability, which suggest high biocompatibility of the ensembles.

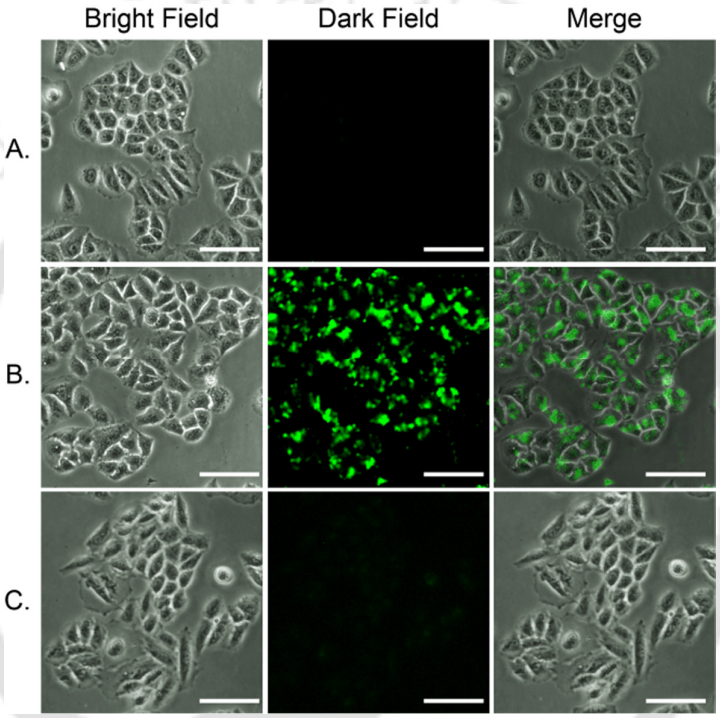

Figure 5.8 Fluorescence microscopic images of HeLa cells after adding 15 μM of **L**$_1$ (row A) and after subsequent treatment with 30 μM Zn^{2+} (row B) and 30 μM PPi (row C). Scale bar for the images is 100 μm.

The non-toxic nature of the developed chemosensor **L**$_3$ and its Zn^{2+}-ensemble suggests that the probe could perhaps be deployed for fluorescence-based intracellular detection of Zn^{2+} in live cells. Therefore, to ascertain the potential of **L**$_3$ in intracellular sensing of Zn^{2+}, HeLa cells are incubated with 15 μM **L**$_3$ followed by 30 μM of $Zn(ClO_4)_2$ to promote the formation of intracellular **L**$_3$-Zn^{2+} complex. It is observed that **L**$_3$ alone fail to elicit any fluorescence signals as evidenced by the absence of any intracellular fluorescence (Figure 5.8). However, addition of zinc led to the manifestation of bright green fluorescence in HeLa cells (Figure 5.8). The fluorescence microscopic analysis strongly suggests that compound **L**$_3$ could readily cross the cell membrane, infuse into HeLa cells, and sense Zn^{2+} through the formation of intracellular **L**$_3$-zinc complex. It must be also mentioned that bright field images suggests that HeLa cells

retained their characteristic morphology, which reiterated the biocompatibility of **L3** and **L3**-Zn^{2+} ensemble (Figure 5.8). Interestingly, subsequent incubation of the cells with excess PPi resulted in a dramatic loss of fluorescence (Figure 5.8), perhaps originating from fluorescence quenching behavior of PPi on **L3**-Zn^{2+} ensemble as evidenced from previous solution-based studies (Figure 5.6).

5.7 Conclusions

A novel benzothiazole containing dipodal Schiff base renders relay recognition of Zn^{2+} and PPi in physiological medium. The dipodal framework has improved selectivity and sensitivity in chemosensor in sensing Zn^{2+} ion. The Zn^{2+} sensing is evident in mixed buffered medium and also in the physiological milieu in presence of HSA, BSA and SBF. In presence of Zn^{2+}, the colourless chemosensor solution display a strong greenish fluorescence and thus enable naked eye detection of the metal. The chemosensor also exhibits a strong affinity ($K = 1.25\times10^5\ M^{-1}$) for Zn^{2+} even in the presence of the other interfering metal ions and is ultrasensitive as it can respond even to 1 nM Zn^{2+} (LOD for Zn^{2+} = 71 ppb). A facile application of the chemosensor can be demonstrated through successful detection of Zn^{2+} using the sensor-coated paper strips. The Zn^{2+}-chemosensor ensemble also responds to PPi in the same experimental medium through fluorescence quenching. On the basis of the selectivity of **L3** for Zn^{2+} in physiological medium and its biocompatible attribute, the probe can facilitate fluorescence-based sensing of intracellular Zn^{2+} in live HeLa cells. It is envisaged that the developed probe holds considerable potential as a Zn^{2+} sensor for future environmental and biomedical applications.

References

1. L. Xue, C. Liu and H. Jiang, *Org. Lett.,* 2009, **11**, 1655-1658.
2. Z. Xu, K. H. Baek, H. N. Kim, J. Cui, X. Qian, D. R. Spring, I. Shin and J. Yoon, *J. Am. Chem. Soc*., 2010, **132**, 601-610.
3. Y. Xu, L. Xiao, S. Sun, Z. Pei, Y. Peia and Y. Pang, *Chem. Commun.,* 2014, **50**, 7514-7516.
4. R. K. Pathak, A. G. Dikundwar, T. N. G. Row and C. P. Rao, *Chem. Commun*., 2010, **46**, 4345-4347.

Appendix 4

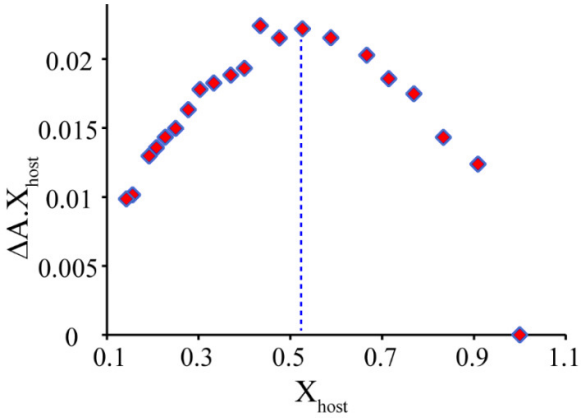

Figure A5.1 The Job's plot presentation for finding the binding stoichiometry between **L_3** with Zn^{2+} (1:1 host-guest complex).

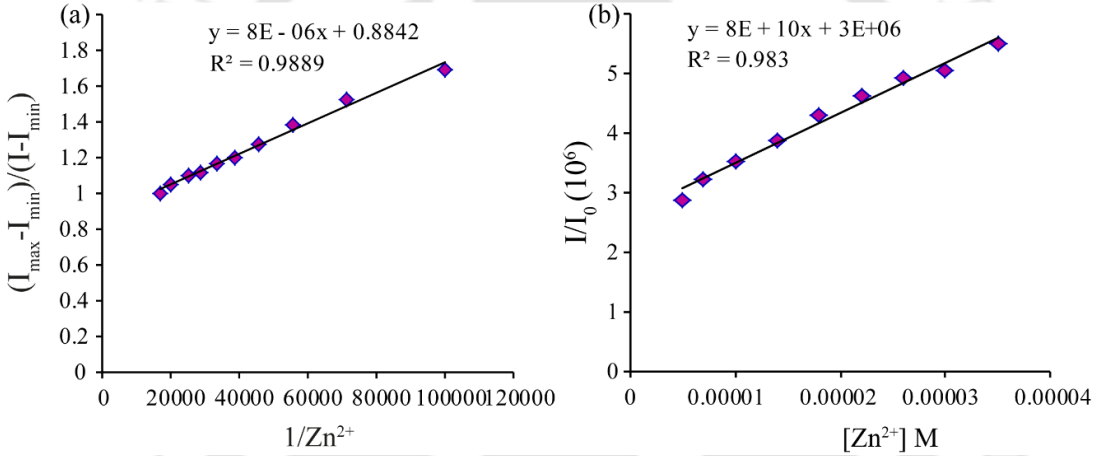

Figure A5.2 (a) The Bensei-Hildebrand plot to calculate the binding constant for Zn^{2+} ion in buffered ethanol solution. (b) Ratio of fluorescence emission intensity change at 510 nm versus Zn^{2+} concentrations for the LOD calculation.

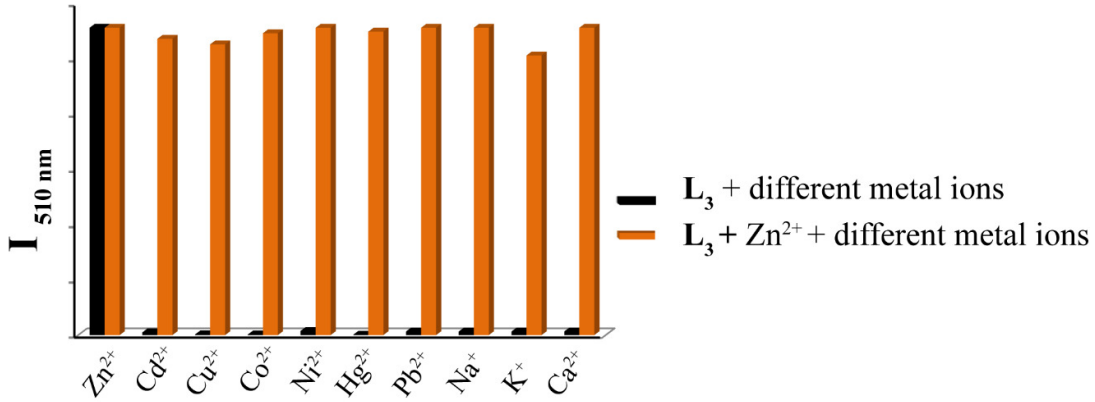

Figure A5.3 Bar plot presentation of **L_3** and Zn^{2+} in the presence of various other metal ions.

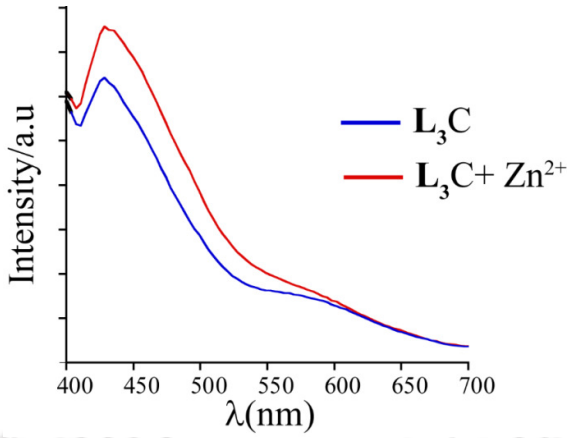

Figure A5.4 Fluorescence emission change after addition of Zn^{2+} to **L3c** under the same experimental condition.

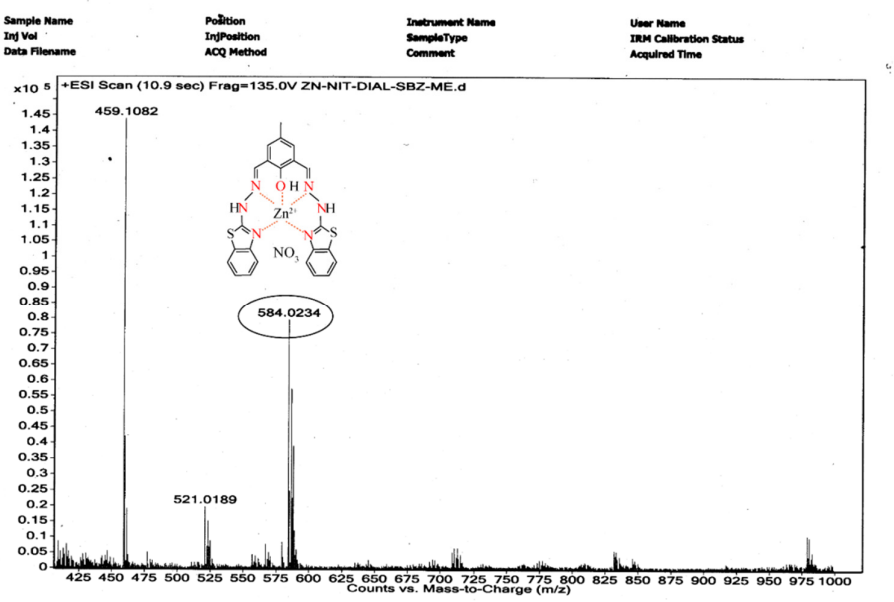

Figure A5.5 HRMS analysis of the solution of **L3** with $Zn(NO_3)_2$.

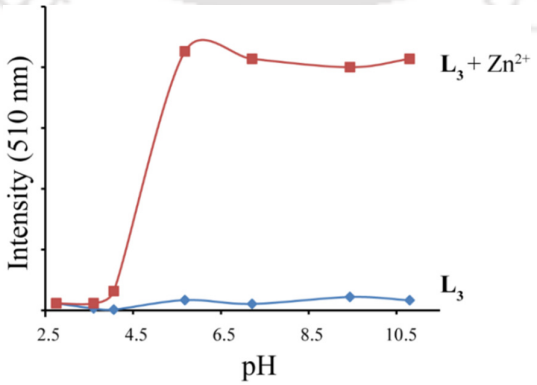

Figure A5.6 Effect of pH on emission behaviour of **L3** and '**L3**-Zn^{2+} ensemble' (Blue line represents the change for **L3**, whereas the changes for '**L3**-Zn^{2+} ensemble' is represented by red line).

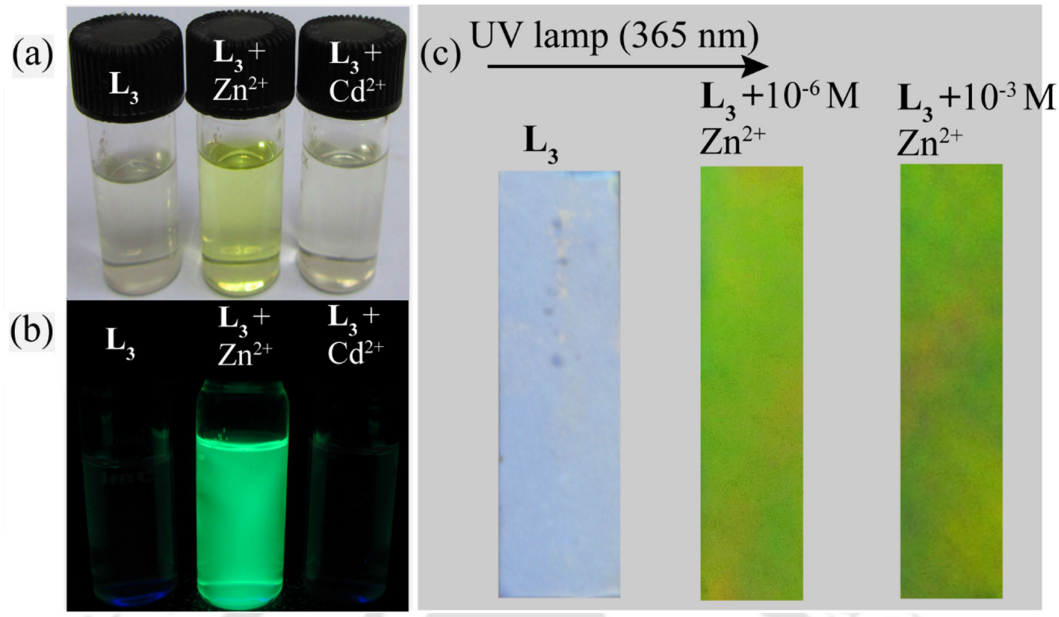

Figure A5.7 Visual colour changes to **L3** after addition of Zn^{2+} and Cd^{2+} ions (a) under normal light and (b) under the UV lamp. (c) The **L3** coated paper strips with different concentration of Zn^{2+} ion under the UV lamp (λ_{ex} = 365 nm).

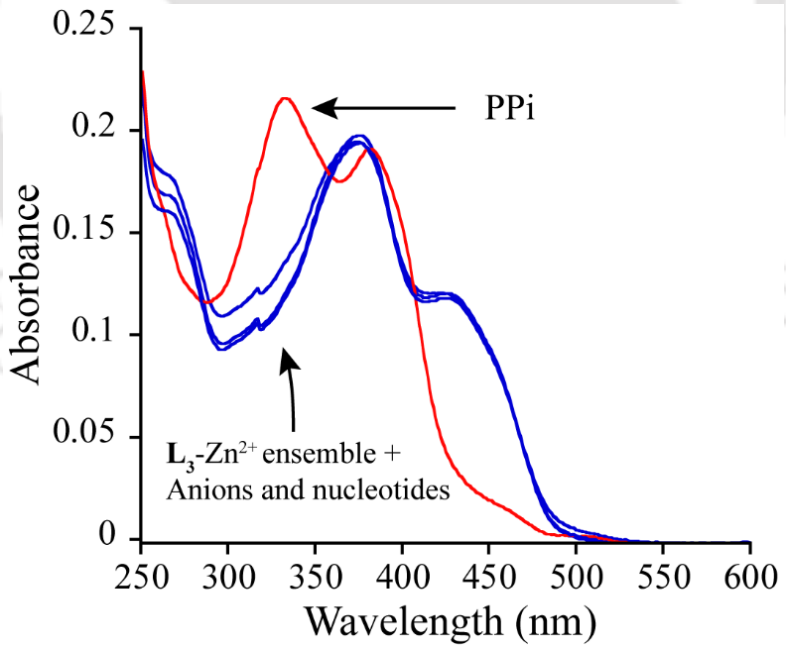

Figure A5.8 Changes in UV-Vis absorption spectra of '**L3**-Zn^{2+}' ensemble with different anions in the buffered ethanol (1:1:: EtOH: 10 mM HEPES buffer, pH~7.2).

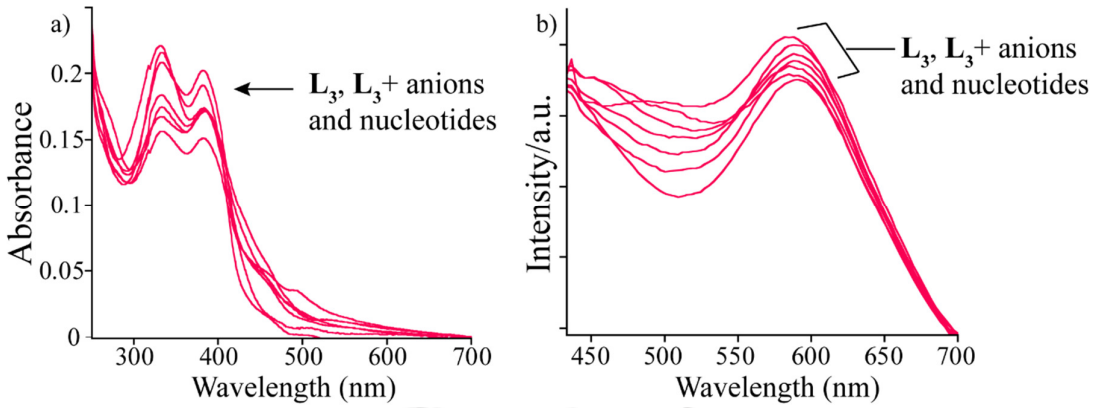

Figure A5.9 a) UV-Vis and b) fluorescence selectivity study of the naked probe **L_3** with anions and nucleotides in buffered ethanol (1:1 EtOH:10 mM HEPES buffer, pH~7.2).

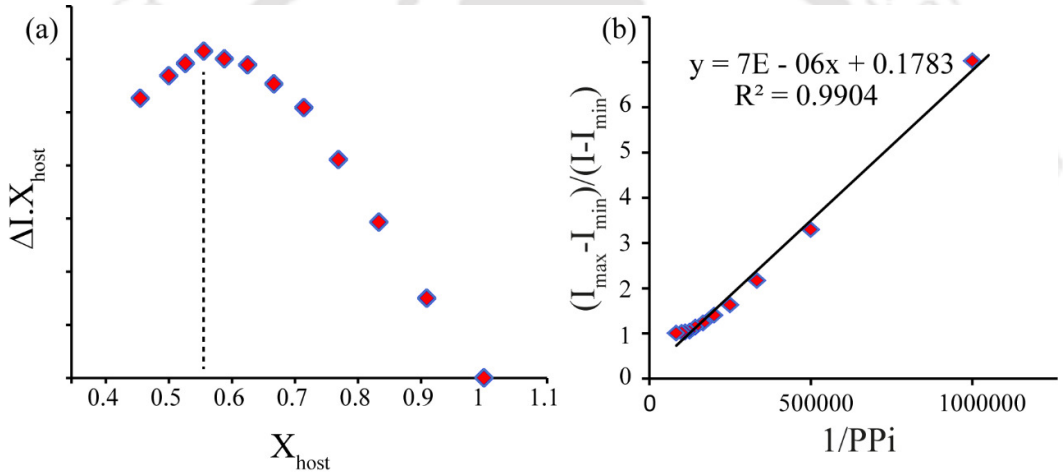

Figure A5.10 (a) Job's plot for determining the stoichiometry of '**L_3**-Zn^{2+}' and PPi ion and (b) the corresponding Benesi–Hildebrand plot for binding constant determination.

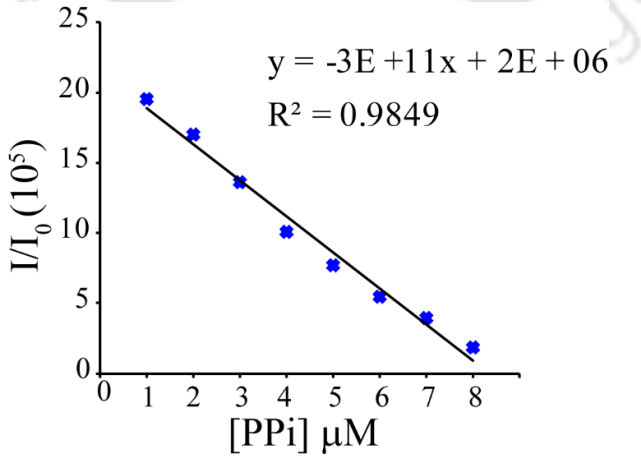

Figure A5.11 Ratio of fluorescence emission intensity change at 510 nm versus PPi concentrations for lowest detection limits (LOD) calculation.

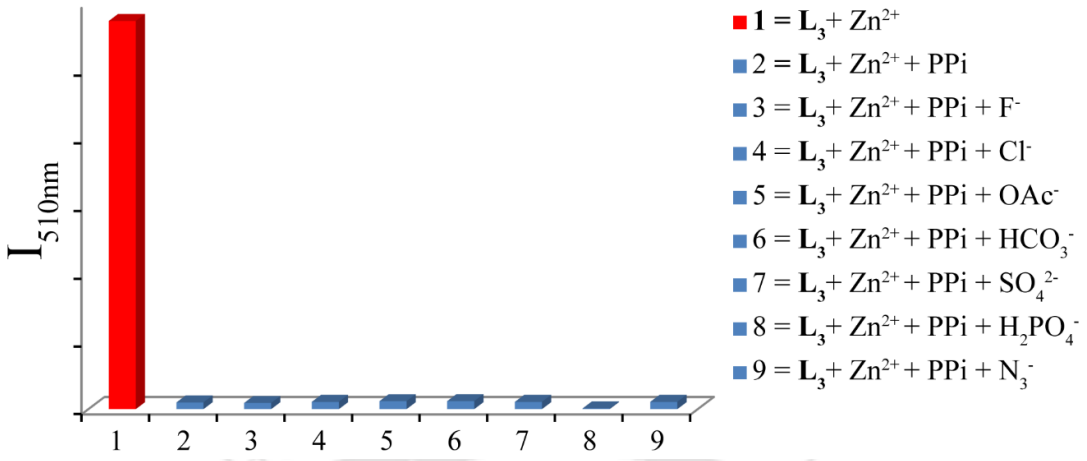

Figure A5.12 Competitive binding affinity of PPi towards the flourish 'L_3-Zn^{2+}' ensemble in presence of other anions (10 equivalents).

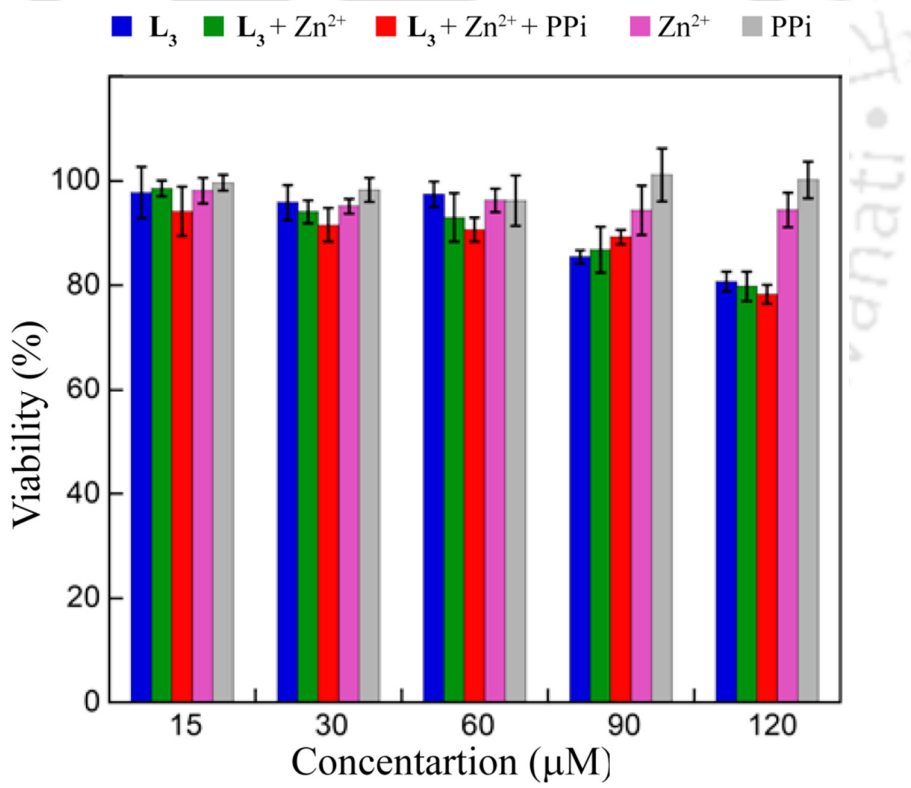

Figure A5.13 MTT based cytotoxicity assay for L_3 and L_3-zinc complex.

Table A5.1 Comparison of metal sensing aptitude of some reported dipodal Schiff base type chemosensor.

References	Experimental Medium	Sensed Metal ion with LOD	*In vivo* application	Anion Sensing with LOD	*In vivo* application
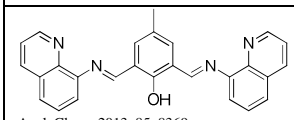 Anal. Chem, 2013, 85, 8369	Methanolic HEPES Buffer (3:2), pH 7.4	Zn^{2+} sensor LOD for Zn^{2+} **56 ppb**	Zn^{2+} imaging	PPi sensing, LOD for PPi **2 ppb**	PCR
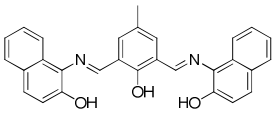 Sensors and Actuators B 2013, 188, 1132–1140	CH_3CN/aqueous HEPES buffer (1:4, v/v)	Zn^{2+} sensor LOD for Cu^{2+} **3 ppb**	Cu^{2+} imaging	No anion sensing	-------
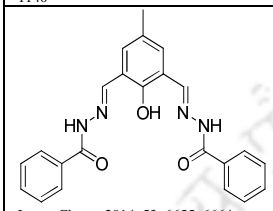 Inorg. Chem., 2014, 53, 6655–6664	CH_3CN/ buffer (2:8, v/v)	Zn^{2+} and Cu^{2+} sensing LOD not discussed	Zn^{2+} and Cu^{2+} images in HELa cells	PPi sensing, LOD for PPi **123 ppb**	No imaging Crystals of Zn and Cu
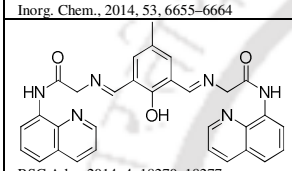 RSC Adv., 2014, 4, 18270–18277	CH_3CH_2OH–Tris–HCl buffer solution (50 mM Tris, 50 : 50, v/v, pH 7.2)	Zn^{2+} sensor LOD for Zn^{2+} **0.1μM**	No imaging	S^{2-} sensing, LOD for S^{2-} **10^{6-} M**	No imaging Crystals of Zn and Cu

Table A5.2 Comparison of some latest reported Zn^{2+} chemosensors with the present work.

Sl No.	References	LOD of Zn^{2+}	Solvent system
1	Present work	25 ppb	7:3, v/v, MeOH, HEPES buffer, pH 7.2
2	B. K. Datta, S. Mukherjee, C. Kar, A. Ramesh, and G. Das; Org. Biomol. Chem., 2014,12, 4975-4982	56 ppm	MeOH: aqueous HEPES buffer (1 mM, pH 7.4; 3:2 v/v)
3	S. Kaur, V. Bhalla and M. Kumar; Chem. Commun., 2014,50, 9725-9728	110 nm	(8:2, v/v H_2O:THF)
4	Z. Dong, X. Le, P. Zhou, C. Dong and J. Ma; RSC Adv., 2014, 4, 18270	0.1μM	CH_3CH_2OH–Tris–HCl buffer solution (50 mM Tris, 50 : 50, v/v, pH 7.2)
4	M. Kumar, N. Kumar and V. Bhalla ; Chem. Commun., 2013,49, 877-879	20×10^{-8} mol L^{-1}	H_2O : CH_3CN (2 : 8, v/v) HEPES buffer, pH=7.0
5	J. Guan, P. Zhang, T. Wei, Q. Lin, H. Yao and Y. Zhang; RSC Adv., 2014, 4, 35797	0.13μM	DMSO–H_2O (8 : 2, v/v, containing 0.01 M HEPES, pH 7.24
6	Z. Liu, C. Zhang, Y. Chen, F. Qian, Y. Bai, W. He and Z. Guo; Chem. Commun., 2014, 50, 1253-1255	0.5 nM	HEPES buffer (50 mM, 0.1 M KNO_3, pH 7.2,
7	V. Luxami, K. Paula and I. H. Jeong; Dalton Trans., 2013, 42, 3783	-------	CH_3CN–H_2O::1 : 1) (HEPES buffer, pH = 7.0)
8	J. Wang, B. Liu, X. Liu, M. J. Panzner, C. Wesdemiotisa and Y. Pang; Dalton Trans., 2014,43, 14142-14146	-------	EtOH

Chapter 6

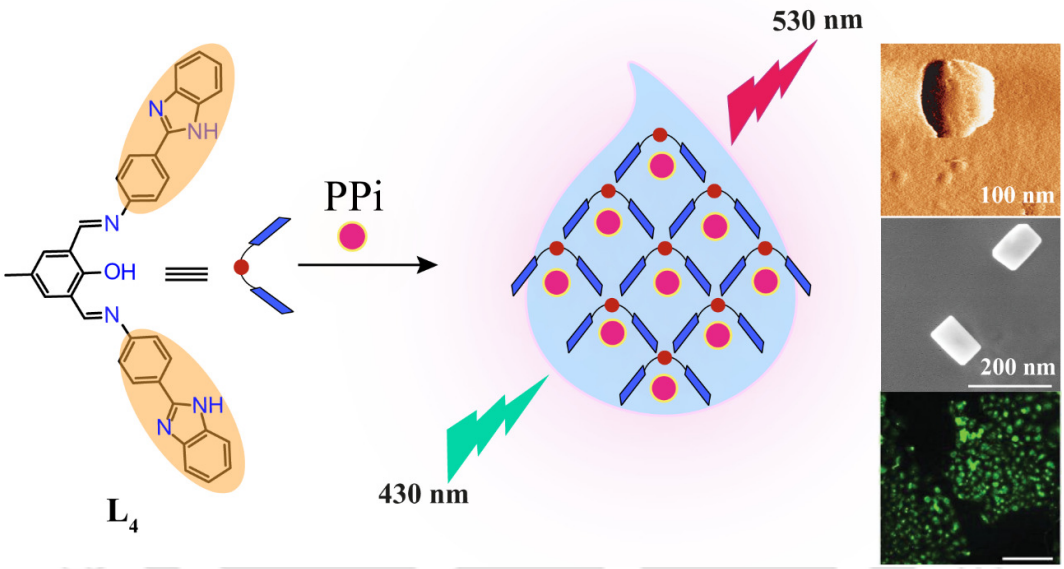

Benzimidazole Functionalized Sensor for PPi: Aggregation-Induced Metal-Free Chemosensing Platform

Chapter 6

6.1 Background and focus of the chapter

Water is the ultimate medium for all forms of life and also the most abundant solvent on earth. It is the first and simplest form of hydrogen bond donor and acceptor compound. Water can hydrogen bonded to ions or neutral polar compounds. Anions are too essential for life and has a great affinity for water. Thus to protect it, nature seal the anions in hydrophobic pockets of anion binding proteins. For that, it requires only a few building blocks, such as OH groups of serine, threonine, or tyrosine, the NH group in the indole moiety of tryptophan and the guanidinium group of arginine. The NH functionality from protein backbone additionally contributes to anion coordination. In that way, the anion binding proteins bind with the anions in water and transport them inside the cells.[1-2]

However, such receptors have complicated designs and their synthesis in laboratory is highly laborious. On the other hand, fluorescence based chemosensor design would be beneficial for the easy and fast visualization of the anion in the targeted biological species. Thus, in the recent few decade enormous effort have been given in designing new chemosensors for various anions. But the low solubility of the most organic chemosensors in water and higher solvation energies of the anions keep most chemosensors away from the realistic application world. A metal-chemosensor ensemble is a new hope in this field as they can tackle the solvation issue to some extent. The potential of such metal-chemosensor ensembles as secondary anion sensors are already reported in the earlier chapters. The natural affinity of the anions for the positively charged metals ion is the backbone in designing such ensembles. However, as the interaction between the chemosensor and metal ion is completely non covalent in nature, it suffers relatively lower stability. Again, a metal free chemosensor is superior to that of metal-chemosensor ensemble on the basis of simplicity and ease of handling. Thus the chase for new methods and technologies for metal free anion sensing in aqueous medium is still going on.

In order to harness the potential of an anion sensor in the biological milieu, it is critical that the developed sensor functions in an aqueous medium. Further, owing to the complexity of biological samples and the possibility of signal interference from non-specific molecules, the target analyte is often detected using high concentrations of the sensor. However, in this backdrop, sensing may be impeded as it has been shown previously that increasing the concentrations of the sensor may lead to an aggregation-caused quenching (ACQ) phenomenon. In 2001, Tang *et. al.* has made a revolutionary scientific discovery in this arena. They had

observed that a series of silole derivatives which were non-emissive in dilute solutions became highly luminescent when their molecules were aggregated in concentrated solutions or in solid films. They coined the process as ‘‘aggregation induced emission’’ (AIE) which is now one of the most cited technique in sensing world. On contrary to the notorious ACQ (aggregation caused quenching), this type of aggregation if beneficial for application purpose. Thus, suitably designed chemosensors which are insoluble in water may be aggregated in water in a way to offer AIE. The biggest advantage of this process is the constructive role of the most common solvent water.[3-4]

Aiming this, a dipodal benzimidazole functionalized sensor has been developed, which is AIE-active and could directly sense pyrophosphate (PPi) without any metal-mediator through an enhanced ‘turn-on’ fluorescence emission. The developed chemosensor is highly selective towards PPi with nanomolar level of detection limit in physiological medium. Interestingly, the sensor could readily detect inherent PPi levels in HeLa cells as evidenced in cellular imaging studies.

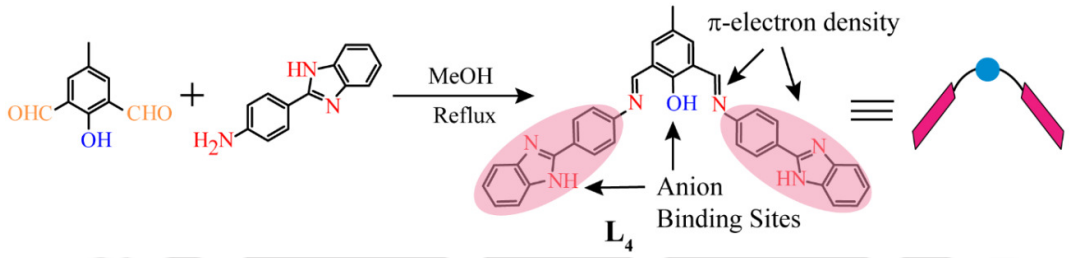

Scheme 6.1 Synthetic scheme of the probe **L4**.

6.2 Design principle

The design principle of the PPi sensor working on aggregation induced emission principle should encompass the following cardinal features: (1) The probe should be an aromatic system with extended conjugation with the possibility of stacking and (2) it should possess sufficient convergent H-bond donor sites for efficient anion coordination. Based on the above rational, we have synthesized a benzimidazole-functionalized imine-based chemosensor (**L4**) bearing phenolic OH and benzimidazole NH as H-bond donors. The imine functionality and the benzimidazole functionality are intended to increase the π electron density and also the extent of π delocalization in the system.

6.3 AIE phenomenon

The photophysical properties of the chemosensor are elucidated by UV/Vis absorption and fluorescence emission study in various solvents. For this, a stock solution of **L4** is prepared in

DMSO (5.0 mM) and diluted accordingly with the experimental solutions. As depicted in figure 6.1, the chemosensor **L4** (10 μM) is very weakly emissive in THF. However, the aqueous solution of the chemosensor, which is a poor solvent for **L4**, is strongly emissive at ~530 nm with a Stokes shift of 125 nm (λ_{ex} = 430 nm, slit = 2 nm / 2 nm). This suggests the possibility of aggregation induced emission (AIE) phenomenon.[5] To elucidate the AIE process, **L4**'s emission intensities at ~530 nm are recorded with increasing water fractions in THF. As evident in figure 6.1a, the solution is very weakly emissive upto f_w = 90 %. However, further increase in the water content lead to a remarkable increase in emission intensity at the same wavelength. At 99 vol% f_w, the emission intensity of solution is nearly 9.0 times than that at f_w = 0% (Figure 6.1b). Furthermore, a light green fluorescence of the solution is apparent under a 365 nm UV lamp (Figure 6.1b, inset).

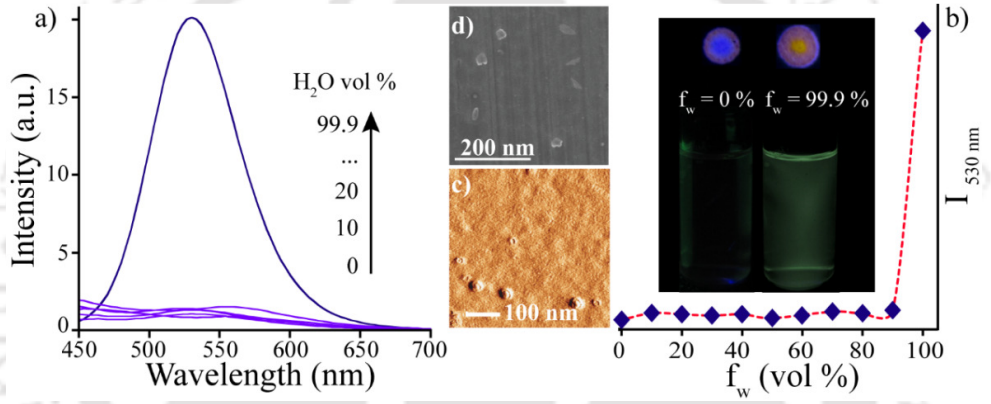

Figure 6.1 a) Fluorescence intensity changes of the chemosensor (**L4**, 10 μM) with increasing water fraction in THF. b) A plot of intensity ($I_{530\ nm}$) versus fraction of water (f_w) content in THF-water mixture (λ_{ex} = 430 nm, slit 2/2 nm). c) AFM and d) FESEM images of **L4**.

A close inspection of the receptor design reveal that it is very flexible and can adopt various conformations through several possible combinations of C-C or even C=N imine bond rotations/isomerization.[6] These rotations or conformational changes leads to the non-radiative deactivation of the excited state, which perhaps accounts for the weak fluorescence of the probe in THF. However, as the chemosensor is insoluble in water, addition of higher water fraction triggers aggregation of **L4**'s molecules, wherein the intermolecular and intramolecular hydrogen bonding between various H-donors and H-acceptors in the chemosensor would be the driving force. These interactions lock the conformation and thus, the restriction of intramolecular rotation (RIR) around single bond finally leads to fluorescence enhancement. Given that aggregation of **L4** is the plausible reason for fluorescence enhancement, it is anticipated that **L4** would be strongly fluorescent in viscous solvents, which are known to hinder intramolecular rotation. Prominent fluorescence emission spectra of **L4** recorded in glycerol (Figure A6.1)

supports this premise. Subsequently, THF solution of **L4** is spotted on filter a paper and to one of the spot, drop of water is added. Following drying, the spot in THF displayed bluish-violet fluorescence, whereas the aqueous spot exhibits yellowish like color under the 365 nm UV lamp (Figure 6.1b, inset). This also validates the aggregation caused fluorescence emission behavior of **L4**.

However, naked eye observation indicates that the aqueous **L4** solution is transparent and macroscopically homogeneous with no visible precipitation, which perhaps suggests the formation of sub-micron aggregates in solution. Formation of smaller aggregates is also supported by the changes in absorption spectra of **L4** in water. The probe **L4** exhibits an absorption maximum at 325 nm and a hump at 375 nm in THF whereas, in water the absorption maxima is slightly blue shifted to 321 nm along with a broad hump like peak around 439 nm (Figure A6.1b). The weak absorption peaks at 321 nm or 325 nm can be attributed to the π---π* transition of benzimidazole-benzene.[7] Upon close inspection, a trailing trace beyond 500 nm is also observable, which suggests light scattering or Mie effect originating from the smaller aggregates present in the solution (Figure A6.1b).

In order to ascertain the formation of nano-aggregates of **L4** in aqueous medium, field emission scanning electron microscope (FESEM) and atomic force microscope (AFM) analysis are pursued. AFM analysis of a10 μM aqueous solution of **L4** reveals the formation of aggregates of average particle size ranging from 40-50 nm (Figure 6.1c). This is corroborated by FESEM image of block-shaped aggregates of particle size 50-60 nm in case of a 10 μM aqueous solution of **L4** (Figure 6.1d). Collectively, these results strongly suggest aggregation of the probe molecules in water.

6.4 Anion sensing aptitude of L4

It has been reported that the AIE nature of a chromophore can be tuned by guest molecules.[8-10] In the present study, the chemosensor **L4** has potential anion binding sites (NH and OH). Hence, it is pertinent to scrutinize its anion sensing aptitude in water. To this end, changes in the UV-visible spectra of a 10 μM aqueous solution of **L4** are recorded upon addition of 10 equivalents of sodium or tetrabutyl salts of various anions such as F^-, Cl^-, Br^-, I^-, NO_3^-, OAc^- ($CH_3CO_2^-$), HSO_4^-, SO_4^{2-}, ClO_4^- and PPi. Interestingly, a distinct change in the UV-visible spectra is observed only after addition of pyrophosphate anion (PPi), which lead to the emergence of new absorption peaks at 270 nm and 439 nm (Figure 6.2). These spectral changes are accompanied by a distinct visual change in the color of the solution of the probe **L4** from colorless to faint yellowish in case of the interaction of **L4** with PPi (Figure 6.2b, inset). This visual color change

is encouraging as it renders facile naked eye detection of PPi in water. Further inspection of the UV-Vis spectra after the addition of PPi anion reveals the formation of isosbestic points at 266 nm, 321 nm and 391 nm, which indicates the formation of a new species. It may also be mentioned that addition of PPi induced further aggregation, which is evident from the trailing UV-visible trace of the probe solution in presence of PPi (Figure 6.2b). Our next endeavour is to determine the selectivity and sensitivity of **L4** towards PPi for which fluorescence-based experiments are pursued.

Upon addition of increasing concentrations of PPi, the fluorescence intensity of **L4** increases systematically to attain a magnitude, which is nearly 17 times more than the probe alone at 530 nm (Figure 6.3). The **L4**-PPi solution also exhibits intense yellowish-green like fluorescence when observed under the 365 nm UV lamp (Figure 6.3a).

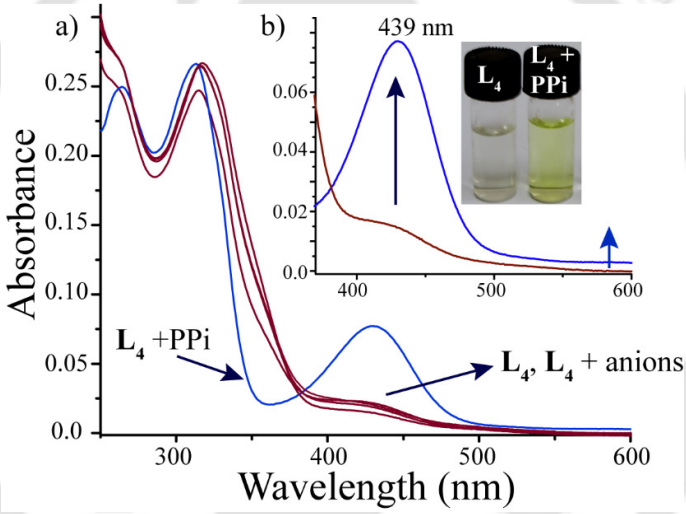

Figure 6.2 UV-Visible changes of **L4** with a) various anions (10 equivalents) and b) magnified view with PPi in water. Inset: Change in the color of **L4** after PPi addition.

The steep enhancement in the fluorescence emission intensity of the aforesaid solution suggests the possibility that PPi promoted further aggregation of the probe **L4**. This tenet is validated by AFM and FESEM analysis of **L4**-PPi complex, which indicate the formation of aggregates (Figure 6.3b,6.4.c), whose average particle sizes (130-170 nm) appeared to be bigger than that of **L4** alone in water (Figure 6.2c, 6.2d). Job's plot analysis suggested that **L4** and PPi form a 1:1 host guest complex (Figure A6.2). The apparent binding constant as calculated by B-H plot is 4.2×10^5 M^{-1} (Figure A6.2b). The limit of detection (LOD) of **L4** for PPi is 1.67 nM, with a signal: noise ratio of 3:1 (Figure A6.3). This detection limit of PPi compares well with those reported in previous studies (Table A6.1).

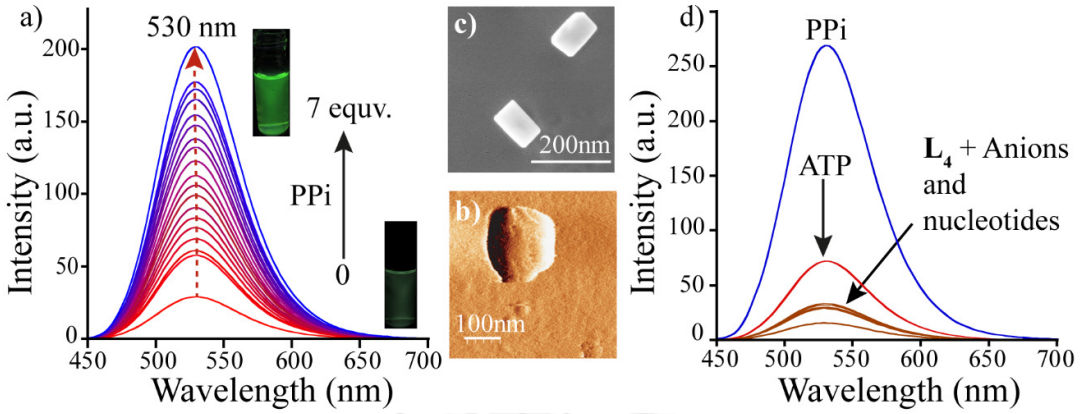

Figure 6.3 a) The systematic increase in fluorescence emission intensity change of **L4** with increasing concentrations of PPi (λ_{ex} = 430 nm, slit 2/2 nm). b) AFM and c) FESEM image of **L4** after addition of PPi. d) Fluorescence based anion selectivity profile of **L4**.

The specificity of **L4** towards PPi is verified in solution based experiments wherein other tested anions such as F^-, Cl^-, Br^-, I^-, NO_3^-, OAc^-, HSO_4^-, SO_4^{2-}, ClO_4^-, $H_2PO_4^-$, PO_4^{3-} HPO_4^{2-}, ADP and AMP etc. cause no change to the emission spectra of **L4**. However, a prominent enhancement in the emission intensity of **L4** is also recorded in presence of ATP (Figure 6.3d). Competitive binding studies are also carried out with these anions by mixing 10 equivalents of the aforesaid anions to a solution of **L4** containing 1.0 equivalent of PPi (Figure A6.4). It is significant to mention that the PPi-induced manifold enhancement of the emission intensity of **L4** remains almost unaffected by the presence of these anions, which indicates the strong selectivity of the developed sensor for PPi. We have also tested some biologically relevant anions such as citrate, tartrate, succinate and oxalate for possible interference. Interestingly, none of the aforesaid anions cause any significant change in the fluorescence emission intensity of **L4** (Figure A6.5). The chemosensor can also detect PPi in a mixed aqueous medium and cause similar changes. Prior to PPi addition, **L4** in a 1:1 (v/v) MeCN-5.0 mM HEPES buffer (pH~7.4) mixture exhibited weak fluorescence. However, addition of 10 equivalents of PPi resulted in strong fluorescence at 530 nm (Figure A6.6).

It can be construed that the higher acetonitrile (MeCN) content in this experimental solution prevent the **L4** molecules to aggregate, which results in comparatively weak fluorescence emission of the solution. However, presence of PPi perhaps trigger the aggregation of **L4** molecules, which results in enhanced fluorescence emission. Other anions fail to produce similar optical signal with **L4** under alike experimental conditions. It may be mentioned here that even in pure dry acetonitrile medium (f_w = 0), PPi-induced aggregation of the probe is visible (Figure A6.7).

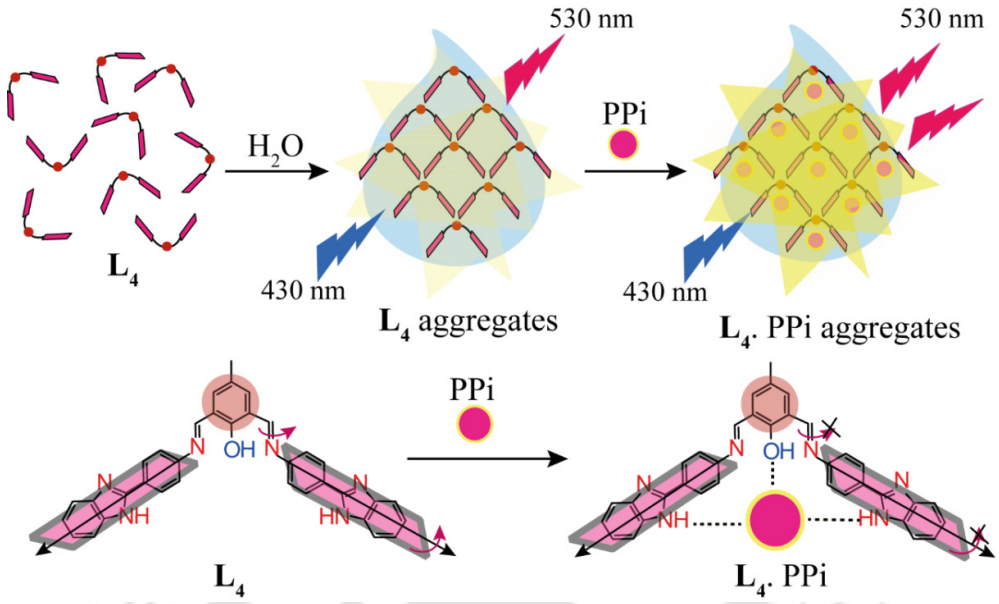

Scheme 6.2 The plausible binding scheme of **L4** with PPi.

Ca^{2+} has a high affinity for PPi and is known to form a strong complex with the same. It is thus envisaged that addition of Ca^{2+} is likely to disrupt the **L4**-PPi ensemble owing to strong Ca^{2+}-PPi interactions and this would also provide strong evidence for the involvement of PPi in inducing aggregation and thereby enhancing the fluorescence emission intensity of **L4** manifold. As anticipated, upon addition of Ca^{2+}, the solution turned colorless and the fluorescence diminished considerably, which implies the involvement of PPi in the enhancement of fluorescence emission (Figure A6.8). UV-Vis and fluorescence-based studies indicate that the initial aggregation induced emission of **L4** in water is further intensified with the addition of PPi. This suggests that addition of PPi would lead to the generation of comparatively larger aggregates in aqueous medium. This is corroborated by FESEM and AFM analysis, as discussed earlier. Further, dynamic light scattering (DLS) measurement shows an average particle size of 258 nm (PdI = 0.554, Figure A6.9) in a 10 µM solution of **L4** in water interacted with 10 equiv. of pyrophosphate anion. Collectively, all these evidence support the PPi-induced aggregation of **L4** in aqueous medium probably through the involvement of OH and NH groups (Scheme 6.2).

6.5 Paper strip based detection of PPi

For practical application of a chemosensor, it is preferable to perform the detection on solid supports in order to circumvent the involvement of complex and expensive equipment and render the detection rapid and facile. To this end, filter papers are soaked with the chemosensor solution and checked for fluorescence and colorimetric changes following addition of aqueous pyrophosphate solution. Interaction with PPi anion resulted in a light yellowish colour on the

filter papers, which could be readily deciphered with naked eye (Figure A6.10a). Furthermore, under a 365 nm UV lamp, the faint bluish-green **L4**-impregnated papers emit strong yellowish-green like fluorescence following PPi addition (Figure A6.10b). Similar changes are also observed on the silica plates (Figure A6.10b, inset).

6.6 Detection of intracellular PPi by imaging

Pyrophosphate (PPi) has emerged as an anion of significant biological relevance as it has been shown to have a profound role in several cellular processes.[11-14] This has spurred considerable interest amongst analytical chemists to design chemosensors that can be deployed for PPi sensing in the cellular milieu. In the present study, the excellent selectivity of the probe **L4** for PPi and its strong fluorescence in aqueous medium suggest that the probe could perhaps be used for bio-imaging of intracellular pyrophosphate.

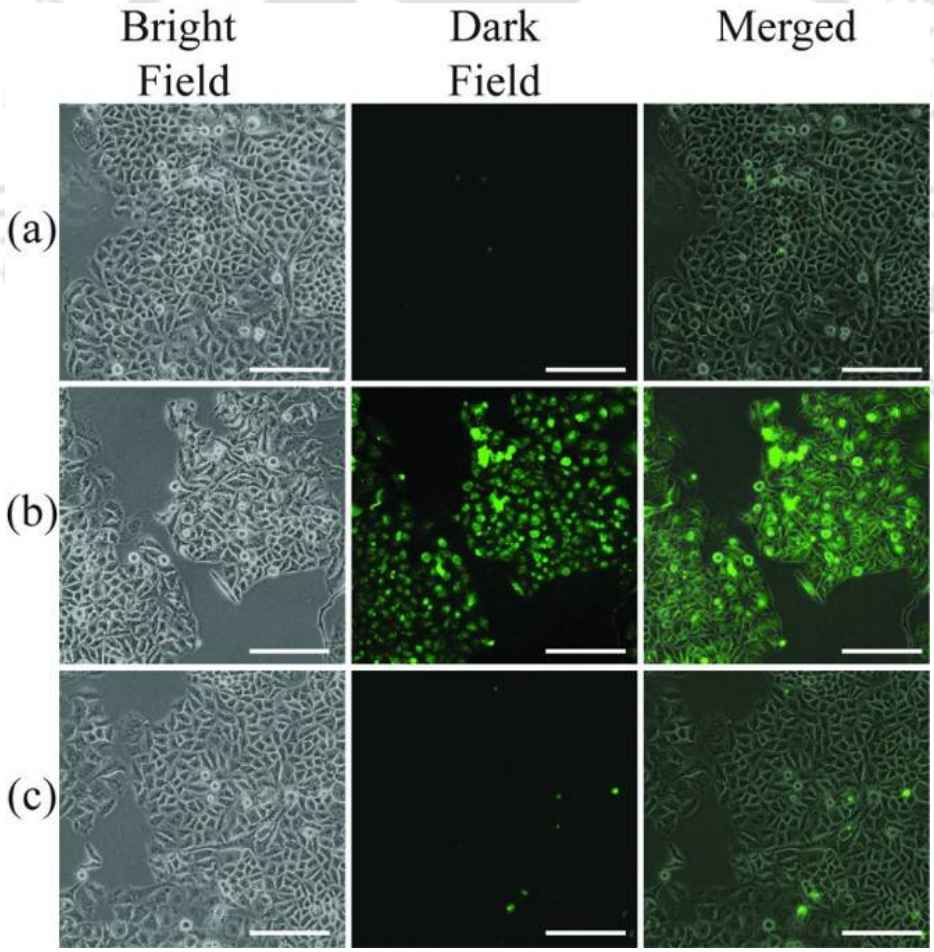

Figure 6.4 Fluorescence microscope images of HeLa cells incubated with (a) probe **L4** (2.5 μM) only, (b) probe **L4** (subsequent addition of 2.5 μM) and (c) Ca^{2+} (50 μM) following addition of **L4**.

An important pre-requisite for this endeavour is to ascertain the cytotoxic potential of the probe. To that end, the well-established MTT-based cytotoxicity assay on HeLa cell line (human cervical carcinoma cells) are carried out. Interestingly, even at very high concentrations of the probe or probe-PPi complex (60 μM) the viability of the cells is as high as 80% (Figure A6.11). Considering the non-toxic nature of **L4** as well as **L4**-PPi ensemble, it is envisaged that the probe could be used for detecting intracellular PPi through imaging studies. To this end, when **L4** is added to HeLa cells at 2.5 μM followed by an incubation for 1 hour, the observed cellular fluorescence is negligible (Figure 6.4a). However, on further addition of 2.5 μM **L4**, a prominent green fluorescence can be detected in the cells (Figure 6.4b).

These results suggest that the probe **L4** facilitates sensing of the inherent PPi levels present in the cell. On careful observation, intracellular clusters emitting intense green fluorescence could be deciphered in some cells, which perhaps represent intracellular aggregates of **L4**-PPi complex. Interestingly, subsequent addition of Ca^{2+} to HeLa cells results in a dramatic quenching of the fluorescence of HeLa cells (Figure 6.4c), which further support the relevance of PPi in inducing aggregation of the probe, and consequently manifold increase in the fluorescence exhibited by HeLa cells.

6.7 Conclusion

In conclusion, we have developed a promising AIE active chemosensor for the selective 'switch-on' colorimetric and fluorimetric detection of pyrophosphate anion in physiological medium. The sensing is reported in 100% water with a benzimidazole functionalized chemosensor and it ruled out the need of a metal-chemosensor ensemble for anion sensing. Interaction with the PPi anion boosted the fluorescence through aggregation, which is well supported by FESEM, AFM and DLS experiments. The high sensitivity for the PPi anion is observed both in aggregated as well as non-aggregate (solution) form of the chemosensor. Importantly, the PPi selectivity does not alter even in the presence of higher concentration of other competing anions, including biologically relevant anions. Furthermore, paper strips of the chemosensor can also be used to detect the PPi. Finally, based on the non-toxic nature of the probe, the PPi-induced enhanced fluorescence emission could be garnered to ascertain inherent levels of PPi produced in live HeLa cells.

References

1. S. Kubik, *Chem. Soc. Rev*., 2010, **39**, 3648-3663.
2. S. Kubik, *Chem. Soc. Rev*., 2009, **38**, 585-605.
3. J. Luo, Z. Xie, J. W. Y. Lam, L. Cheng, H. Chen, C. Qiu, H. S. Kwok, X. Zhan, Y. Liu, D. Zhu and B. Z. Tang, *Chem. Commun*., 2001, 1740-1741.
4. B. Z. Tang, X. Zhan, G. Yu, P. P. S. Lee, Y. Liu and D. Zhu, *J. Mater. Chem*., 2001, **11**, 2974-2978.
5. Y. Cao, M. Yang, Y. Wang, H. Zhou, Z. Jun, X. Zhang, J. Wu, Y. Tiana, Z. Wud, *J. Mater. Chem. C,* 2014, **2**, 3686-3694.
6. A. Maity, F. Ali, H. Agarwalla, B. Anothumakkool and A. Das, *Chem. Commun.*, 2015, **51**, 2130-2133.
7. L.Wang, Y. Shen, M. Yang, X. Zhang, W. Xu, Q. Zhu, J. Wu, Y. Tian and H. Zhou, *Chem. Commun*., 2014, **50**, 8723-8726.
8. C. Gao, G. Gao, J. Lan and J. You, *Chem. Commun*., 2014, **50**, 5623-5625.
9. J. Chang, Y. Lu, S. He, C. Liu, L. Zhaoab and X. Zeng, *Chem. Commun*., 2013, **49**, 6259-6261.
10. S. Gui, Y. Huang, F. Hu, Y. Jin, G. Zhang, L. Yan, D. Zhang and R. Zhao, *Anal. Chem*., 2015, **87**, 1470-1477.
11. A. E. Timms, Y. Zhang, R. G. G. Russell and M. A. Brown, *Rheumatology,* 2002, **41**, 725-729.
12. S. Xu, M. He, H. Yu, X. Cai, X. Tan, B. Lu and B. Shu, *Anal Biochem*., 2001, **299**, 188-193.
13. M. Doherty, C. Belcher, M. Rehan, A. Jones and J. Ledingham, *Ann. Rheum. Dis*., 1996, **55**, 432-436.
14. R. A. Terkeltaub, *Am. J. Physiol. Cell Phydiol*., 2001, **281**, C1-C11.

Appendix 5

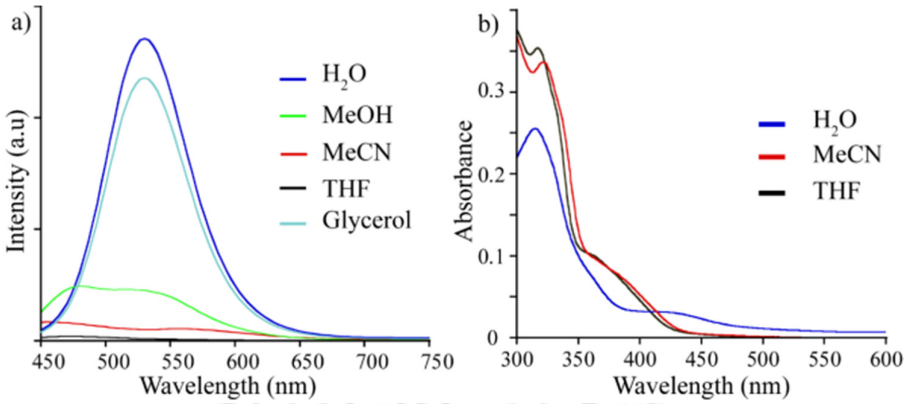

Figure A6.1 a) Fluorescence emission and (b) absorption spectra of **L4** in various solvents.

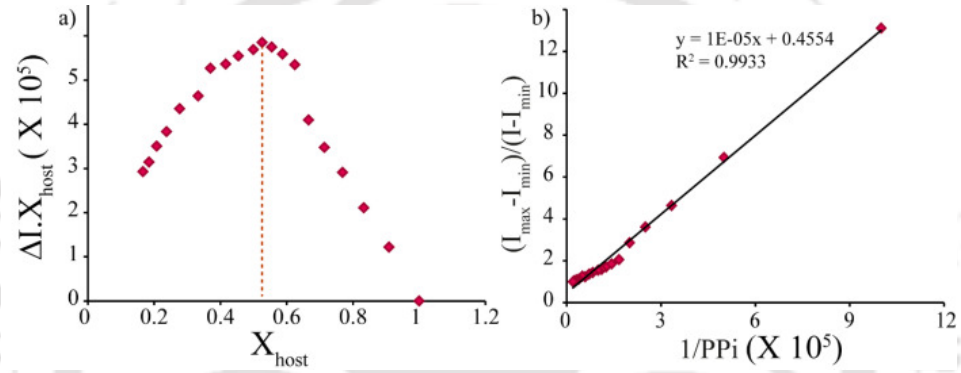

Figure A6.2 a) Job's plot for determining the binding stoichiometry of **L4** with PPi (1:1 host-guest complex). b) The corresponding Bensei-Hildebrand plot for PPi ion.

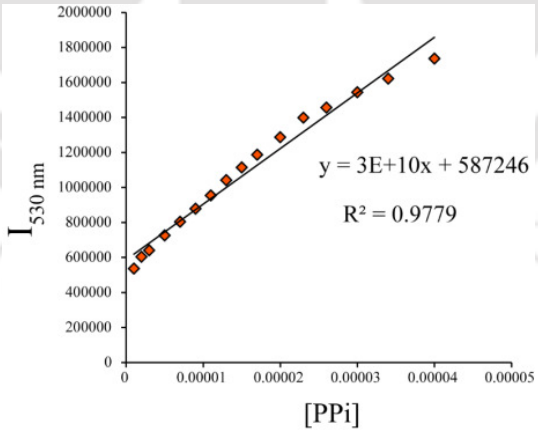

Figure A6.3 Fluorescence emission intensity at 530 nm of **L4** against pyrophosphate (PPi) concentrations (in molarity) for calculation of limit of detection (LOD).

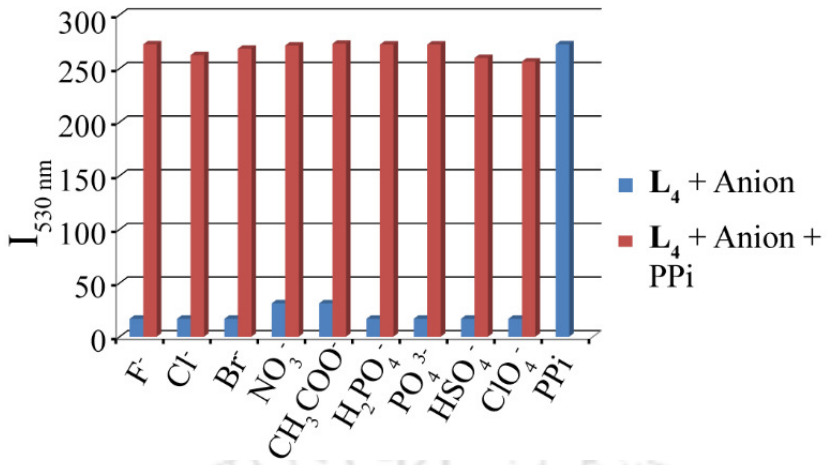

Figure A6.4 Bar plot presentation of interference of other anions in the PPi induced 'turn-on' fluorescence of **L4**.

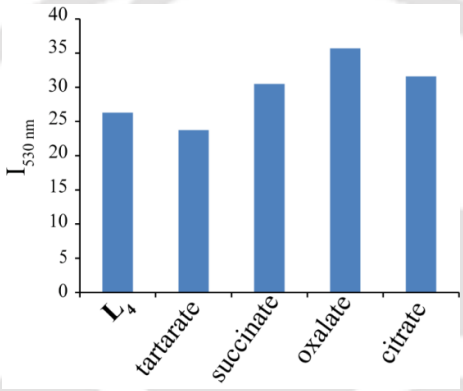

Figure A6.5 Fluorescence intensity changes of **L4** with the some biologically important anions in water.

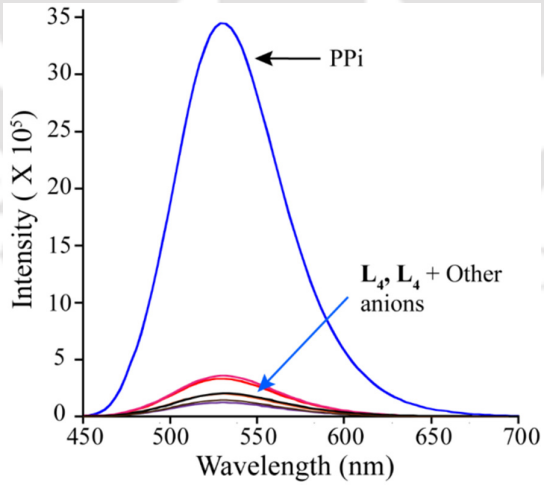

Figure A6.6 Fluorescence based anion selectivity study of **L4** in MeCN-water (1:1, v/v) mix at room temperature (λ_{ex} = 430 nm, slit = 2nm / 2nm).

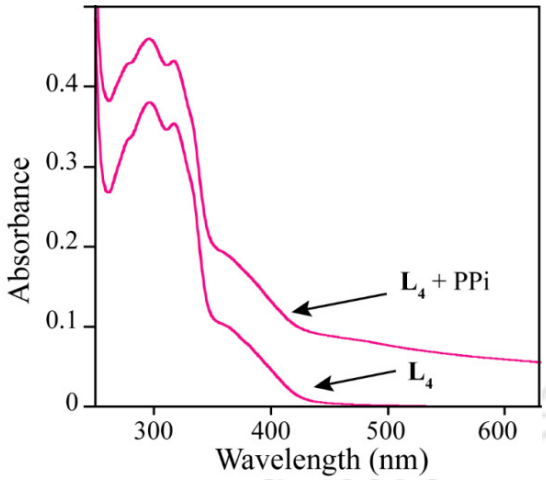

Figure A6.7 UV-Vis changes of the **L4** (10 μM) with PPi (10 equivalent) in dry acetonitrile at room temperature.

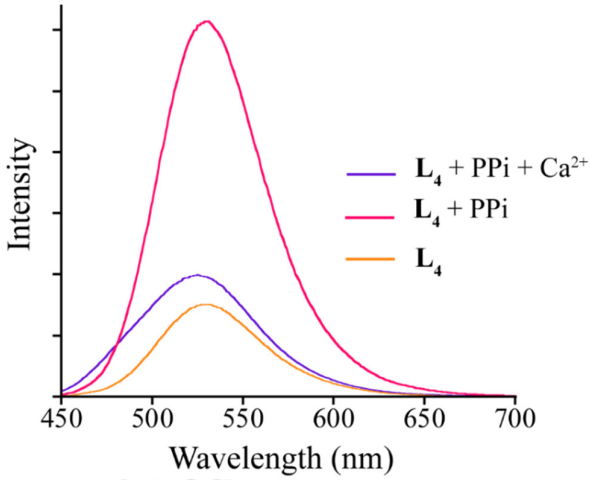

Figure A6.8 Fluorescence emission changes '**L4**-PPi' ensemble after addition of Ca^{2+} (λ_{ex} = 430 nm, slit = 2nm/ 2nm).

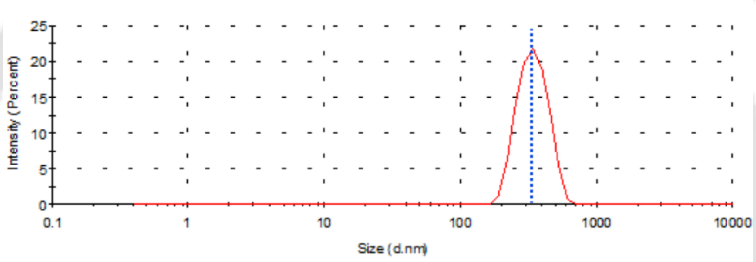

Figure A6.9 DLS analysis of **L4** (10 μM) after addition of PPi (10 equiv.) in water.

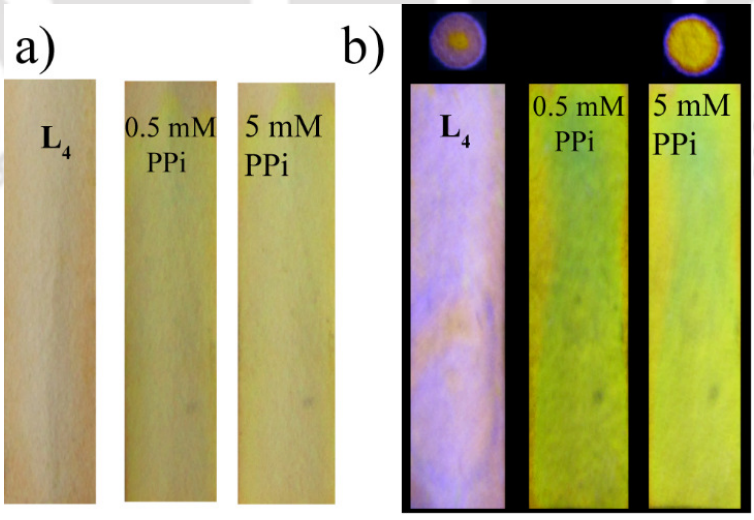

Figure A6.10 Paper strip test of **L4** with different concentrations of PPi. Visual color changes of **L4** after PPi addition a) in day light and b) under 365 nm UV lamp. Inset of panel b: The color change experiment on TLC plates after PPi addition.

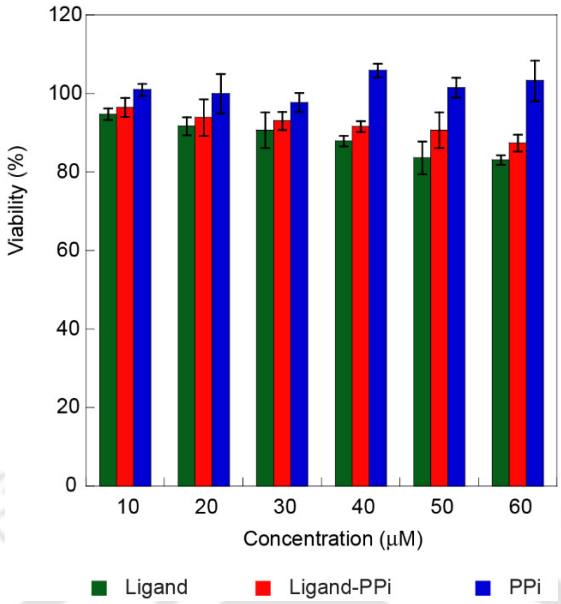

Figure A6.11 MTT based cytotoxicity assay for ligand and **L4**-PPi ensemble.

Table A6.1. Recent progress in the field of PPi sensing, a comparative study of their LOD values in different binding environments.

Sl No.	References	Used system	LOD of PPi	Solvent system
1.	**Present work**	**Probe alone**	**1.67 nM**	**Water**
2.	*J. Am. Chem., Soc*. **2014**, 136, 5543	Probe-Zn(II) ensemble	0.8 nM	10 mM HEPES buffer (pH = 7.4)
3.	*RSC Adv*., **2015**, 5, 10505–10511	Probe-Zn(II) ensemble	7.27×10^{-6} M	10 mM HEPES buffer (pH = 7.4)
4.	*Chem. Commun*., **2013**, 49, 877-879	Probe-Zn(II) ensemble	40×10^{-8} M	H_2O:CH_3CN (2:8, v/v) buffered with HEPES, pH =7.0
5.	*Chem. Commun*., **2012**, 48, 1784-1786	Probe-Cu(II) ensemble	2.02 mM	10 mM MOPS buffer (pH = 7.0)
6.	*J. Org. Chem*., **2012**, 77, 11405−11408	Probe-Zn(II) ensemble	Not reported	50 mM HEPES buffer (pH = 7.4)
7.	*Inorg. Chem*., **2013**, 52, 8294–8296	Probe-Zn(II) ensemble	155×10^{-9} M	0.02 mM HEPES buffer (pH = 7.4)
8.	*Org. Lett*., **2014**, 16, 2220–2223	Probe-Cu(II) ensemble	Not reported	10 mM HEPES buffer (pH = 7.4)
9.	*Dalton Trans*., **2015**, 44, 1358-1365	Probe-Cd(II) ensemble	3.39 μM	1:1 CH_3CN:10 mM HEPES buffer (pH = 7.4)
10.	*RSC Adv*., **2014**, 4, 484	Probe-Zn(II) ensemble	Not reported	10 mM HEPES buffer (pH = 7.0)
11	*Org. Lett*., **2011**, 13, 5294	Probe-Zn(II) ensemble	1.5 μM	5:95 CH_3CN:20 mM HEPES buffer (pH = 7.4)
12	*Anal. Chem*., **2010**, 82, 4628-4636	Probe-Zn(II) ensemble	0.4 μM	30% ethanol/water (v/v) solution at (pH 7.4)

This thesis report the efforts made in designing and improvising certain benzothiazole and benzimidazole functionalized chemosensors for colorimetric and fluorescent sensing of biologically important cations and anions. The present findings provide an insight in designing the chemosensors to apply them in aqueous solution for biological application with better spectral properties.

Ninhydrin functionalized benzothiazole probe **L_1** is an excellent Zn^{2+} sensor and emits in the NIR (near infrared) region without any interference from other metal ions. A visual distinction of $H_2PO_4^-$ from other phosphate related anions is also achieved with the probe-Zn^{2+} ensemble. However, to improve the water solubility, a modified benzothiazole functionalized Schiff base probe **L_2** was synthesized, which can sense Zn^{2+} and Cd^{2+} ions at physiological medium. Again, the corresponding metal-ensembles are sensitive to $H_2PO_4^-$ and PPi anions. The design of such multi-ion sensors is highly desirable as they can reduce the cost involved in synthesis of multiple sensors meant for the same task. Proceeding on the same lines, two benzothiazole and two imine functionalities are introduced to **L_3**. It is highly selective and sensitive only to Zn^{2+} ion at physiological conditions with lowest detection limit of 71 ppb. Finally, in an attempt to synthesize metal-free chemosensors for anions in aqueous medium, few benzimidazole type functionalities are introduced in designing **L_4**. The new chemosensor demonstrates the positive impact of aggregation in the sensing process. Addition of PPi anion facilitate the aggregation of **L_4**'s molecules and thereby enhances the fluorescence emission through a process known as aggregation induce emission (AIE). Paper strips of the chemosensor can also be used for the quick detection of PPi.

The chemistry of chromo-fluorogenic chemosensors for cation and anions has grown considerably since the pioneering work of Sousa with the naphthalene compounds. After the Nobel Prize in supramolecular chemistry in 1987 to Charles J. Pedersen, Jean-Marie Lehn and Donald J. Cram, the design and application of fluorescent molecular devices increased exponentially. Since then different combinations of binding sites and signalling units are coupled in different ways to develop selective systems for different anionic species. Moreover, for practical applications, new probes with good water solubility and response in NIR region (650–900 nm) are essential. AIE active chemosensors are relatively new the sensing world and there are various scopes available with this technique. Again, the design of new chemosensor ensembles apart from metal based one for various analytes except anions is also desirable.

Abhijit Gogoi

Date of Birth: 31-12-1986

Place of Birth: Natun Nirmali Gaon, Dibrugarh, Assam, India.

Nationality: Indian

Email: abhijit.gogoi@iitg.ernet.in, jitgogoi@gmail.com

Academic Summary

2010-present: Ph.D. student at Indian Institute of Technology Guwahati, India.
(Thesis has been submitted)
Thesis title: "**Benzimidazole and Benzothiazole Based Chemosensors For Biologically Important Analytes**".

2009-2010: Project Assistance at Natural Product Chemistry division, CSIR-NEIST, Jorhat, India

2007-2009: Masters in Chemistry (Specialization: Organic Chemistry)
Dibrugarh University, Assam, India.

2004-2007: Graduation (Chemistry), DHSK College, Dibrugarh, Assam, India.

2004: 12th (Science), AHSEC.

2002: 10th, SEBA.

Honours and awards

- Qualified National Eligibility Test (NET) for Junior Research Fellowship, 2010

Research Interests

- Design and synthesis of fluorescent probes
- Fluorescence sensing of biologically important ions and molecules
- Applications of new sensor technologies in biotechnology and environmental analysis

Expertise

- Spectroscopic techniques (UV, Fluorescence, FT-IR, Atomic absorption), Optical and fluorescence microscopy, NMR spectroscopy, mass spectrometry, DLS, single crystal x-ray diffraction

Publications

1. Charge-Assisted Complexation of Anions of Different Dimensionality by Benzimidazole-Based Receptors Bearing -OH Functionality.
   Abhijit Gogoi and Gopal Das, *Crystal Growth & Design*, 2012, **12**, 4012–4021.
2. Electronic substitution effects on anion coordination of a tripodal thiourea receptor: Evidences of deprotonation of oxy-anions in solid and solution.
   Abhijit Gogoi and Gopal Das, *Supramol Chem*, 2013, **25**, 819-830.
3. A benzothiazole containing CHEF based fluorescence turn-ON sensor for Zn^{2+} and Cd^{2+} and subsequent sensing of $H_2PO_4^-$ and $P_2O_7^{4-}$ in physiological pH.
   Abhijit Gogoi, Soham Samanta and Gopal Das, *Sensor Actuat B-Chem*, 2014, **202**, 788-794.
4. NIR sensing of Zn(II) and subsequent dihydrogen phosphate detection by a benzothiazole functionalized ninhydrin based receptor.
   Abhijit Gogoi and Gopal Das, *RSC Adv*., 2014, **4**, 55689-55695.
5. AIE Active Metal-Free Chemosensing Platform for Highly Selective Turn-ON Sensing and Bioimaging of Pyrophosphate Anion.
   Abhijit Gogoi, Sandipan Mukherjee, Ramesh Aiyagari and Gopal Das, *Anal. Chem.*, 2015, **87**, 6974–6979.
6. Nanomolar Zn(II) sensing and subsequent PPi detection in physiological medium and live cells with a benzothiazole functionalized chemosensor.
   Abhijit Gogoi, Sandipan Mukherjee, Ramesh Aiyagari and Gopal Das, *RSC Adv*., 2015, **5**, 63634-63640.
7. Anion complexation with cyanobenzoyl substituted first and second generation tripodal amide receptors: Crystal structures and solution studies
   Md. Najbul Hoque, **Abhijit Gogoi** and Gopal Das, *Dalton Trans*., 2015, **44**, 15220-15231.
8. Competitive anion binding aptitude of benzimidazole and amide functionality of a non-symmetrical receptor in solid state and solution phase.
   Nilotpal Borah, **Abhijit Gogoi** and Gopal Das, *Supramol Chem.* (accepted)
9. Colorimetric and Fluorescence Improvement in F^- and OAc^- Sensing with A series of benzothiazole based receptors
   Abhijit Gogoi and Gopal Das (Manuscript under preparation).

Poster Presentation

- Poster presented in ***Frontiers in Chemical Science,*** Indian Institute of Technology Guwahati, Guwahati, 2014.